

THE SCHWINGER-DYSON EQUATIONS AND GLUON BOUND STATES OF QCD

by

Joseph W. Meyers

B.S. in Engineering Physics, University of Pittsburgh, 2009

M.S. in Physics, University of Pittsburgh, 2010

Submitted to the Graduate Faculty of
the Kenneth P. Dietrich School of Arts and Sciences in partial
fulfillment

of the requirements for the degree of

Doctor of Philosophy

University of Pittsburgh

2014

UNIVERSITY OF PITTSBURGH
DIETRICH SCHOOL OF ARTS AND SCIENCES

This dissertation was presented

by

Joseph W. Meyers

It was defended on

December 3, 2014

and approved by

Eric Swanson, Associate Professor, University of Pittsburgh

Ayres Freitas, Assistant Professor, University of Pittsburgh

Vladimir Savinov, Associate Professor, University of Pittsburgh

Andrew Zentner, Associate Professor, University of Pittsburgh

Colin Morningstar, Professor, Carnegie Mellon University

Dissertation Director: Eric Swanson, Associate Professor, University of Pittsburgh

Copyright © by Joseph W. Meyers
2014

THE SCHWINGER-DYSON EQUATIONS AND GLUON BOUND STATES OF QCD

Joseph W. Meyers, PhD

University of Pittsburgh, 2014

Nonperturbative techniques in quantum field theory, such as lattice gauge theory, Schwinger-Dyson equations, and applications of the renormalization group, have been successful in describing both the propagator functions and bound states of various theories, most notably those of quarks and hadrons in Quantum Chromodynamics (QCD). The Schwinger-Dyson theoretical framework is presented from basic principles and developed, through examples in a variety of quantum field theories, as a general numerical approach which can yield valuable insight into quantum phenomenology. Explorations include the studies which I have performed to extend bound state theory to the gauge sector of QCD, including the influence of both gluon and ghost fields. This allows for the description of gluon bound states (“glueballs”), which are theoretically viable explanations for previously unidentified resonances in experimental particle searches, and is treated for the first time using the Bethe-Salpeter formalism. This description is sufficiently robust to explore the spectrum of glueballs and provide commentary on the potential for investigation of valence gluon content in meson bound states. Additionally, the first investigation of the full two-loop gluon gap equation is presented and discussed, along with general commentary on the current state of nonperturbative QCD. This computation yields the dressed propagators for quarks, gluons, and ghosts from the coupled set of equations.

TABLE OF CONTENTS

1.0 INTRODUCTION	1
2.0 FORMALISM	13
2.1 Path Integrals	13
2.2 Generating Functionals	15
2.2.1 Definitions	15
2.2.2 Legendre Transform	16
2.3 Schwinger-Dyson Equations	18
2.3.1 Derivation	18
2.3.2 Diagrammatics	21
2.3.3 Truncation	22
2.3.4 Renormalization	25
2.4 The Bethe-Salpeter Equation	29
3.0 GAP EQUATIONS	34
3.1 Numerical Methods	34
3.1.1 Discretization	35
3.1.2 Convergence and Stability of Solutions	38
3.1.3 Renormalization in Practice	41
3.2 ϕ^4 theory	44
3.3 QED	48
3.3.1 Electrons	49

3.3.2	Photons	52
3.3.3	QED Interactions	55
3.3.4	QED Renormalization	56
3.3.5	Results	58
3.4	QCD	60
3.4.1	Quark Sector	62
3.4.2	Yang-Mills Sector	65
3.4.2.1	Ghosts	65
3.4.2.2	Gluons	67
3.4.3	QCD Interactions	73
3.4.4	QCD Renormalization	80
3.4.5	Truncation Examples	83
3.4.5.1	Swimming with Quarks	83
3.4.5.2	Fits to Lattice Gluons	86
3.4.5.3	Mandelstam's Equation	92
3.4.5.4	vSHA Equations	94
3.4.6	Fully Coupled System	97
3.4.7	Comparison to Other Work	102
4.0	BOUND STATES	109
4.1	Analytic Continuation	109
4.1.1	Necessity	109
4.1.2	Methods – Direct Continuation	111
4.1.3	Methods – Cauchy-Riemann Continuation	112
4.1.4	Methods – Double-Grid Continuation	114
4.1.5	Methods – Contour Continuation	115
4.2	Numerical Methods	117
4.2.1	Eigensystem Representation	118
4.2.2	Chebyshev vs. Super-Index	119

4.2.2.1	Point Basis Diagonalization	119
4.2.2.2	Chebyshev Basis Diagonalization	119
4.2.2.3	Results and Comparison	121
4.3	Glueballs	122
4.3.1	Symmetries of the 2-gluon Valence Contribution	125
4.3.2	The 0^{-+} Glueball	128
4.3.2.1	Perturbative Vertices	129
4.3.2.2	Dressed Vertices	129
4.3.3	The 0^{++} Glueball	131
4.3.4	Glueball Results	135
4.4	Glueball + Meson Studies	137
5.0	CONCLUSIONS	139
	BIBLIOGRAPHY	144

LIST OF TABLES

1	Set of Renormalization parameters for the QCD propagator functions of Figure 8	40
2	Toy model renormalization parameters for the QED propagator functions of Figure 19.	60
3	Set of parameters for the Maris-Tandy gluon propagator model.	89
4	Comparison of anomalous dimension parameters γ_i exhibited by Lattice QCD results and the numerical results of our fully coupled system.	108

LIST OF FIGURES

1	Plot of the Running Coupling of QCD as obtained from lattice gauge theory and multiple experimental measurements as compiled by the Particle Data Group ^[56]	7
2	Diagrams representing the (source-dependent) propagators in QCD	22
3	Diagrams representing the perturbative vertices in QCD	23
4	General diagram for a nonperturbative vertex in QCD	23
5	Diagrams representing the classical field variables in QCD	24
6	Diagrammatic representation of functional derivatives with respect to a generic classical field variable X	24
7	Diagrammatic representation of the Bethe-Salpeter amplitude $\Gamma_{ij}(q_+, q_-; \lambda)$, where $P = q_+ - q_-$	30
8	Plots of the QCD propagator dressing functions obtained under various combinations of radial and angular grid spacing. The scalar functions $A(p^2)$ and $B(p^2)$ are part of the quark propagator as defined in §3.4.1, while $G(p^2)$ and $Z(p^2)$ are defined in §3.4.2.2 as two ways of parametrizing the gluon propagator. Solutions were obtained with $g^2 = 1$ and the set of renormalization parameters shown in Table 1.	39
9	Schwinger-Dyson Master Equation for ϕ^4 theory.	44
10	Schwinger-Dyson equation of motion for the phion propagator in ϕ^4 theory.	44
11	Perturbative vertex for ϕ^4 theory.	44

12	Plot of the pion propagator $F(p^2)$ as obtained from the nonperturbative equation of motion. The propagator was renormalized using the toy model convention with $F(0) = 1$ and $F(10,000) = \frac{1}{10,000}$.	47
13	Photon Schwinger-Dyson Master Equation	49
14	Electron Schwinger-Dyson Master Equation	49
15	Perturbative vertex for QED	50
16	Electron Gap Equation	50
17	Photon Gap Equation	52
18	Electron-Photon Vertex Equation.	55
19	Plot of the electron propagator dressing functions A and B and the photon propagator dressing functions G and Z under a variation in momentum grid resolution. Solutions were obtained with $g^2 = 1$ and the set of toy model renormalization parameters shown in Table 2.	59
20	Quark Schwinger-Dyson Master Equation	61
21	Ghost Schwinger-Dyson Master Equation	62
22	Gluon Schwinger-Dyson Master Equation	62
23	Quark Gap Equation	63
24	Ghost Gap Equation	65
25	Gluon Gap Equation	67
26	Quark-Gluon Vertex Equation	73
27	Ghost-Gluon Vertex Equation	75
28	3-Gluon Vertex Equation	76
29	4-Gluon Vertex Equation	79
30	Comparison of solutions to the Swimming with Quarks ^[58] model obtained through the integral form (3.180) and the differential form (3.184). Solutions were obtained with $g^2 = 50$ and toy model renormalization parameter (or boundary condition) $B(0) = 5$.	86

31	Comparison of solutions to the Swimming with Quarks ^[58] model which have: (a) Identical (toy model) boundary conditions of $B(0) = .3$ but coupling values of $\alpha \equiv \frac{g^2}{4\pi} = 3$ (red) and $\alpha = 10$ (purple), and (b) Identical coupling $\alpha = 3$ but different (toy model) boundary conditions $B(0) = .3$ (blue) and $B(0) = .6$ (green).	87
32	Plot of the Lattice Gluon Propagator as provided by Bogolubsky <i>et al.</i> ^[15] . . .	88
33	Demonstration of dynamical chiral symmetry breaking using the (a) Maris Tandy and (b) Aguilar-Papavassiliou gluon propagator models. Note that XSB solutions do not allow for renormalization of the equation for $B(p^2)$, but the renormalization parameter $A(9 \text{ GeV}^2) = 1$ was used, where the units of GeV arise from the scales introduced by the lattice $G(p^2)$	90
34	Plots of the quark propagator dressing functions A and B using the $n = 2$ CBC vertex and a variety of couplings and perturbative masses, obtained using the entire gluon model. The renormalization parameters $A(9 \text{ GeV}^2) = 1$ and (for massive quark cases) $B(9 \text{ GeV}^2) = .65 \text{ GeV}$ were used, and again the entire model fit to the lattice $G(p^2)$ implies units of GeV.	91
35	Plots using the entire gluon model of the quark propagator dressing functions A and $M = \frac{B}{A}$ with perturbative and $n = 0$ CBC vertices in comparison to the quenched massive quark lattice data of Bowman <i>et al.</i> ^[16] . Renormalization parameters $A(9 \text{ GeV}^2) = 1$ and $B(9 \text{ GeV}^2) = .033 \text{ GeV}$ were used.	92
36	Results for the gluon propagator functions G and Z from Mandelstam's equa- tion under two different approaches to renormalization. The solutions were obtained with $g^2 = 1$ and renormalization parameters were $G(0 \text{ GeV}^2) =$ 10 GeV^{-2} and $G(.01 \text{ GeV}^2) = \frac{1}{.01} \text{ GeV}^2$	93

37	Results of the von Smekal, Hauck, and Alkofer propagator equations for the Yang-Mills system under two different approaches to renormalization of the gluon equation. Solutions were obtained with $g^2 = .11$ and renormalization parameters $G(0 \text{ GeV}^2) = 10 \text{ GeV}^{-2}$, $G(.01 \text{ GeV}^2) = \frac{1}{.01} \text{ GeV}^2$, and $h(16 \text{ GeV}^2) = 1.24$	96
38	Plots of the solutions to the fully coupled system of QCD propagator dressing functions under two sets of renormalization parameters and a universal coupling value. The renormalization parameters for quarks, ghosts, and the IR point for gluons were $A(.25 \text{ GeV}^2) = 1.39$, $B(.25 \text{ GeV}^2) = .43$, $h(1 \text{ GeV}^2) = 1.9$, and $G(0 \text{ GeV}^2) = 10$ for all curves, while the second gluon renormalization point was $G(.25 \text{ GeV}^2) = 8 \text{ GeV}^{-2}$ with $g^2 = .36$ for the blue curves and $G(21.5 \text{ GeV}^2) = .0665$ with $g^2 = .83$ for the purple curves.	105
39	Plot of the relative contributions of the diagrams from (3.123) (Figure 25) to the gluon propagator's vacuum polarization, under two different sets of renormalization parameters. The renormalization parameters for quarks, ghosts, and the IR point for gluons were $A(.25 \text{ GeV}^2) = 1$, $B(.25 \text{ GeV}^2) = .033$, $h(1 \text{ GeV}^2) = 1.9$, and $G(0 \text{ GeV}^2) = 10$, while the second gluon renormalization point was $G(.25 \text{ GeV}^2) = 8 \text{ GeV}^{-2}$ with $g^2 = .36$; and (b) $G(21.5 \text{ GeV}^2) = .0665$ with $g^2 = .83$	106
40	Comparison of the quark propagator dressing functions A and $M \equiv \frac{B}{A}$ to the lattice data of Bowman <i>et al.</i> ^[16] Solutions were obtained with differentiated coupling values and variety of vertex models. Renormalization parameters were $A(.25 \text{ GeV}^2) = 1$, $B(.25 \text{ GeV}^2) = .033$, $h(16 \text{ GeV}^2) = 1.24$, $G(0 \text{ GeV}^2) = 10$, and $G(.25 \text{ GeV}^2) = 8 \text{ GeV}^{-2}$, while the couplings were $g_{AAA}^2 = .2$ and $g_{cAc}^2 = 1.57$, with $g_{\psi A\psi}^2 = 5.29$ for the bare vertex, $g_{\psi A\psi}^2 = 12.08$ for the $n = 0$ CBC vertex, $g_{\psi A\psi}^2 = 7.2$ for the $n = 1$ CBC vertex, and $g_{\psi A\psi}^2 = 3.85$ for the $n = 2$ CBC vertex.	107

41	Comparison of the ghost and gluon propagator dressing functions h and Z to the lattice data of Bogolubsky <i>et al.</i> ^[15] The solutions were obtained using differentiated coupling values and two sets of renormalization parameters in the gluon equation. Renormalization parameters were $A(.25 \text{ GeV}^2) = 1$, $B(.25 \text{ GeV}^2) = .033 \text{ GeV}$, $h(16 \text{ GeV}^2) = 1.24$, and $G(0 \text{ GeV}^2) = 10 \text{ GeV}^{-2}$, with $G(.25 \text{ GeV}^2) = 8 \text{ GeV}^{-2}$ with couplings $g_{AAA}^2 = .2$, $g_{cAc}^2 = 1.6$, and $g_{\psi A\psi}^2 = 6.5$ for the blue curves, and $G(21.5 \text{ GeV}^2) = .0665 \text{ GeV}^{-2}$ with couplings $g_{AAA}^2 = .54$, $g_{cAc}^2 = 1.97$, and $g_{\psi A\psi}^2 = 8.4$ for the purple curves	108
42	Plot of the real and imaginary parts of $Z(s)$ as obtained through direct continuation.	110
43	Plot of the magnitude and phase of the quark propagator function $\sigma_S(s)$ on the complex plane, as obtained using the entire gluon model and a Cauchy-Riemann algorithm.	113
44	Comparison of the eigenvalue curves for the 0^{-+} glueball, calculated using both the Point Basis (lines) and Chebyshev Basis (points) methods, obtained with $g^2 = 1$ and the entire gluon model.	122
45	Functional expression for the 2-gluon glueball Bethe-Salpeter amplitude . . .	123
46	Functional expression for the ghost-antighost mixing contribution to the glueball Bethe-Salpeter amplitude	123
47	Functional expression for the quark-antiquark mixing contribution to the glueball Bethe-Salpeter amplitude	124
48	Equation for the gluon Bethe-Salpeter amplitude which was used in the present computation.	124
49	Equation for the ghost Bethe-Salpeter amplitude which was used in the present computation.	124
50	Equation for the quark Bethe-Salpeter amplitude which was initially attempted for the extension to glueball-meson mixing of §4.4.	125

51	Extended equation for the gluon Bethe-Salpeter amplitude which was initially attempted for the extension to glueball-meson mixing of §4.4.	125
52	Bethe-Salpeter terms involving the gluon-ghost mixing kernel.	130
53	Comparison of resonance eigenvalues to the lattice results for glueball masses of Morningstar <i>et al.</i> ^[52] . Solid lines represent 0^{++} eigenvalues, dashed lines are 0^{-+} . All solutions were obtained with the entire gluon model and $g^2 = .1681$	136

Acknowledgements

I am grateful to everyone who made it possible for me to take part in the continual progress of Quantum Field Theory research.

I would like to thank Reinhard Alkofer, Hans Bethe, Martina Blank, Jacques Bloch, Freeman Dyson, Gernot Eichmann, Christian Fischer, Andreas Hauck, Markus Huber, Francis Low, Murray Gell-Mann, Stanley Mandelstam, Pieter Maris, Noboru Nakanishi, Michael Pennington, Craig Roberts, E.E. Salpeter, Julian Schwinger, Peter Tandy, Lorenz von Smekal, Richard Williams, David Wilson, and the many other physicists whose work has informed my studies of nonperturbative and bound state techniques in quantum field theory.

I am thankful for my wife Melanie Good Meyers and my children Sarah Good-Lang, Ashley Good-Lang, and Rigel Meyers for their persistent encouragement, patience and support. I would also like to thank my parents, Bill and Anne Meyers, for nurturing my curiosity and interest in science and mathematics.

I would like to thank the many former Professors who have taken great interest in the progress and development of their students, including Steven Dytman for his mentorship and guidance during my undergraduate physics education and research, and Ayres Freitas, Vladimir Savinov, Andrew Zentner, and Colin Morningstar for their continued advising and participation in my Dissertation Committee.

Finally and most of all, I would like to thank Eric Swanson for his mentorship and support through my graduate research career. Eric has been a teacher, advisor, and friend while guiding my efforts in theoretical physics.

1.0 INTRODUCTION

The study of Quantum Field Theory has been invaluable to modern physics, where the behavior of the smallest known constituents of matter and energy are described by a combination of mathematics and physical principles developed through the contributions of many physicists. The known symmetries of nature have been incorporated into a set of quantum field theories known as the Standard Model, which describe nearly all phenomena observed in over a century of particle physics experiments. The Standard Model includes the most fundamental particles ever observed or shown to exist in predictive theories, and successfully describes electromagnetism and both the strong and weak nuclear forces. These theories are based on gauge symmetry, which codifies the invariance of the fundamental degrees of freedom under transformations by the set of operators which represent the generators of that particular gauge group. The typical structure of these symmetries involves the invariance of a (fermion) matter particle under this transformation, with a “force-carrier” (gauge particle) that couples to the matter field and ensures the invariance of the complete theory under the transformation.

The motivation for my research efforts has been to apply nonperturbative methods to calculate various dynamical quantities of quantum field theory. The particular focus has been on obtaining solutions for the dressed propagators for a variety of field theories and models, as well as the spectra of composite objects composed of the fundamental particles whose behavior is described by those theories. In addition, the particular nonperturbative formalism I employ provides opportunities for insight into the analytic structure of quantum field theory and the general patterns and behaviors which are common to all of the seemingly

disparate quantum theories of modern interest. Many aspects of modern technology and most of the fundamental physical laws which we have identified in nature are described by the behavior of objects in the quantum realm, and so this nonperturbative formalism can be used to develop powerful intuition and calculational tools.

The main focus of the research presented here is the theory which describes the strong nuclear force known as Quantum Chromodynamics (QCD). This theory of the strong interaction is a part of the Standard Model, but unlike the other components it is hidden from our ordinary low-temperature, low-energy experiences. In the cases of electromagnetism or radioactive decay, there are consequences of the fundamental interactions which produce physical phenomena which can be more easily observed, and thus provide an easier means of accessing and investigating the laws behind these phenomena. The more abstract link between the strong interaction, nuclear and atomic structure, and the chemical elements contributed to the fact that it was the last of the four fundamental forces of nature which it has become possible to study and understand to the extent which we do today.

QCD contains fundamental matter particles called “quarks” and gauge particles called “gluons” (along with, in certain choices of gauge, the Faddeev-Popov “ghosts”), and is built upon the concept of the color charge first conjectured by Greenberg and others to describe the quark bound states that had been discovered and seemed at the time to resist systematic categorization. The color charges are described by a basis of 8 traceless 3×3 hermitian matrices, which allow for 3 possible color charges for the quarks and 8 possible color states for the gauge particles.

QCD is described by the Lagrangian (which we shall see again in Chapter 3):

$$\mathcal{L}_{\text{QCD}} = -\frac{1}{2}\text{Tr}_{\text{SU}(3)} [F_{\mu\nu}F^{\mu\nu}] + \bar{\psi}(i\not{D} - m)\psi + \mathcal{L}_{\text{gauge}} + \mathcal{L}_{\text{gh}}, \quad (1.1)$$

where:

$$A_\mu = T^A A_\mu^A \quad (1.2)$$

$$F_{\mu\nu} = D_\mu A_\nu - D_\nu A_\mu, \quad (1.3)$$

$$D_\mu = \partial_\mu + ig_s T^A A_\mu^A. \quad (1.4)$$

The as-yet unspecified terms appearing in the Lagrangian are chosen for a covariant gauge, and are given by:

$$\mathcal{L}_{\text{gauge}} = -\lambda \text{Tr}_{\text{SU}(3)} [(\partial \cdot A)^2], \quad (1.5)$$

$$\mathcal{L}_{\text{gh}} = -\bar{c}_A \left(\delta_{AB} \square + f_{ACB} A_C \cdot \partial \right) c_B. \quad (1.6)$$

This Lagrangian is designed to be invariant under the $\text{SU}_{\text{color}}(3)$ gauge symmetry, but introduction of the gauge fixing term (1.5) and ghost contribution (1.6) complicate this fact. The most general gauge symmetry transformation found to leave this Lagrangian invariant is due to Rouet, Stora, and Tyutin, and is thus known as BRST-invariance^[9,38]. The set of transformations^[69], with a constant Grassmann parameter θ , is given by:

$$A_\mu^A \rightarrow A_\mu^A + \theta D_\mu^{AB} c^B, \quad (1.7)$$

$$\psi \rightarrow \psi - ig\theta T^A c^A \psi, \quad (1.8)$$

$$\bar{c}^A \rightarrow -\lambda\theta(\partial \cdot A^A), \quad (1.9)$$

$$c^A \rightarrow -\frac{g}{2}\theta f^{ABC} c^B c^C. \quad (1.10)$$

In addition to this transformation, an additional “auxiliary field” B^A is introduced which is invariant under the BRST transformation. This field must be included in the set of path integral variables, and introduces additional terms \mathcal{L}_{aux} to (1.1):

$$\mathcal{L}_{\text{aux}} = B^A(\partial \cdot A^A) + \frac{1}{2\lambda} B^A B^A. \quad (1.11)$$

The resulting Lagrangian $\mathcal{L}_{\text{QCD}} + \mathcal{L}_{\text{aux}}$ is then invariant under the symmetry transformation. This modified Lagrangian can then be used to obtain a set of identities^[65,66] which represent the gauge symmetry of QCD and are called the Slavnov-Taylor identities (STIs). These identities are the QCD equivalent of the Ward-Takahashi identities which represent the gauge symmetry in QED. Both sets of identities provide relationships between various correlation functions in their respective theories, and, for example, can be used to partially constrain the structure of dressed interaction vertices in terms of the dressing functions of propagators and other interactions. We will discuss in Chapter 3 how these identities have been used^[2,7,8,28,30,57,67] in this capacity to design vertex models for nonperturbative studies using the Schwinger-Dyson equations.

QCD contains a number of unusual properties that distinguish it from previous theories and those that describe the electroweak (electromagnetism + weak nuclear) interactions. These properties are among the reasons that perturbation theory cannot be used to describe the dynamical behavior within the realm of interest for the various bound states which have been observed.

One of these properties is “asymptotic freedom”, which is a means of describing the fact that the running (or dressed) coupling of interactions in QCD becomes weaker in the ultraviolet (UV, or high-momentum) regime, and so it is there that the perturbative power expansion in coupling can most successfully describe the theory. At these momenta, the dynamical quantities of QCD (which are correlation functions between the particles’ field operators) approach the non-interacting limit of the quantum field theory (thus the name, in the limit in which momentum becomes infinite). The particle interactions and “dressing” of dynamical quantities become more significant as the momentum scale is reduced, such that before one reaches the scale of bound states ($O(1 \text{ GeV})$ and below) it is practically infeasible to rely on perturbation theory. The cutoff at which perturbation theory ceases to be dependable is frequently written as Λ_{QCD} , which implies that the perturbative series in coupling does not yield a good approximation to the quantum corrections.

Another characteristic of QCD is complementary to asymptotic freedom, and is known as

“confinement”. In conducting a Fourier transform between the four-momentum and space-time variables, the strongest correlations hold for combinations which produce little variation in the exponential factor $e^{ip \cdot x}$. As such, large values of momentum have their greatest influence over short distances, and for QCD this translates to $O(1 \text{ fm})$, which is about the size of a typical nucleon. When a high-momentum state attempts to propagate beyond this distance, it tends to decay through a process known as “fragmentation” (or “hadronization”) to yield a color-neutral combination of final state particles. Confinement thus describes the process by which an asymptotic (observable) state of QCD cannot possess a nonzero color charge. The name confinement is used because any dynamics or interactions of a color-charged entity are confined to a tiny region of spacetime volume. A proper treatment of the dynamical quantities in QCD should be consistent with this restriction, and at the very least the correlation functions should not possess any poles which correspond to the propagation of a color-charged state. Since the perturbative gluon propagator behaves as $\frac{1}{p^2}$, the IR limit of the dressed propagator is of particular importance. The perturbative form would imply a massless asymptotic state of the gluon field, which would certainly violate confinement. The absence of an IR pole in this propagator is obtained in “decoupling” solutions for the gluon propagator, which approach a finite, nonzero value as $p^2 \rightarrow 0$. Cases where the gluon propagator vanishes in the IR are referred to as “scaling” solutions due to their lack of obvious dependence on rescaling of external momenta.

QCD also possesses a peculiar unsolved property known as the “strong-CP problem”. This issue arises from additional terms that could be added to the Lagrangian and do not respect the otherwise CP-symmetric formulation of QCD. The particular term can be written as:

$$\mathcal{L}_{\mathcal{CP}} = -\frac{\theta}{64\pi^2} \epsilon^{\alpha\beta\gamma\delta} F_{\alpha\beta}^A F_{\gamma\delta}^A. \quad (1.12)$$

Expressions of this form (though without color indices) were obtained when investigating the axial anomaly^[1,10] of the Electroweak theory. This anomaly was shown to arise from quantum corrections to the classically conserved axial-vector current. In QCD, the term

(1.12) presents its own puzzle, as experimental evidence^[69] such as the neutron electric dipole moment places severe restrictions on the parameter θ to be many orders of magnitude smaller than the other constants in the theory, which is inconsistent with expectations of naturalness. Proposed solutions include the possibility of at least one flavor of massless quark, or introduction of a dynamical variable that leads to hypothetical particles known as axions and allows for a symmetry transformation to suppress this additional term.

These properties of QCD are difficult to describe successfully in perturbation theory. The perturbative propagator for the gluon possesses a pole at zero four-momentum, implying that it should be a massless particle like the photon. The infrared (IR) is a region where perturbation theory cannot be trusted at low (or even accessible) orders of the coupling constant, and so elimination of this built-in mass pole (to prevent the possibility of a propagation as an asymptotic state) requires other “nonperturbative” methods to describe those dynamics. There are multiple nonperturbative tools available that have been applied to QCD. The most successful of these are lattice QCD, renormalization group (RG) methods, and the functional Schwinger-Dyson equations.

The most commonly known method is lattice gauge theory (or when applied to this theory, lattice QCD), which discretizes the spacetime dependence of this quantum field theory and simulates various states and interactions. Lattice QCD^[71] has to date been the most successful means of describing the nonperturbative physics of QCD, but possesses certain weaknesses. In discretizing the variables to implementing Monte Carlo methods upon a multidimensional grid, the computational requirements of lattice QCD become rather intense. The algorithmic simplicity of lattice QCD means that it is fairly easy to implement when the resources are available, and in fact it has become the preferred means of measuring the computational power of the world’s largest supercomputers. The spacetime discretization likewise yields a discretized momentum dependence, and extrapolation to the continuum limit is difficult unless one uses progressively larger grids, which can quickly outstrip the available resources. Despite these troubles, lattice QCD has contributed a vast amount of information to the knowledge of nonperturbative QCD, and remains at the forefront of

progress in advancing studies.

Studies of the renormalization group have also been able to provide nonperturbative information about QCD. The renormalization group allows one to evolve the dynamical quantities of a quantum field theory from the regions well approximated by perturbation theory into nonperturbative regimes. For QCD, this means that one can start with perturbative expressions in the UV, and extrapolate down to regions of interest close to Λ_{QCD} . This approach is used for example in “Effective Field Theories”, which use an expansion in non-renormalizable interactions with the intent of cutting off the momentum dependence at some scale and using the RG expressions in the UV.

The renormalization group can be described by a relation known as the Callan-Symanzik equation, which can be expressed (for a single, self-interacting, massless field theory) as^[61]:

$$\left[\mu \frac{\partial}{\partial \mu} + \beta(\lambda) \frac{\partial}{\partial \lambda} + n\gamma(\lambda) \right] G^{(n)}(\{x_i\}; \mu, \lambda) = 0, \quad (1.13)$$

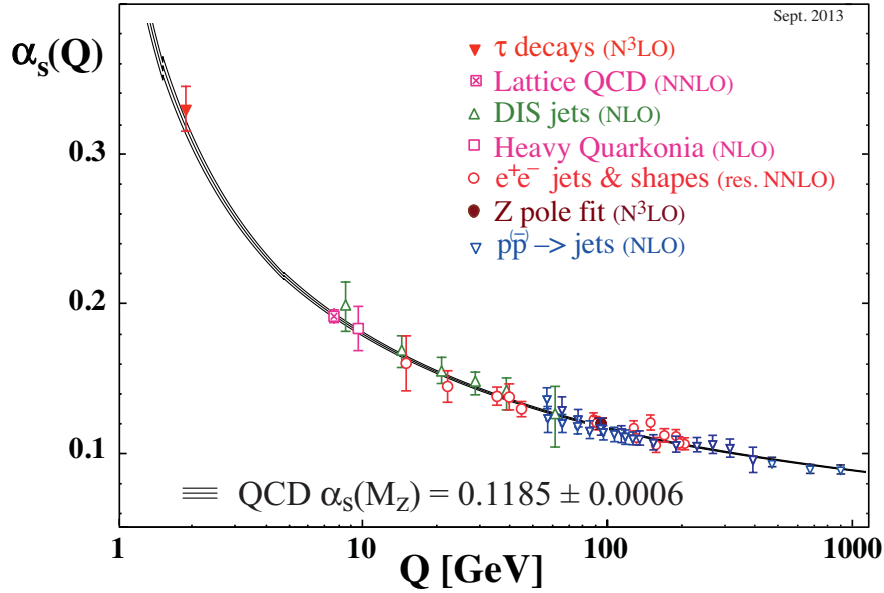


Figure 1: Plot of the Running Coupling of QCD as obtained from lattice gauge theory and multiple experimental measurements as compiled by the Particle Data Group^[56]

where G is the renormalized Green function described by the n external particle lines, λ the renormalized coupling, and μ the renormalization scale (suppose for example we are discussing ϕ^4 theory). This expression introduces quantities known as the beta-function $\beta(\mu^2) \equiv \mu \frac{\partial \lambda}{\partial \mu}$ and the anomalous dimension $\gamma \equiv \frac{\mu}{Z_\phi} \frac{\partial Z_\phi}{\partial \mu}$ (with Z_ϕ the field renormalization constant) which characterize the dependence of renormalized quantities on the momentum scale used in renormalization. The beta-function describes the rate of change in the dressed coupling at various scales, and thus determines the region of renormalization scales (and momentum regimes) in which the quantum field theory is well described by perturbation theory. For theories like QED, this provided confirmation that the low-momentum dependence exhibited perturbative behavior, and allowed for the accuracy of early applications of quantum field theory to the fine structure of the hydrogen atom. As described above and shown in Figure 1, the asymptotic freedom of QCD implies that the dressed coupling^[56] becomes perturbative in the UV instead of the IR, and it is the theory’s beta-function that provides this information. The anomalous dimension γ provides information regarding additional logarithmic contributions to the behavior of correlation functions on their approach to the perturbative limit, which for QCD lies in the UV. This behavior can be used as verification across the nonperturbative methods, as consistency has been demonstrated between lattice, RG, and Schwinger-Dyson approaches. A final contribution from RG theory regards the existence of a “fixed-point” in the IR limit, where the asymptotic behavior of the gauge particles is found to be constrained and is useful in the treatment of running coupling computations^[14,30,67]. The fixed-point represents a constraint on the gluon and ghost propagators at vanishing momenta, and features heavily in IR analyses of QCD.

The last of these major nonperturbative methods are the Schwinger-Dyson equations of motion. The original form was obtained by Freeman Dyson^[23], who found a way to sum classes of diagrams to all orders in perturbation theory. These equations represented the full contribution of all interactions and dressings to the dynamical quantities, but required extensive intuition and insight into the perturbative dynamics. The same set of equations were later obtained by Julian Schwinger^[62], who employed the functional approach to quantum

field theory and thus generalized the patterns and tools of Dyson’s approach. The treatment we present here is based on the generating functionals obtained from the path integral formalism, which provide a direct means of deriving the equations of motion for an arbitrary quantum field theory. Using this formalism, one can obtain the nonperturbative equations of motion for any field theory, as well as the proper means of introducing renormalized variables and constants. The well-noted weakness of these equations is that they very clearly display a dynamical dependence on progressively higher sets of correlation functions, and have thus come to be called the “infinite-tower” of Schwinger-Dyson equations. These equations compose an infinite-dimensional set of relations, and furthermore tend to be expressed (in physically-relevant spacetimes) as nonlinear integral equations which implicitly define the nonperturbative quantities. Since the calculation of an infinite set of equations is unrealistic, one must typically introduce a form of truncation or modeling to obtain a computationally feasible set of equations. Despite these truncations, the content of the Schwinger-Dyson equations includes information to all orders in perturbation theory, and so this reduction is not directly comparable to an order-by-order calculation in that method. It is possible (and in fact quite easy) to produce nonperturbative dynamical features in the correlation functions from even very simple or naive truncations, as we shall demonstrate.

The relative strengths and weaknesses of lattice gauge theory and the Schwinger-Dyson equations, along with their ability to complement each other, provide a compelling reason to devote significant efforts to the continued progress and understanding of how these methods relate to each other and to quantum field theory in general. The Schwinger-Dyson equations comprise an infinite set of coupled equations and so the relation to interactions involving many particles must be modeled or truncated to allow for practical calculation. Conversely, lattice gauge theory is able to include the complete theory with every possible physical contribution. While this eliminates the need for models or approximations, it also makes it difficult to access the details of how different processes and theoretical ingredients can affect each other or contribute to the solutions as a whole. The truncation of Schwinger-Dyson equations amounts to making some approximation to the complete theory, but also allows

for a clear and controlled analysis of how different approximations compare and how significantly the various quantities and equations can influence each other. The inclusion of more sophisticated or complex interactions, whether obtained through dynamical calculations or modeling, can be relatively difficult due to the rapid increase in complexity as more particles and tensors become involved, whereas the many particle contributions are automatically included and described very well by the lattice. The approximations made in lattice gauge theory relate mostly to the resolution or granularity of the discretized spacetime and the restriction to a finite volume, both of which can affect the method's ability to describe phenomena which require correlation across wide ranges of momenta and particularly those which have significant dependence on either very large or very small scales. The analytic representation of Schwinger-Dyson equations allows for careful development and study of asymptotic forms of the equations, and so extrapolation to extreme values of momenta are much more accessible than on the lattice. This allows the treatment of theories which can exhibit chiral symmetry breaking, and can be applied to both the broken and unbroken regions of the theory's phase transition. Other theoretical applications familiar from perturbation theory, such as scattering or investigation of condensed matter states, are also relatively difficult to implement on the lattice, but the expression of Schwinger-Dyson equations as relationships among dressed correlation functions allows many such applications to be easily generalized and studied in nonperturbative realms. It is clear from these and many other reasons that there is compelling motivation to continue to pursue both methods of nonperturbative research and to look for further opportunities for the calculations and insights from each one to contribute to the other.

Beyond the nonperturbative correlation functions of QCD, there is also interest in the bound states of the theory. The Schwinger-Dyson equations will be applied to correlation functions of the fundamental degrees of freedom, but we also need a theoretical formalism to discuss composite objects. Treatment of these states is done by means of the Bethe-Salpeter equation. This equation was first published^[55] without derivation, but was soon derived by Hans Bethe and E.E. Salpeter^[60], and was rapidly confirmed and reproduced by many

others^[33,42,45,63]. This equation describes a quantity called the Bethe-Salpeter amplitude, which is a dynamical quantity that represents the coupling of the fundamental (constituent) particles into the bound state current. The Bethe-Salpeter equation makes use of an interaction kernel between the constituent particles to describe the binding, and takes the form of a resonance condition for the existence of a bound state. Once a resonance is found and the amplitude obtained and normalized^[21,43,53], it can be used to compute other dynamical properties of the bound state such as form factors and decay constants. The ability of these calculations to describe fermion fields and their bindings through electromagnetic and nuclear interactions has been demonstrated and successfully applied to many experimentally observed states, and has thus grown into an important and highly active field of particle physics research. In the current discussions, we are particularly interested in how these techniques may be applied to the binding and interactions of other potential states in nature, particularly the possibility of QCD’s gluons producing experimentally observable composite objects.

In Chapter 2: [Formalism](#), the necessary framework of path integrals and generating functionals will be presented in a pedagogical manner. The Schwinger-Dyson equations will then be extracted from the functional approach by considering symmetries of the path integral. The general properties of Schwinger-Dyson equations will be presented and discussed, including a diagrammatic representation, the role of truncation in the set of infinitely-coupled equations, and the introduction of appropriate renormalization factors into the functional calculus. Finally, the appearance of bound states in quantum field theory will be discussed through a derivation and examination of the Bethe-Salpeter equation.

In Chapter 3: [Gap Equations](#), a numerical approach to solving the Schwinger-Dyson equations for the dressed propagators of an arbitrary quantum field theory will be discussed. The general structure of these “gap equations” for the one-particle-irreducible (1PI) two-point correlation functions will be obtained from the second derivatives of the effective action using the Schwinger-Dyson formalism. A reliable and robust method for obtaining solutions to these equations will be discussed, as will the general approach to performing

renormalization in nonperturbative quantum field theory. These techniques will be demonstrated through examples in ϕ^4 theory, QED, and QCD. The QCD examples will include a number of truncated examples that have been explored in the standard literature of the field, as well as the first calculation within the fully-coupled system of gap equations under vertex-level truncations and the full suite of nonperturbative diagrams. The results of these QCD examples will be compared and discussed in the context of lattice QCD.

In Chapter 4: [Bound States](#), application of the Bethe-Salpeter equation to the bound states of QCD will be presented. Given the Euclidean-space formalism which is traditionally employed in the investigation of gap equations, the necessity of analytic continuation on the complex 4-momentum plane will be presented and discussed. A discretized form of the Bethe-Salpeter equation will be presented alongside an expansion in well-known analytic functions, and the merits and weaknesses of both approaches will be discussed. The methods of solving Bethe-Salpeter equations will be presented with the investigation of gluon bound states (glueballs) in one of the truncated models of Chapter 3. The extension and interpretation of this computation to include valence states including quarks and/or gluons will be discussed.

2.0 FORMALISM

The framework of functional calculus, based upon the path integral approach to quantum field theory (QFT), forms the (predominant) basis of investigation presented in this work. The formalism of QFT will be presented and developed in terms of two sample cases, with a bosonic and fermionic fields. The distinction of these two cases in the functional calculus are more fundamental than the variation in quantum numbers, as these other properties will be shown to be automatically included if properly expressed in the Lagrangian. Fields of a bosonic nature are represented by c-number functional variables, which are defined by their behavior upon commuting with other fields. Fields of a fermionic nature are represented by Grassmann functional variables, which are defined by their behavior under anti-commutation with each other. We will show that the definition of a QFT through its Lagrangian will produce the appropriate functional calculus to describe the nonperturbative structure of the theory.

2.1 PATH INTEGRALS

The functional representation of quantum field theory is built upon the path integral formalism as introduced by Feynman^[27]. The transition element from a field configuration B to a field configuration A is given by a sum over all possible intermediate states weighted by a factor involving the Lagrangian density (hereafter referred to as the Lagrangian) that defines the theory. The standard method of incorporating these boundary conditions involves

identifying a path that matches the endpoints A and B , then summing over all functional variations that keep these endpoints fixed. Working in natural units (where $\hbar = c = 1$), this is expressed as:

$$\langle A|B\rangle = \int_{\text{Field Configuration } B}^{\text{Field Configuration } A} \mathcal{D}(\bar{\psi}, \psi, A) e^{iS(\bar{\psi}, \psi, A)}. \quad (2.1)$$

By allowing the field configuration B to become the limit of the quantum vacuum at some infinite time in the past, and A to become a similar limit an infinite time in the future, we obtain the vacuum to vacuum transition element, $\langle \Omega|\Omega\rangle$:

$$\langle \Omega|\Omega\rangle = \int \mathcal{D}(\bar{\psi}, \psi, A) e^{iS(\bar{\psi}, \psi, A)}. \quad (2.2)$$

This particular function has a number of important properties. First, this determines the proper normalization factor for any expectation value we seek to calculate. Second, this function reveals the weighted averaging procedure which is necessary to compute statistical averages in the QFT. Finally, modification of this path integral will define the generating functional upon which the functional approach to QFT is based.

The vacuum expectation value (VEV) for a time-ordered set of field operators can be obtained by performing the functional path integral with the set of field variables, corresponding to each operator, included in the integrand^[6,68]. Note that we use the normalization factor in this proper definition of the expectation value, and so this can be written (using the time-ordering operator \mathcal{T}) as:

$$\begin{aligned} & \langle \Omega | \mathcal{T}(\psi_1 \dots \psi_{n_1} \bar{\psi}_1 \dots \bar{\psi}_{n_2} A_1 \dots A_p) | \Omega \rangle \\ &= \frac{1}{\langle \Omega|\Omega\rangle} \int \mathcal{D}(\bar{\psi}, \psi, A) (\psi_1 \dots \psi_{n_1} \bar{\psi}_1 \dots \bar{\psi}_{n_2} A_1 \dots A_p) e^{iS(\bar{\psi}, \psi, A)}. \end{aligned} \quad (2.3)$$

2.2 GENERATING FUNCTIONALS

The functional approach to quantum field theory is due to Schwinger, and employs the approach of generating functions in the context of the path integral. Since the path integral is expressed in terms of (formally unknown) functions rather than coordinate or momentum variables, the derivatives acting upon the generator are functional in nature, and thus the generator is considered a generating functional.

2.2.1 Definitions

The expression of quantum field theory in terms of functional calculus begins with the definition of the Generating Functional Z . By introducing a source parameter into the integrand of the path integral, one can obtain the (normalized) VEV of any desired combination of field operators through functional differentiation. In order to properly normalize the expectation values, it is necessary to divide by the norm^[6,40,47,68] $\langle \Omega | \Omega \rangle = Z|_{\text{All Sources}=0}$ (note that some sources build this normalization factor into the path integral measure such that $\langle \Omega | \Omega \rangle = 1$). We define Z according to:

$$Z[\bar{\eta}, \eta, J] = \int \mathcal{D}(\bar{\psi}, \psi, A) e^{i[S(\bar{\psi}, \psi, A) + \int d^4x (\bar{\eta}\psi + \bar{\psi}\eta - J \cdot A)]}, \quad (2.4)$$

and express the generic form for a VEV (suppressing all spacetime dependence and tensor indices) with proper normalization as:

$$\langle \Omega | \mathcal{T}(\psi_1 \dots \psi_{n_1} \bar{\psi}_1 \dots \bar{\psi}_{n_2} A_1 \dots A_p) | \Omega \rangle \quad (2.5)$$

$$= \frac{(i)^{p+n_2-n_1}}{Z[0, 0, 0]} \left[\left(\frac{\delta}{\delta \bar{\eta}_1} \dots \frac{\delta}{\delta \bar{\eta}_{n_1}} \right) \left(\frac{\delta}{\delta \eta_1} \dots \frac{\delta}{\delta \eta_{n_2}} \right) \left(\frac{\delta}{\delta J_1} \dots \frac{\delta}{\delta J_p} \right) Z[\bar{\eta}, \eta, J] \right]_{\bar{\eta}=\eta=J=0}.$$

Automatic inclusion of the proper normalization factor, as well as the subtraction of all “disconnected” or “bubble” diagrams can be accomplished by introducing the connected

generating functional W [6,40,68]. The corresponding Feynman diagrams demonstrate that the resulting expectation values consist only of those in which all external fields represented by the functional derivatives are attached to the same set of internal particle lines. This generating functional is defined as:

$$W[\bar{\eta}, \eta, J] = -i \ln(Z[\bar{\eta}, \eta, J]), \quad (2.6)$$

with the connected functions obtained through functional derivatives according to:

$$\begin{aligned} \langle \Omega | \mathcal{T}(\psi_1 \dots \psi_{n_1} \bar{\psi}_1 \dots \bar{\psi}_{n_2} A_1 \dots A_p) | \Omega \rangle_{\text{conn}} \\ = (i)^{p+n_2-n_1+1} \left[\left(\frac{\delta}{\delta \bar{\eta}_1} \dots \frac{\delta}{\delta \bar{\eta}_{n_1}} \right) \left(\frac{\delta}{\delta \eta_1} \dots \frac{\delta}{\delta \eta_{n_2}} \right) \left(\frac{\delta}{\delta J_1} \dots \frac{\delta}{\delta J_p} \right) W[\bar{\eta}, \eta, J] \right]_{\bar{\eta}=\eta=J=0}. \end{aligned} \quad (2.7)$$

2.2.2 Legendre Transform

The removal of propagators (dressed two-point correlation functions) on the external field lines is accomplished via a Legendre Transform, in which dependence upon the functional source variables is substituted in terms of the “Classical Fields”, a set of functional variables which correspond to the (normalized) VEV of each field operator in the presence of nonzero source variables and serve as conjugate variables to the functional sources. The resulting functional generates “1-Particle Irreducible”(1PI) functions and is called the effective action. The 1PI functions cannot be separated by removal of any internal line, and have all external lines amputated.

The variable substitution is performed by first defining the classical field variables, here represented by $\bar{\psi}_{\text{cl}}$, ψ_{cl} , and A_{cl} for the sample field types. Note that the definition of the classical field $\bar{\psi}_{\text{cl}}$ is actually the opposite sign from the proper VEV, this is done for simplicity in the formalism and diagrammatics to come later. Once each conjugate variable is defined,

the proper forms for the effective action and the source variables as functional derivatives are easily obtained. We define the conjugate pairs:

$$\begin{aligned}\overline{\psi}_{b\text{cl}} &= \frac{\delta W}{\delta \eta_b} & \psi_{a\text{cl}} &= \frac{\delta W}{\delta \overline{\eta}_a} & A_{\mu\text{cl}} &= -\frac{\delta W}{\delta J^\mu}, \\ \eta_b &= \frac{\delta \Gamma}{\delta \overline{\psi}_{b\text{cl}}} & \overline{\eta}_a &= \frac{\delta \Gamma}{\delta \psi_{a\text{cl}}} & J_\mu &= \frac{\delta \Gamma}{\delta A^\mu_{\text{cl}}},\end{aligned}\tag{2.8}$$

and so the effective action is defined by the Legendre Transform:

$$\Gamma [\overline{\psi}_{\text{cl}}, \psi_{\text{cl}}, A_{\text{cl}}] = W [\overline{\eta}, \eta, J] - \int d^4x (\overline{\eta} \psi_{\text{cl}} - \overline{\psi}_{\text{cl}} \eta - J \cdot A_{\text{cl}}).\tag{2.9}$$

As stated above, functional derivatives of the effective action produce the 1PI correlation functions of the quantum field theory. It is important to note two details of these functional derivatives. First, the functional now depends only on the classical fields as defined from the VEVs. Second, fermionic classical field variables correspond to their role in the interaction Lagrangian of perturbation theory, in which ψ ($\overline{\psi}$) is paired with the external lines as created or annihilated by $\overline{\psi}$ (ψ). The 1PI functions are then found to be:

$$\begin{aligned}\langle \Omega | \mathcal{T} (\psi_1 \dots \psi_{n_1} \overline{\psi}_1 \dots \overline{\psi}_{n_2} A_1 \dots A_p) | \Omega \rangle_{\text{1PI}} \\ = i \left[\left(\frac{\delta}{\delta \overline{\eta}_1} \dots \frac{\delta}{\delta \overline{\eta}_{n_1}} \right) \left(\frac{\delta}{\delta \eta_1} \dots \frac{\delta}{\delta \eta_{n_2}} \right) \left(\frac{\delta}{\delta J_1} \dots \frac{\delta}{\delta J_p} \right) \Gamma [\overline{\psi}_{\text{cl}}, \psi_{\text{cl}}, A_{\text{cl}}] \right]_{\overline{\eta}=\eta=J=0}.\end{aligned}\tag{2.10}$$

In order to properly develop the Schwinger-Dyson equations, we must also take note of a class of identities relating the connected and 1PI expectation values. From the definition of the connected generating functional W , we examine the two-point functions of the QFT in the presence of nonzero sources. The propagators are defined from W as:

$$\frac{\delta^2 W}{\delta J_2 \delta J_1} = i \langle \Omega | \mathcal{T} (A_2 A_1) | \Omega \rangle_{\text{conn}} \equiv i \Delta'_{A_2 A_1},\tag{2.11}$$

$$\frac{\delta^2 W}{\delta \bar{\eta}_2 \delta \eta_1} = -i \langle \Omega | \mathcal{T} (\psi_2 \bar{\psi}_1) | \Omega \rangle_{\text{conn}} \equiv -i \Delta'_{\psi_2 \bar{\psi}_1}. \quad (2.12)$$

Since we have expressed the source variables in terms of the effective action and classical fields, we can identify that these source-dependent propagators are actually the inverted 1PI two-point functions. This identification will become useful in the development of the Schwinger-Dyson framework and in obtaining the Gap Equations for the fully dressed propagators from those equations of motion. The precise inverse relationship can be expressed as:

$$\frac{\delta^2 \Gamma}{\delta A^\mu_{\text{cl}}(y) \delta A^\nu_{\text{cl}}(x)} = \left(\frac{\delta^2 W}{\delta J_\mu(y) \delta J_\nu(x)} \right)^{-1} = i \left(\Delta'_{A^\mu(y) A^\nu(x)} \right)^{-1}, \quad (2.13)$$

$$\frac{\delta^2 \Gamma}{\delta \psi_{a\text{cl}}(y) \delta \bar{\psi}_{b\text{cl}}(x)} = \left(\frac{\delta^2 W}{\delta \bar{\eta}_a(y) \delta \eta_b(x)} \right)^{-1} = -i \left(\Delta'_{\psi_a(y) \bar{\psi}_b(x)} \right)^{-1}. \quad (2.14)$$

The identities shown correspond to field combinations which yield a physical result in the source-free limit, but we will later employ a diagrammatic representation in which these relations will be properly incorporated alongside functions which imply an unphysical mixing of fields. While these mixing terms do not result in physically relevant correlation functions for the QFT, they are in fact essential to obtaining all necessary diagrams in the Schwinger-Dyson equations. Relations of the type (2.13) and (2.14) can also be considered in the mixed-field cases, and consistency with the full set of such identities (physical and unphysical) has been incorporated into our diagrammatic rules in a way that requires no special treatment.

2.3 SCHWINGER-DYSON EQUATIONS

2.3.1 Derivation

Derivation of the Schwinger-Dyson equations begins by noting that the expectation values produced by the generating functionals would remain unchanged by an arbitrary shift in any

of the field variables in the Lagrangian. Consider the shift:

$$X(x) \rightarrow X'(x) \equiv X(x) + \delta X(x), \quad (2.15)$$

where X denotes any of the theory's fields:

$$X \in [\bar{\psi}, \psi, A]. \quad (2.16)$$

We make a variable substitution within the path integral for X' , which leaves the path integral measure unchanged. What we recover is the identical form for the generating functional as defined in (2.4). If we allow δX to become an infinitesimal shift in the fields, we learn that the functional variation of Z with respect to any of the functional variables in the path integral is precisely zero (as we would expect from having integrated over all possible variations in X). Coupled with the invariance of the path integral measure under such a transformation, we obtain:

$$0 = \int \mathcal{D}(\bar{\psi}, \psi, A) \left(\frac{\delta S}{\delta X(x)} + \zeta_X Y_X(x) \right) e^{i[S(\bar{\psi}, \psi, A) + \int d^4x (\bar{\eta}\psi + \bar{\psi}\eta - J \cdot A)]}, \quad (2.17)$$

where we have introduced a factor ζ_X depending on the particular field being considered. The appropriate value for a particular X is given by (2.18).

X	$\bar{\psi}$	ψ	A
ζ_X	1	-1	-1
$Y_X(x)$	η	$\bar{\eta}$	J

(2.18)

Since neither the factor ζ_X nor the source Y_X depend upon the path integral variables, they can be factored outside of the integration. Isolating them on the left hand side and dividing by the path integral Z which appears, we obtain:

$$-\zeta_X Y_X = \frac{1}{Z[\bar{\eta}, \eta, J]} \int \mathcal{D}(\bar{\psi}, \psi, A) \frac{\delta S}{\delta X} [\bar{\psi}, \psi, A] e^{i[S(\bar{\psi}, \psi, A) + \int d^4x (\bar{\eta}\psi + \bar{\psi}\eta - J \cdot A)]}, \quad (2.19)$$

$$\frac{\delta\Gamma}{\delta X_{\text{cl}}} = -\zeta_X \frac{1}{Z[\bar{\eta}, \eta, J]} \int \mathcal{D}(\bar{\psi}, \psi, A) \frac{\delta S}{\delta X} [\bar{\psi}, \psi, A] e^{i[S(\bar{\psi}, \psi, A) + \int d^4x (\bar{\eta}\psi + \bar{\psi}\eta - J \cdot A)]}. \quad (2.20)$$

Noting that $\zeta_X^2 = 1 \forall X$, we can move it onto the right hand side, and also express Y_X as $\frac{\delta\Gamma}{\delta X}$ since it holds for all of our sample fields. From this form as expressed in (2.20), we can substitute any arbitrary term of $\frac{\delta S}{\delta X}$ in terms of the corresponding functional derivatives with respect to each appropriate source. This allows us to factor $\frac{\delta S}{\delta X}$ out of the integral since it no longer contains explicit dependence on the path integral variables. We thus obtain a general form in which $\frac{\delta\Gamma}{\delta X_{\text{cl}}}$ can be obtained in terms of the connected generating functional W :

$$\frac{\delta\Gamma}{\delta X_{\text{cl}}} = -\zeta_X e^{-iW[\bar{\eta}, \eta, J]} \frac{\delta S}{\delta X} \left[\frac{i\delta}{\delta\eta}, -\frac{i\delta}{\delta\bar{\eta}}, \frac{i\delta}{\delta J} \right] e^{iW[\bar{\eta}, \eta, J]}. \quad (2.21)$$

Finally, we note that the functional variables expressed as such can have one of two actions. Either the derivative will act upon another functional derivative in the same term of $\frac{\delta S}{\delta X}$ which lies between itself and the generating functional at the far right, or it will act upon the generating functional to produce one of the classical field variables. Using the chain rule, we can commute the generating functional through to cancel with the factor $\frac{1}{Z} = e^{-iW}$ by including the classical field terms in the arguments of $\frac{\delta S}{\delta X}$. We obtain (2.22) with the understanding that a functional constant of value unity still exists at the far right (expressed as the $\cdot 1$ below), and so any functional derivative acting beyond its own term of $\frac{\delta S}{\delta X}$ yields zero. We thus have a general form for the **Schwinger-Dyson Master Equation**:

$$\frac{\delta\Gamma}{\delta X_{\text{cl}}} = -\zeta_X \frac{\delta S}{\delta X} \left[\frac{i\delta}{\delta\eta} - \bar{\psi}_{\text{cl}}, -\frac{i\delta}{\delta\bar{\eta}} + \psi_{\text{cl}}, \frac{i\delta}{\delta J} + A_{\text{cl}} \right] \cdot 1. \quad (2.22)$$

In order to properly calculate the general functional derivatives such as $\frac{\delta X_{\text{cl}}}{\delta Y_{X'}}$, it is necessary to consider all possible expressions of the form (2.13) – (2.14). These expressions are properly considered by implementing a form such as $\frac{\delta}{\delta Y_X} = \sum_i \frac{\delta X_i}{\delta Y_X} \frac{\delta}{\delta X_i}$. It is possible and in fact much simpler to employ a diagrammatic representation which is sufficiently robust

to incorporate these factors. In the following section regarding the diagrammatic expression of Schwinger-Dyson equations, these factors have been taken into account and properly incorporated into the formalism.

In the various theories we shall consider in Chapter 3: [Gap Equations](#), we will begin with the diagrammatic form of (2.22) as appropriate for each field variable. This will allow us to begin the consideration of each theory starting from the Schwinger-Dyson master equation, and any necessary definitions of propagators (perturbative or dressed) and interaction vertices will be provided. Any difference in tensor indices or quantum numbers from the example of QCD which follows in §2.3.2 should be made clear with those basic definitions.

2.3.2 Diagrammatics

The series expansion of the effective action in terms of all classical field variables is expressed in terms of all possible 1PI diagrams which constitute the QFT. The most convenient and versatile way to formulate these expressions is through a diagrammatic representation, reminiscent of the Feynman diagrams of perturbation theory.

The diagrammatics here will be introduced using the definitions from QCD as an example, but extension to a variety of other theories is simple. We represent the diagrams for the gluons as an example of a bosonic field, the quarks as an example of a fermionic field, and the Faddeev-Popov ghosts to demonstrate a field of that type. These diagrams can be extended to any other QFT by defining lines and propagators for the necessary field variables, including tensor indices and quantum numbers appropriate for the field operators, and defining the perturbative and dressed interactions to represent the physical content.

The necessary ingredient is the expression of the propagators which serve as the internal or “virtual” particle lines. The various propagators of the nonperturbative theory are shown in Figure 2. Each propagator is listed as a general tensor using the symbol Δ with the appropriate field operators as a subscript, and will be later expressed in terms of scalar functions and specific tensors as each theory is considered. The “primed” notation indicates that the propagator is to be understood in the presence of nonzero sources, and is thus active

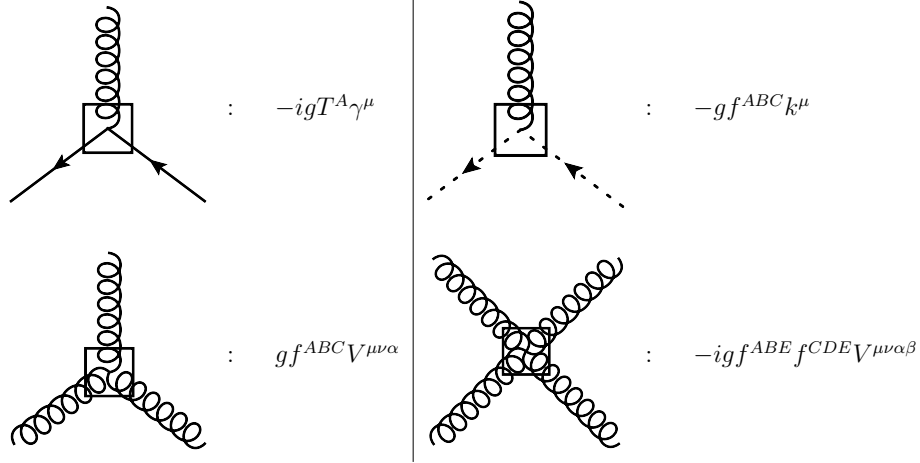


Figure 3: Diagrams representing the perturbative vertices in QCD

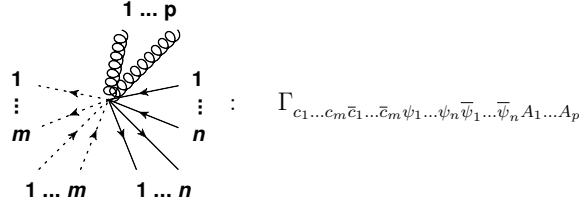


Figure 4: General diagram for a nonperturbative vertex in QCD

referred to as the “Gap Equations”, which describe the dynamics of the 1PI two-point functions (which turn out to be the inverse of the dressed, nonperturbative propagator $\Delta_{X_1 X_2}$). Higher derivatives of the effective action yield equations of motion for the nonperturbative vertices which govern the interactions of the theory. As with the gap equations, we find a set of coupled, nonlinear integral equations. The apparent feature of these equations of motion is that each vertex equation is coupled through one or more of the diagrams to a vertex containing a greater number of field operators. This is what constitutes the so-called “Infi-

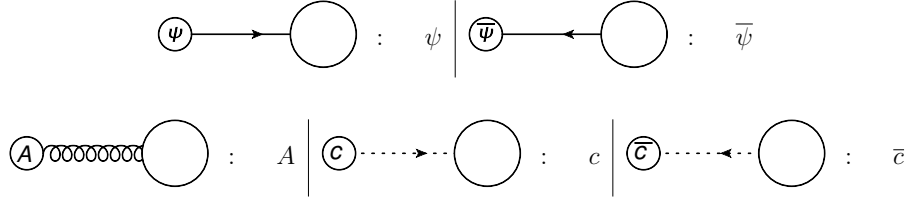


Figure 5: Diagrams representing the classical field variables in QCD

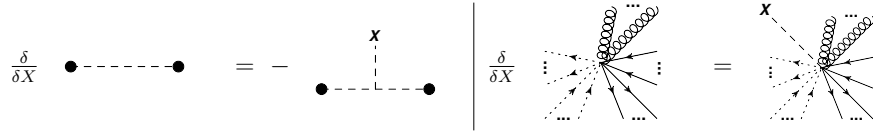


Figure 6: Diagrammatic representation of functional derivatives with respect to a generic classical field variable X

nite Tower” of Schwinger-Dyson equations, where the behavior at a lower level such as the gap equations require a complete simultaneous knowledge of every possible 1PI interaction vertex allowed by the theory.

Complete knowledge of the 1PI functions of a quantum field theory would represent a full solution of the theory, as every dynamical quantity and interaction would thus be specified. Since these equations of motion generally constitute an infinite set of coupled integral equations, performing any practical calculation of the theory requires us to modify the equations into a finite and manageable set. This process, known as truncation, can break the essential symmetries of the theory by imposing some approximation. This truncation is usually carried out at the level of vertex equations, by either employing a model for the interaction, or by reducing the interaction to its simplest perturbative form. While this ultimately breaks the proper formulation of the QFT, it is possible to still obtain solutions

which contain nonperturbative information and can thus be used as a means of studying an approximated version of the theory. In theories which have been studied using lattice gauge theory, such as QCD, comparison to the lattice results is used to evaluate the success of the more analytical Schwinger-Dyson approach given a particular model or truncation.

2.3.4 Renormalization

Due to the presence of loop integrals in the equations of motion, it is necessary to confront the possibility of divergent quantities in the formalism as presented thus far. The first step is to regulate these integrals, by which we mean the introduction of a parametrization scheme to describe these divergences. Popular methods include Dimensional Regularization, Pauli-Villars Regularization, or Momentum Cutoff Regularization. Each of these methods renders the integrals finite, but at the cost of introducing an unphysical parameter which depends on the particular regulator used. The parameter is considered in the limit where it would correspond to no regulator having been introduced, and thus exhibits the divergent pieces of the integral. The second step is then to renormalize the dynamical quantities, which is done by absorbing those unphysical divergences into the theory’s input parameters by means of previously undetermined “ Z -factors”. This is ideally done by setting these factors to produce agreement with physically measurable quantities, in which case the theory will then have the ability to predict other experimentally accessible quantities. In theories such as QCD where the fundamental degrees of freedom may not be physically observable, we instead choose proxies for these measurable quantities such as results of lattice QCD or observable properties of bound states.

In modern perturbation theory, the preferred regulator is Dimensional Regularization, which replaces the spacetime dimensions with a continuous dependence on some infinitesimal parameter ϵ (usually as $d = 4 \mp K\epsilon$ for some constant K) and allows small variations around the integer number of dimensions in the physical theory. While this method is robustly able to respect a theory’s symmetries, especially in gauge theories, it is difficult to implement in our numerical and nonperturbative techniques. The preferred method which will be used

here is to discuss the divergences present in the bare theory using a momentum cutoff regulator. As will be shown in the description of numerical techniques in §3.1, our integrals are defined using discretized grids which suffice to compute our integrals over the full volume of four-momentum space. Our discussions of renormalization will be framed using examples of a momentum-cutoff regulator, but this is only to demonstrate the ability of nonperturbative momentum subtraction to render the equations finite. Once the renormalization is performed, we are able to apply our numerical techniques to entirely finite and convergent integrals in which the cutoff is already understood to have been removed.

We implement the renormalization process by introducing Z -factors in the Lagrangian to convert the bare fields into renormalized fields. The field renormalization is carried out through the definition of Z_X as the field renormalization constant for the field X . Mass terms will gain coefficients dictated by the type of field they describe, but in general we will identify some mass renormalization factor Z_m . Interaction terms in the Lagrangian will pick up a combination of field renormalization terms and bare coupling constants. For each interaction i in the theory, the vertex renormalization constant is defined as Z_{g_i} . The Lagrangian for the renormalized theory is then obtained by substituting the field renormalization constants according to:

$$X_{\text{bare}} = \sqrt{Z_X} X_{\text{renormalized}}, \quad (2.23)$$

which results in the following definitions in the mass and interaction terms:

$$Z_X m_{X \text{ bare}} = Z_m m_{X \text{ renormalized}}, \quad (\text{Fermions}) \quad (2.24)$$

$$Z_X m_{X \text{ bare}}^2 = Z_m m_{X \text{ renormalized}}^2, \quad (\text{Bosons}) \quad (2.25)$$

$$\left(\prod_n \sqrt{Z_{X_n}} \right) g_{i \text{ bare}} = Z_{g_i} g_{i \text{ renormalized}}, \quad (2.26)$$

where the vertex renormalization involves the n fields X_n which participate in the interaction. Depending on the theory being considered, there may be more than one field or

interaction which needs to be defined in terms of the renormalized fields variables. This can be accomplished by considering the set $\{X\}$ of field variables in the context of (2.23), each particle's mass term in the context of (2.24) or (2.25), and each individual interaction with coupling g_i in the context of (2.26). In instances where various interactions are related by gauge symmetry, then one can only define as many independent renormalization constants as there are bare couplings and fields in the Lagrangian, as will be discussed in detail when renormalizing QCD.

Once all renormalization factors have been introduced into the Lagrangian, the development of generating functionals and functional calculus proceeds exactly as discussed above, where all functional variables are understood to refer to the renormalized fields. This means that only the renormalization constants which appear in the Lagrangian can appear in the Schwinger-Dyson equations after any combination of functional derivatives. Each diagrammatic term in a Schwinger-Dyson equation will contain exactly one of the perturbative or “boxed” symbols, and the renormalization factors which accompanied that symbol's term in the Lagrangian are those which should appear on any diagrammatic term which it contributes to the theory. In the renormalizable theories we discuss here, the two types of dynamical variables which can appear in “boxed” form are either propagators or interactions. As such, we will see in specific examples that the only renormalization factors which should appear in an equation of motion are introduced by the substitutions:

$$\Delta_{XX \text{ bare}}^{(0)} = Z_X \Delta_{XX \text{ renormalized}}^{(0)} , \quad (2.27)$$

$$\Gamma_{\{X\}_i \text{ bare}}^{(0)} = Z_{g_i} \Gamma_{\{X\}_i \text{ renormalized}}^{(0)} , . \quad (2.28)$$

We must note that these expressions (2.27) and (2.28) are only to be used in the approach discussed above, where the Lagrangian is expressed entirely in renormalized field variables along with the functional calculus.

The equations of motion also exhibit a property called multiplicative renormalizability^[12,13,14,20,30,67,70] (which is also frequently used in the construction of vertex models). This replaces the use of the discussion which led to (2.27) and (2.28) in favor of considering only the renormalization of dressed N -point functions of a quantum field theory. Using this approach, we could obtain the identical renormalized equations of motion directly from the bare ones. In order to express this method, we introduce the field renormalization Z -factors into the expectation values by replacing a bare field operator with a renormalized one:

$$\left\langle \Omega \left| \mathcal{T} \left(\prod_i X_i(x_i) \right) \right| \Omega \right\rangle_{\text{bare}} = \left\langle \Omega \left| \mathcal{T} \left(\prod_i Z_{X_i}^{\frac{1}{2}} X_i(x_i) \right) \right| \Omega \right\rangle_{\text{renormalized}}, \quad (2.29)$$

which applies to both the VEV and connected functions. Due to the Legendre transform and corresponding amputations, the 1PI functions exhibit a different modification:

$$\left\langle \Omega \left| \mathcal{T} \left(\prod_i X_i(x_i) \right) \right| \Omega \right\rangle_{\text{1PI bare}} = \left\langle \Omega \left| \mathcal{T} \left(\prod_i Z_{X_i}^{-\frac{1}{2}} X_i(x_i) \right) \right| \Omega \right\rangle_{\text{1PI renormalized}}. \quad (2.30)$$

We see that dynamical quantities such as propagators or classical field variables introduce positive powers of the appropriate Z -factors according to (2.29), while amputated vertices of the type used in our diagrammatics introduce negative powers of the appropriate Z -factors according to (2.30).

As mentioned, there is one important caveat to this approach, that the expressions above pertain only to the expectation values or dressed dynamical quantities. For instance, the perturbative propagators or interactions under this approach are to be viewed simply as tensors or (spatial) derivative operators. Upon inspection of the equations of motion shown in Chapter 3: [Gap Equations](#), one can confirm that the equations resulting from redefinition of the Lagrangian and functional calculus in terms of renormalized fields produces equivalent equations of motion to the introduction of factors according to the Multiplicative Renormalizability described by (2.29) and (2.30).

2.4 THE BETHE-SALPETER EQUATION

The Bethe-Salpeter equation serves as a method for obtaining quantitative information about the bound states of a quantum field theory. The most general information about the contribution of two valence particles i and j to the quantum bound state is represented by the Bethe-Salpeter amplitude (2.31), and its conjugate (2.32):

$$\Phi_{B,r}(x_a, x_b; P_B, \{r\}) \equiv \langle 0 | \mathcal{T}(\phi_i(x_a) \phi_j(x_b)) | B, \{r\} \rangle, \quad (2.31)$$

$$\bar{\Phi}_{B,r}(x_a, x_b; P_B, \{r\}) \equiv \langle B, \{r\} | \mathcal{T}(\phi_i^\dagger(x_a) \phi_j^\dagger(x_b)) | 0 \rangle, \quad (2.32)$$

where $|B, \{r\}\rangle$ is an eigenstate of four-momentum with eigenvalue P_B and quantum numbers $\{r\}$, hereafter to be referred to collectively using the index r . We perform a Fourier Transform, and impose the necessary conservation of four-momentum:

$$\Phi_{B,r}(x_a, x_b; P_B) \equiv \int \frac{dq_+}{(2\pi)^4} \frac{dq_-}{(2\pi)^4} e^{iq_+ \cdot x_a} e^{iq_- \cdot x_b} \phi_{B,r}(q_+, q_-; P_B) \delta(P + q_- - q_+), \quad (2.33)$$

thus

$$\phi_{B,r}(q_+, q_-; P_B) \equiv \langle 0 | \mathcal{T}(a_i^\dagger(q_+; t) a_j^\dagger(q_-; t)) | B, r \rangle, \quad (2.34)$$

$$P = q_+ - q_-. \quad (2.35)$$

For convenience, we have chosen to use the momenta of the fundamental particles as the variables to this amplitude. Using the parametrizations $q_\pm = q \pm \eta_\pm P$, with $\eta_+ + \eta_- = 1$, we automatically satisfy the conservation of four momentum in our expressions above.

The diagrammatic form of (2.34) is shown in Figure 7.

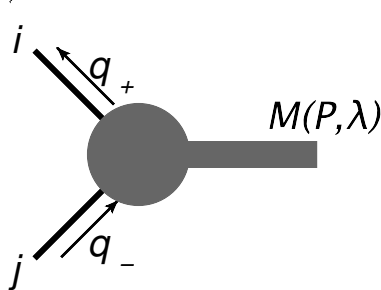


Figure 7: Diagrammatic representation of the Bethe-Salpeter amplitude $\Gamma_{ij}(q_+, q_-; \lambda)$, where $P = q_+ - q_-$.

Following the example of Nakanishi^[54], we investigate the 4-point Green function of the theory in order to derive the Bethe-Salpeter equation. The two valence particles of type i and j determine the appropriate Green function to use. In situations involving more than two valence particles or two or more identical particle types, substituting the quantum field operators into an expression analogous to (2.36) produces the generalization. The Green function dictates the most general motion in the Quantum Field theory in which (here) particle i travels between x_2 and x_1 , and particle j travels between y_2 and y_1 . For the time being we have allowed the particles i and j to potentially mix into another valence state composed of i' and j' , but the derivation presented here is most easily understood by considering a no-mixing (or better yet, a “valence eigenstate”) case. These type of extensions will be introduced when we consider specific theories in the [Bound States](#) Chapter. The general form for this function is:

$$G_{ij;i'j'}(x_1, y_1; x_2, y_2) = \left\langle 0 \left| \mathcal{T} \left(\phi_i(x_1) \phi_j(y_1) \phi_{i'}^\dagger(x_2) \phi_{j'}^\dagger(y_2) \right) \right| 0 \right\rangle. \quad (2.36)$$

This Green function can be factorized into two main pieces. First, we define a quantity $I \equiv \Delta_{X_i X_{i'}} \Delta_{X_j X_{j'}}$ as the “fly-through” operator, as this represents the contribution where both particles travel according to their own 1PI propagators without interacting with each other. The other required quantity is the “Interaction Kernel” K , which contains all possible

2-Particle Irreducible (2PI) interactions that the particles may have with each other. The meaning of 2PI can also be explained as $(i + j)$ Irreducible, as any intermediate state which contains only a single particle i and a single particle j (or two of the same if these are identical particles) would not fit this definition. Much as the 1PI diagrams of the Schwinger-Dyson formalism, this also means that the pair of external particle lines for the i and j fields are amputated to the point of connection into the 2PI process. The equation for the Green function G can thus be expressed schematically using:

$$G = I + I \cdot K \cdot G, \quad (2.37)$$

$$= I + I \cdot K \cdot I + I \cdot K \cdot I \cdot K \cdot I + \dots, \quad (2.38)$$

where we understand the dot notation to imply attaching the external points of G or I to the appropriate corresponding stubs of K and integrating over the momenta of any closed loops which result. By performing amputations on this equation with I^{-1} , we obtain:

$$I^{-1} \cdot G = 1 + K \cdot G, \quad (2.39)$$

$$G = (I^{-1} - K)^{-1}. \quad (2.40)$$

Further consideration of (2.36) as it relates to a physical bound state of the particle types i and j , then we should expect the times x_1^0 and y_1^0 at which the final state particles are observed would both be later than both times x_2^0 and y_2^0 at which the initial particles were observed. This would suggest a rewriting of $G \rightarrow G^{\text{BS}}$ as:

$$G_{ij;i'j'}^{\text{BS}}(x_1, y_1; x_2, y_2) = \left\langle 0 \left| \mathcal{T} \left(\phi_i(x_1) \phi_j(y_1) \right) \mathcal{T} \left(\phi_{i'}^\dagger(x_2) \phi_{j'}^\dagger(y_2) \right) \right| 0 \right\rangle. \quad (2.41)$$

With this separation, we can then expand G^{BS} by inserting a complete set of states which can connect the initial and final states. It can be shown that an appropriate complete set is formed by the combination of all physical and bound states in the theory^[54] distinguished

by their quantum numbers r . After incorporating the separation between initial and final state times, Nakanishi shows that the Green function can be written as:

$$G_{ij;i'j'}^{\text{BS}}(x_1, y_1; x_2, y_2) = \sum_r \int \frac{d^4 P}{(2\pi)^4} \frac{\Phi_{B,r}(x_1, y_1; P_B) \bar{\Phi}_{B,r}(x_2, y_2; P_B)}{(P^2 - P_B^2 + i\epsilon)} e^{-iP \cdot (X-Y)} + \text{finite}, \quad (2.42)$$

where:

$$X \equiv x_1 - y_1, \quad (2.43)$$

$$Y \equiv x_2 - y_2. \quad (2.44)$$

Performing the Fourier transform, we then find in momentum space:

$$G_{ij;i'j'}^{\text{BS}}(q, k, P) = \sum_r \frac{\Phi_{B,r}(q_+, q_-; P_B) \bar{\Phi}_{B,r}(k_+, k_-; P_B)}{(P^2 - P_B^2 + i\epsilon)} + \text{finite}. \quad (2.45)$$

We observe that each bound state corresponds to a pole in G , and for the moment we will assume that there are no degenerate bound states. The Bethe-Salpeter equation is developed from the combination of (2.37) and (2.45). Equating these two forms, and focusing on the pole region around a particular bound state r' , yields:

$$\begin{aligned} & \frac{\Phi_{B,r'}(q_+, q_-; P_B) \bar{\Phi}_{B,r'}(k_+, k_-; P_B)}{(P^2 - P_B^2 + i\epsilon)} + \text{finite} \\ &= \frac{I \cdot K \cdot \Phi_{B,r'}(q_+, q_-; P_B) \bar{\Phi}_{B,r'}(k_+, k_-; P_B)}{(P^2 - P_B^2 + i\epsilon)} + \text{finite}'. \end{aligned} \quad (2.46)$$

Approaching the location of pole P_B eliminates the finite quantities, and by comparing the pole residues which remain we find:

$$\Phi_{B,r'}(q_+, q_-; P_B) \bar{\Phi}_{B,r'}(k_+, k_-; P_B) = I \cdot K \cdot \Phi_{B,r'}(q_+, q_-; P_B) \bar{\Phi}_{B,r'}(k_+, k_-; P_B). \quad (2.47)$$

Finally, noting that the common $\bar{\Phi}_{B,r'}$ factor is not involved in any contractions or loop integrals allows us to remove it and obtain the final form of the Bethe-Salpeter equation:

$$\Phi_{B,r'}(q_+, q_-; P_B) = I \cdot K \cdot \Phi_{B,r'}(q_+, q_-; P_B). \quad (2.48)$$

In the cases we will explore in Chapter 4: [Bound States](#), we find it to be more convenient to handle the tensors if we consider the amputated Bethe-Salpeter amplitude $\chi \equiv I^{-1}\Phi$. In terms of this amplitude, the Bethe-Salpeter equation now reads:

$$\chi_{B,r'}(q_+, q_-; P_B) = K \cdot I \cdot \chi_{B,r'}(q_+, q_-; P_B). \quad (2.49)$$

Applying this equation to a particular theory or bound state is accomplished by identifying the scattering kernel K which contains the proper physical content, and the various tensor forms which are needed to describe χ . The form of χ can be easily explored by placing the appropriate field operators in (2.31) and (2.32), and considering any symmetries which may be useful in constraining the general set of structure functions.

As will be discussed in §4.2.1, we employ an eigensystem representation to solve (2.49). This entails interpreting this equation as a resonance condition, and once a resonance is found the corresponding eigenvector represents the solution χ for that bound state. Proper normalization of the amplitude χ is necessary should we intend to use it in the calculation of dynamical quantities such as form factors or decay constants. For the investigation presented here, we are interested in a preliminary exploration of the Glueball mass spectrum and so identifying resonances will be the focus.

3.0 GAP EQUATIONS

We will present the nonperturbative treatment of multiple quantum field theories as obtained from the general form (2.22) for the Schwinger-Dyson master equation. The equations of motion for the propagators of a quantum field theory are obtained through analysis of the functional second derivatives of the effective action, $\frac{\delta^2 \Gamma}{\delta X_i \delta X_j}$. Upon taking the limit of all functional sources vanishing, the physically relevant equations of motion result. In general, the Schwinger-Dyson equations can be reduced to nonlinear integral equations in momentum-space in which an inverse propagator is related to one (or more) integral expression(s) as obtained from the various loop structures of the diagrammatic approach. We will discuss here a set of robust numerical techniques which can be used to solve a wide range of such equations, and demonstrate their usefulness in the context of several popular textbook and/or physically relevant quantum field theories.

3.1 NUMERICAL METHODS

The equations of motion for the propagators Δ_i in a quantum field theory are expressed as nonlinear integral equations. In all but the simplest cases, transforming these equations into an algebraic or differential equation is not a useful approach. A number of numerical methods can be applied to equations of this type, including minimization of a form such as:

$$|\Delta_i - f(\Delta_i)| \rightarrow 0, \tag{3.1}$$

or expansion in a complete set of functions and computing the resulting coefficients. The method employed here is to iterate the equations of motion in terms of a set of parameters which represent the discretized functions, and obtain the set of points which represent the stable solution. This is equivalent to (3.1), as the accrued changes in the discretized function tend to vanish as the proper solution is approached. This iteration is set up in a fashion which can be understood from any of the diagrammatic equations of motion, for example the propagator equation for ϕ^4 theory shown in Figure 10. The unknown function Δ in this case is the propagator for the pion field (ϕ), and the function $f(\Delta)$ is represented by the terms on the right-hand side of the equation of motion. Starting from an initial guess function (which is most assured to converge, and do so rapidly, if already close in behavior to the solution), the function $f(\Delta)$ can be computed numerically, and then used to update the discretized form for Δ . The updated form is then used to recalculate $f(\Delta)$, and so on until a stable solution is obtained.

3.1.1 Discretization

The nonperturbative equations of motion for a renormalizable field theory allow diagrams with no more than two momentum loops, in the variables q_μ and k_μ . Computation of the integrals over these momentum loops is most easily accomplished in a 4-D Euclidean space, where these vectors (along with the external momentum p_μ) can be fully parametrized in terms of two radial and three angular integration variables. We convert our four-momenta into Euclidean quantities through an analogous transformation to the Wick rotation common in perturbation theory. By implementing the integral transform:

$$p_0^M \rightarrow ip_4, \tag{3.2}$$

$$p_i^M \rightarrow p_i, \tag{3.3}$$

where the index i applies to the spatial components, we obtain the desired conversion. The remaining dependence on radial and angular integration variables in momentum space can

be parametrized in terms of 4-dimensional hyperspherical coordinates. These variables are defined through a Gauss-Legendre algorithm^[34] which generates a set of points $r_i \in (0, 1)$ and corresponding weights w_i . We allow different numbers of grid points for each type of variable, including radial momentum variables q and k , 4-D hyperspherical polar angles $x \equiv \cos(\theta_1^{(q)})$ and $y \equiv \cos(\theta_1^{(k)})$, and one 4-D hyperspherical second polar angle $z \equiv \cos(\theta_2^{(k)})$ (the choice of whether the variable is defined as pertaining to q or k is arbitrary, but we make the choice to express it for our original loop variable q). We see that these angular parameters can be analogously defined through the various vector products in Euclidean space, as $x \equiv \frac{q \cdot P}{qP}$, $y \equiv \frac{k \cdot P}{kP}$, and $w \equiv \frac{q \cdot k}{qk}$, where the relationship between z and w is given by (3.8).

The discretized momentum grid serves two purposes in the computation. First, the grid defines the set of points at which the free parameters representing the propagator dressing functions are evaluated and updated. Second, it also serves as the summation grid for the numerical integration variable $q \equiv |q|$ (and analogously for a second variable k when two-loop diagrams are to be considered). These points and their integral measure are mapped onto the interval $q \in (0, \infty)$ according to:

$$q = \frac{1}{1-r}, \quad (3.4)$$

$$dq = \frac{-dr}{(1-r)^2}. \quad (3.5)$$

A second Gauss-Legendre grid is employed to represent the angular integrations which appear in the four-momentum loop integrals. Both types of angular variables are needed over the domain $(-1, 1)$. First, we use a simple mapping for the variable x (and an identical one for y):

$$x = -1 + 2r, \quad (3.6)$$

$$dx = 2dr. \quad (3.7)$$

The remaining angular variable can be parametrized in terms of a variable z defined by the same mapping, and so we express w as:

$$w = xy + \sqrt{(1-x^2)(1-y^2)}z \quad (3.8)$$

The expressions we evaluate inside of the integrands are obtained from a symbolic treatment using Mathematica^[72] of the various traces and contractions which arise in the equations of motion. Given the mappings and integration variables defined above, we can express the various (Euclidean-space) four-momenta in component form as:

$$p^\mu = (p, 0, 0, 0), \quad (3.9)$$

$$q^\mu = (qx, q\sqrt{1-x^2}, 0, 0), \quad (3.10)$$

$$k^\mu = (ky, k\sqrt{1-y^2}z, k\sqrt{(1-y^2)(1-z^2)}, 0). \quad (3.11)$$

We have thus expressed all necessary parameter dependence to perform integrations over the full volume of four-momentum space, including cases where we consider the nonperturbative two-loop diagrams. The same integration grids and symbolic expressions will also turn out to be useful in our treatment of Chapter 4: [Bound States](#).

A final note should be made regarding the discretized form of momenta and dressing functions. In the various models to be discussed, there can be (depending on choices of momentum routing) a necessity to evaluate the propagator functions away from the discretized

points. The sampling of Euclidean momenta includes arguments between grid points as well as above and below the region bounded by the grid. As such, we require means of interpolating or extrapolating the scalar dressing functions over a wide range of momenta. As will be discussed in §3.4.6, consideration of the full suite of diagrams in the gluon propagator's equation of motion (3.123) or Figure 25 resulted in a simple yet robust interpolation routine which is also capable of producing reliable extrapolations into the far UV or deep IR. This interpolation routine is based on a cubic spline fit, which is applied to a log-log form of the dressing function (e.g. $\ln[F(e^{\ln(p^2)})] \rightarrow F'(\ln(p^2))$). We observe that fits performed using this algorithm provide smooth functions over the required range of momenta which are well-suited to stable numerical integration. The results for all of the theories or models discussed in this chapter have been revised to include this particular routine for all propagator dressing functions.

3.1.2 Convergence and Stability of Solutions

At each iteration, an error value ϵ is computed which can be defined as:

$$\epsilon = \sum_i |\Delta(p_i^2) - f(\Delta(p_i^2))|, \quad (3.12)$$

where the index i refers to the discretized momentum points at which we have chosen to define our propagator function(s). Provided that the gap equations have been properly defined and renormalized, the successive iterations will eventually converge on the stable solutions representing the propagators. When this occurs, the parameter ϵ reaches the smallest possible value corresponding to the machine precision in evaluating the loop integrals. At this point, the set of free parameters $\Delta(p_i^2)$ are to be understood as the discretized form of the analytical solutions to the equation of motion being considered.

An example of a properly renormalized, stable solution is shown in Figure 8. This plot displays the dressing functions from the nonperturbative propagators of QCD, and shows the effect of variations in both radial and angular integration grids. The minor variations in

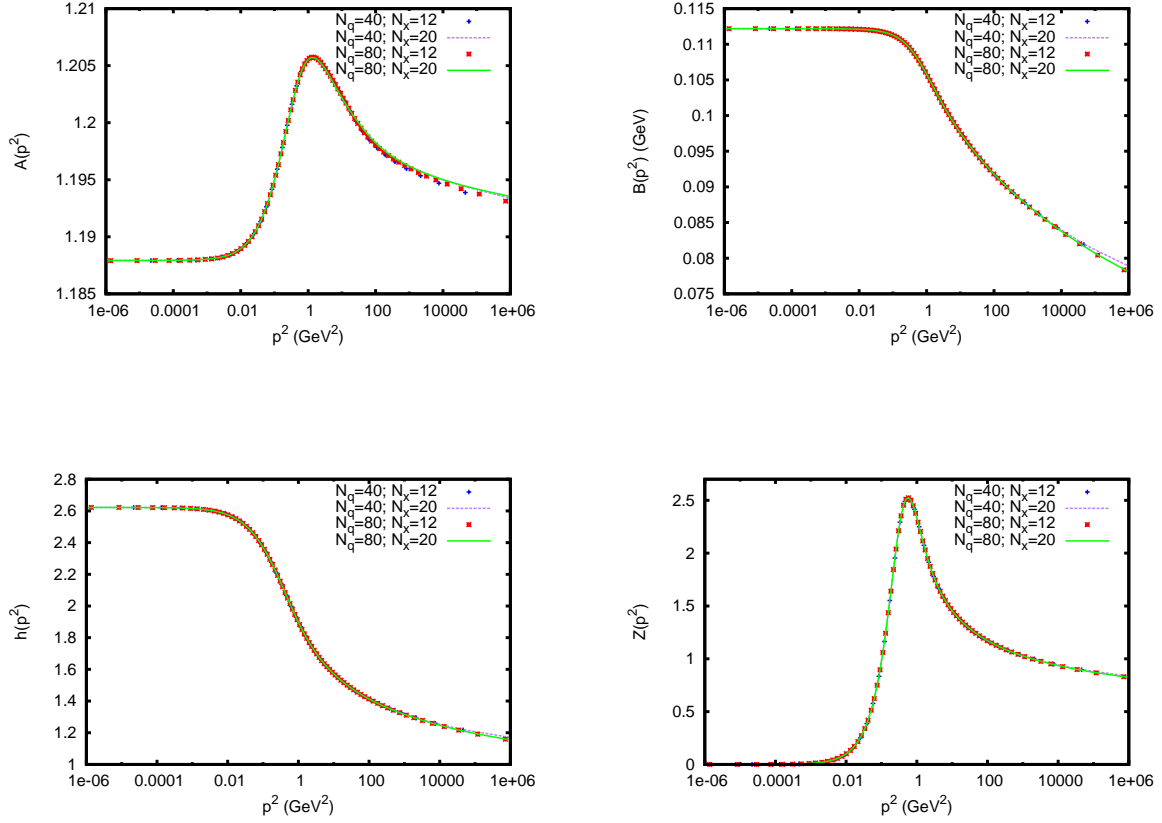


Figure 8: Plots of the QCD propagator dressing functions obtained under various combinations of radial and angular grid spacing. The scalar functions $A(p^2)$ and $B(p^2)$ are part of the quark propagator as defined in §3.4.1, while $G(p^2)$ and $Z(p^2)$ are defined in §3.4.2.2 as two ways of parametrizing the gluon propagator. Solutions were obtained with $g^2 = 1$ and the set of renormalization parameters shown in Table 1.

the functions plotted is demonstration that renormalization was successfully implemented, and that any cutoff or numerical dependence are insignificant sources of error.

In some situations, we find that the convergence of ϵ may not behave in the ideal manner described above. There can be a number of contributing reasons which our computations have identified. First, in situations where the set of renormalization parameters and coupling values are poorly chosen, we have observed that the computation does not converge on a

$A(.25 \text{ GeV}^2)$	1.2
$B(.25 \text{ GeV}^2)$.11 GeV
$h(1 \text{ GeV}^2)$	1.9
$G(0 \text{ GeV}^2)$	10 GeV ⁻²
$G(.25 \text{ GeV}^2)$	8 GeV ⁻²

Table 1: Set of Renormalization parameters for the QCD propagator functions of Figure 8

stable set of solutions. The restriction of our parameter space in these cases is taken to mean either that there is a constraint or relationship between the parameters that has not been properly implemented, that the convergence towards a stable solution is impractical on our computational time scales, or that we have simply chosen a set of parameters which do not correspond to any physical solution (i.e., cases of Chiral Symmetry Breaking). Second, it is possible that the computation will not converge to a stable solution if the integration grids defined through the method of §3.1.1 have been implemented with too few grid points and are thus unable to faithfully evaluate the loop integrals to the necessary level of precision to obtain a solution. In these cases, it is frequently found that increasing the grid resolution will result in improved solutions exhibiting the desired stability at the cost of longer computation time. Third, there are situations (such as when implementing the vertex models described in §3.4.3 or in our consideration of two-loop gluon diagrams in §3.4.6) where the initial guess values for the propagator functions do not have the proper behavior to evaluate the desired computation in a stable manner. In these cases, we obtain useful results by implementing a switch in our code that disables the sensitive quantity until the solutions begin to converge without it, then turn on the quantity and allow the solutions to re-converge on the desired results. Finally, we have observed situations of superficial non-convergence, particularly in the gluon equations of §3.4: QCD. In these situations, we find that ϵ may not begin to converge immediately (and in fact even appear to be diverging) before “turning over” and

converging to the solution. Some cases may even pass through multiple fluctuations before approaching a valid solution. In these cases we find that patience through a large number of iterations (perhaps even up into the thousands) can be quite useful.

3.1.3 Renormalization in Practice

The general means of introducing Z -factors into the Lagrangian of a quantum field theory was discussed in §2.3.4. The functional variables used in the Generating Functionals Z , W , and Γ are thus redefined by coefficients of the field renormalization constants Z_X for each field X . It was also discussed that only those Z -factors which appear explicitly in the Lagrangian will follow the corresponding perturbative or “boxed” diagrammatic symbols through the functional derivatives and appear in the equations of motion. We shall now explain the methods by which these constants are defined in order to obtain physically relevant solutions to the Schwinger-Dyson equations.

We consider a generic equation of motion for a single-field quantum field theory. In addition, we assume for now that there is only one self-energy diagram in the diagrammatics. The equation of motion for the propagator in Euclidean space can be written schematically in the form:

$$\frac{1}{\Delta_{XX}(p^\mu)} = Z_X \frac{1}{\Delta_{XX}^{(0)}(p^\mu)} + iZ_g \Sigma(p^\mu). \quad (3.13)$$

where the perturbative form of the propagator $\Delta_{XX}^{(0)}(p)$ depends strongly on whether we are considering a bosonic or fermionic field X . In the propagators we will consider in this work, all solutions are obtained after projection or tracing with various tensors to eliminate all Dirac, Lorentz, or SU(3) color indices. As a result, we can discuss the general case by describing the renormalization process for a spinless field (and merely exchanging m^2 for m if we have a fermionic equation). The equation (3.13) would then read as:

$$\frac{-i}{\Delta_{XX}(p^2)} = Z_X p^2 + Z_m m^2 + Z_g \Sigma(p^2). \quad (3.14)$$

We consider now that, before regularization, the self-energy $\Sigma(p^2)$ is formally infinite. Introducing a momentum cutoff Λ^2 , we express the divergences of $\Sigma(p^2)$ using the parametrization:

$$\Sigma(p^2) = \Sigma'(p^2) + a\Lambda^2 + bp^2 \log(\Lambda^2) \quad (3.15)$$

We observe now that the logarithmically divergent piece with coefficient b can be absorbed into the definition of the constant Z_X , while the quadratically divergent piece with coefficient a can be absorbed into the definition of the constant Z_m . This would eliminate the infinite contributions of the unregulated $\Sigma(p^2)$ while leaving behind only the finite self-energy contribution $\Sigma'(p^2)$. Identification of the divergent pieces would rely on fitting functions to the self energy integral over variations in both p^2 and Λ^2 , but this becomes difficult due to the numerical techniques we must generally use to solve nonperturbative equations of motion.

Instead, we choose to employ a renormalization scheme based on momentum subtraction. We first choose an arbitrary external momentum scale μ_2^2 at which to define the value of Z_m . This yields:

$$Z_m = \frac{1}{m^2} \left(\frac{-i}{\Delta_{XX}(\mu_2^2)} - Z_X \mu_2^2 - Z_g \Sigma(\mu_2^2) \right) \quad (3.16)$$

Substituting back into (3.14), we obtain:

$$\frac{-i}{\Delta_{XX}(p^2)} = \frac{-i}{\Delta_{XX}(\mu_2^2)} + Z_X (p^2 - \mu_2^2) + Z_g \left(\Sigma(p^2) - \Sigma(\mu_2^2) \right). \quad (3.17)$$

Choosing a second arbitrary external scale μ_1^2 , we solve for the value of Z_X :

$$Z_X = \frac{1}{(\mu_1^2 - \mu_2^2)} \left(\frac{-i}{\Delta_{XX}(\mu_1^2)} - \frac{-i}{\Delta_{XX}(\mu_2^2)} - Z_g \left(\Sigma(\mu_1^2) - \Sigma(\mu_2^2) \right) \right), \quad (3.18)$$

and substitute its value into (3.17), which yields our fully renormalized form for the propagator's equation of motion:

$$\begin{aligned}
\frac{-i}{\Delta_{XX}(p^2)} &= \left(\frac{p^2 - \mu_2^2}{\mu_1^2 - \mu_2^2} \right) \frac{-i}{\Delta_{XX}(\mu_1^2)} + \left(\frac{\mu_1^2 - p^2}{\mu_1^2 - \mu_2^2} \right) \frac{-i}{\Delta_{XX}(\mu_2^2)} \\
&+ Z_g \left[\Sigma(p^2) - \left(\frac{p^2 - \mu_2^2}{\mu_1^2 - \mu_2^2} \right) \Sigma(\mu_1^2) - \left(\frac{\mu_1^2 - p^2}{\mu_1^2 - \mu_2^2} \right) \Sigma(\mu_2^2) \right]. \quad (3.19)
\end{aligned}$$

We can substitute the form of $\Sigma(p^2)$ from (3.15) and confirm that only contributions from the finite piece $\Sigma'(p^2)$ contribute to renormalized solution $\Delta_{XX}(p^2)$. We have thus successfully used the constants Z_X and Z_m to absorb the unphysical divergences, and replaced our dependence on those unspecified constants by dependence on our input parameters $\Delta_{XX}(\mu_1^2)$ and $\Delta_{XX}(\mu_2^2)$. The values for $\Delta_{XX}(\mu_i^2)$ can be chosen as practically any value, and along with the μ_i they serve to set the momentum scales for the renormalized quantities. In cases where the properties of a quantum field theory can be observed and measured, for example, one could set the propagator functions to known or deduced values which produce agreement with observables. In considering theories as “toy models” without a direct link to physical data, the scales are still set by these parameters but do not have a direct interpretation as dimensionally meaningful quantities. Any results of our computations which were obtained using a toy model approach will be described as such to remind the reader that there is not a direct physical meaning to the units of momentum and they instead are to be understood only as proportions relative to the values of momenta chosen as renormalization points.

Finally, we note that renormalization of the gap equation did not determine the value of Z_g , nor are there any divergences left to be eliminated. The preferred interpretation in this work is that the vertex renormalization factors should be left to the treatment of that interaction’s equation of motion until being determined. Since all of the theories we consider here are truncated at the level of propagator equations of motion, these constants are regarded as arbitrary and so we choose to absorb all factors Z_{g_i} into the definition of their corresponding couplings. A situation in which there are multiple interactions constrained by gauge symmetry will be discussed in §3.4.4.

3.2 ϕ^4 THEORY

The first theory we will use to demonstrate the nonperturbative methods of the Schwinger-Dyson equations is ϕ^4 theory. This theory contains only a single interacting field ϕ , and is described by the Lagrangian:

$$\mathcal{L} = \frac{1}{2}(\partial^\mu \phi)(\partial_\mu \phi) - \frac{m_0^2}{2}\phi^2 - \frac{\lambda}{4!}\phi^4. \quad (3.20)$$

Figure 9: Schwinger-Dyson Master Equation for ϕ^4 theory.

Figure 10: Schwinger-Dyson equation of motion for the phion propagator in ϕ^4 theory.

Figure 11: Perturbative vertex for ϕ^4 theory.

As a bosonic field theory with field operators defined through their commutation relations, the “phion” field of ϕ^4 theory can be treated nonperturbatively through the same diagrammatic rules defined for the gluon-type fields of §2.3: [Schwinger-Dyson Equations](#).

The Schwinger-Dyson master equation for this theory is shown in Figure 9. The only explicit modification to the diagrammatic rules (aside from superficial changes in appearance) is the definition of the perturbative interaction vertex as shown in Figure 11.

We identify that the perturbative form for the propagator is given by:

$$\Delta_{\phi\phi}^{(0)}(p^2) = \frac{i}{p^2 - m_0^2}, \quad (3.21)$$

while we define the dressing function for the nonperturbative propagator as:

$$\Delta_{\phi\phi}(p^2) = iF^M(p^2), \quad (3.22)$$

where we include the superscript M to indicate the function as defined in Minkowski space. The equation of motion for the phion propagator is shown in Figure 10. Using the dressing function $F(p^2)$, we cast this in symbolic form as:

$$\begin{aligned} F^{M^{-1}}(p^2) &= p^2 - m_0^2 - \frac{i\lambda_0}{2} \int \frac{d^4q}{(2\pi)^4} F^M(q^2) \\ &+ \frac{i\lambda_0}{6} \int \frac{d^4q d^4k}{(2\pi)^8} \Gamma_{\phi(q+\frac{p}{2})\phi(k+\frac{p}{2})\phi(-q-k)\phi(-p)}^{(4)} \\ &\times F^M\left(\left(q+\frac{p}{2}\right)^2\right) F^M\left(\left(k+\frac{p}{2}\right)^2\right) F^M((q+k)^2). \end{aligned} \quad (3.23)$$

In order to obtain the equation in Euclidean space where our parametrization of hyperspherical coordinates (discussed in §3.1.1) can be applied, we perform the Wick rotation and observe:

$$F^M(p_M^2) \rightarrow F^E(p^2) = -F^M(p_M^2) \equiv F(p^2). \quad (3.24)$$

We also choose to truncate the equation with the perturbative vertex $\Gamma^{(4)} = i\lambda_0$, which yields:

$$\begin{aligned}
F^{-1}(p^2) &= p^2 + m_0^2 - \frac{\lambda_0}{2} \int \frac{d^4 q}{(2\pi)^4} F(q^2) \\
&\quad - \frac{\lambda_0^2}{6} \int \frac{d^4 q d^4 k}{(2\pi)^8} F\left(\left(q + \frac{p}{2}\right)^2\right) F\left(\left(k + \frac{p}{2}\right)^2\right) F((q+k)^2)
\end{aligned} \tag{3.25}$$

The renormalization of ϕ^4 theory is carried out through the introduction of field and mass Z -factors defined by:

$$\phi_0 \rightarrow Z_\phi^{\frac{1}{2}} \phi_r, \tag{3.26}$$

$$\frac{m_0^2}{2} \rightarrow \frac{Z_\phi m_0^2}{2} \equiv \frac{Z_m m_r^2}{2}, \tag{3.27}$$

where we understand all unlabeled couplings and field variables appearing before this point to have represented the unrenormalized quantities, while all unlabeled quantities which follow in our discussion of ϕ^4 theory will be understood as renormalized.

We define the value of the propagator $F(p^2)$ at two external scales, as an example of the “toy model” case discussed in §subsection:RenormalizationPractice, solving for the values of Z_ϕ and Z_m . As discussed, the renormalization in this fashion naturally introduces a regulator based on momentum subtraction. Schematically representing our equation of motion (3.25), we can express this as:

$$F^{-1}(p^2) = Z_\phi p^2 + Z_m m^2 - I_1 - I_2(p^2), \tag{3.28}$$

where I_1 and $I_2(p^2)$ are shorthand for the loop integrals in (3.25). We note especially that the term I_1 from the tadpole diagram of Figure 10 is independent of the external momentum. As a result, this loop integral gets entirely absorbed by the mass renormalization factor Z_m ,

and does not influence the dressed propagator $F(p^2)$ in any way. The renormalized form for the gap equation is:

$$F^{-1}(p^2) = \left(\frac{p^2 - \mu_2^2}{\mu_1^2 - \mu_2^2} \right) F^{-1}(\mu_1^2) + \left(\frac{\mu_1^2 - p^2}{\mu_1^2 - \mu_2^2} \right) F^{-1}(\mu_2^2) - \left[I_2(p^2) - \left(\frac{p^2 - \mu_2^2}{\mu_1^2 - \mu_2^2} \right) I_2(\mu_1^2) - \left(\frac{\mu_1^2 - p^2}{\mu_1^2 - \mu_2^2} \right) I_2(\mu_2^2) \right]. \quad (3.29)$$

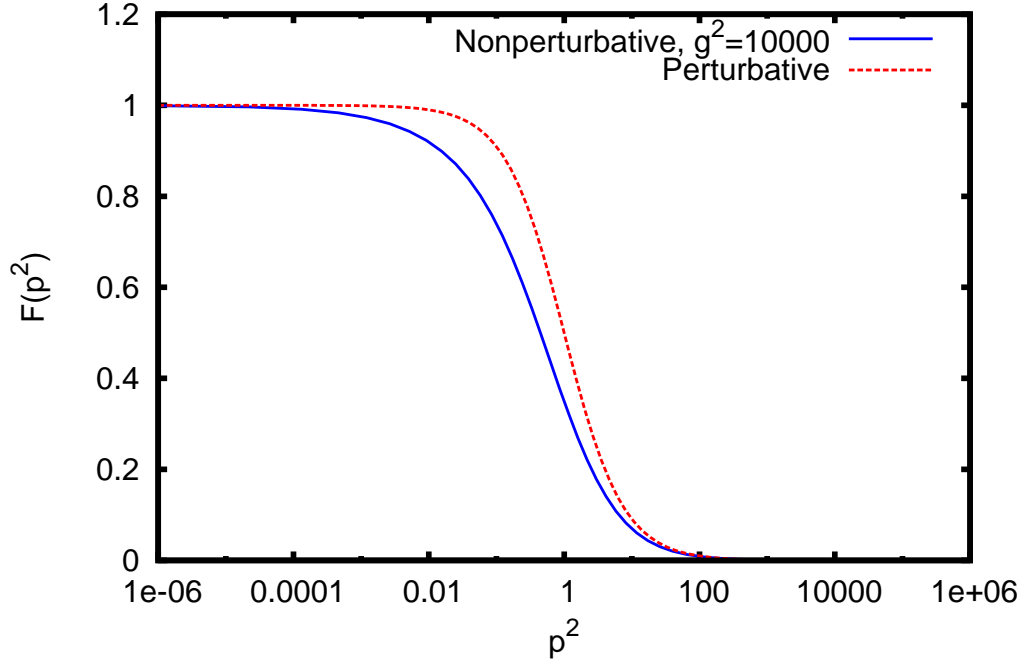


Figure 12: Plot of the phion propagator $F(p^2)$ as obtained from the nonperturbative equation of motion. The propagator was renormalized using the toy model convention with $F(0) = 1$ and $F(10,000) = \frac{1}{10,000}$.

An example of a nonperturbative solution to (3.29) is shown in Figure 12. This solution was obtained with $\lambda^2 = 10000$, as attempts to solve the gap equation for couplings of $O(1000)$ or below displayed very little departure from the perturbative form. The relative weakness of the self-energy in this case is likely due to the truncation to perturbative self-interaction and lack of further momentum dependence in the integration kernel. We shall see an example in §3.4.6 where a similar two-loop diagram has a more significant effect on the propagator with $O(1)$ coupling constants.

3.3 QED

Quantum Electrodynamics (QED) consists of a fermion theory describing electrons and a U(1) gauge theory describing photons. QED is described by the Lagrangian:

$$\mathcal{L}_{\text{QED}} = -\frac{1}{4}F_{\mu\nu}F^{\mu\nu} + \bar{\psi}(i\not{D} - m)\psi + \mathcal{L}_{\text{gauge}} \quad (3.30)$$

where:

$$F_{\mu\nu} = D_\mu A_\nu - D_\nu A_\mu, \quad (3.31)$$

$$D_\mu = \partial_\mu + ieA_\mu. \quad (3.32)$$

We will be considering QED in covariant gauge, so we define the gauge-fixing term:

$$\mathcal{L}_{\text{gauge}} = -\frac{\lambda}{2}(\partial \cdot A)^2 \quad (3.33)$$

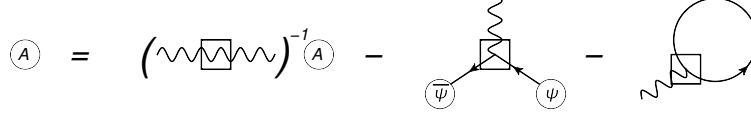


Figure 13: Photon Schwinger-Dyson Master Equation

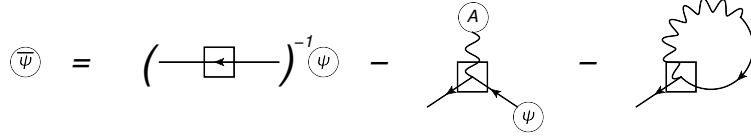


Figure 14: Electron Schwinger-Dyson Master Equation

3.3.1 Electrons

Considering the electron field first, we obtain the bare gap equation as shown diagrammatically in Figure 16:

$$S^{M-1}(p) = -i(\not{p} - m) - ie \int \frac{d^4 q}{(2\pi)^4} \Gamma_{\bar{\psi}(p) A_\nu^A (q-p) \psi(q)} S^M(q) \gamma_\mu P^{\mu\nu}(q-p) G^M(q-p). \quad (3.34)$$

We cast this equation into a pair of equations for scalar dressing functions defined by the ansatz $S^{M-1}(p) = -i(A^M(p^2)\not{p} - B^M(p^2))$. The integrands appearing in the equations of motion are more conveniently expressed in terms of the functions:

$$\sigma_V^M(p^2) = \frac{A^M(p^2)}{(A^M(p^2))^2 p^2 - (B^M(p^2))^2}, \quad (3.35)$$

$$\sigma_S^M(p^2) = \frac{B^M(p^2)}{(A^M(p^2))^2 p^2 - (B^M(p^2))^2}. \quad (3.36)$$

We extract the equations for the quark propagator's dressing functions by performing traces over the Dirac indices. The necessary traces to obtain these are given by:

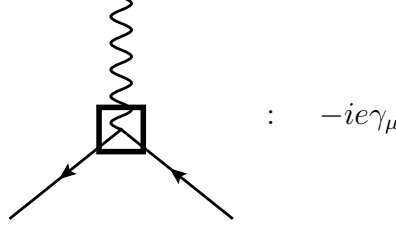


Figure 15: Perturbative vertex for QED

Figure 16: Electron Gap Equation

$$A^M(p^2) = \frac{i}{4p^2} \text{Tr}_{\text{Dirac}} \left[\not{p} S^{M-1}(p) \right], \quad (3.37)$$

$$B^M(p^2) = \frac{-i}{4} \text{Tr}_{\text{Dirac}} \left[S^{M-1}(p) \right]. \quad (3.38)$$

Applying these traces to (3.34), we obtain:

$$A^M(p^2) = 1 + \frac{1}{4p^2} e \int \frac{d^4 q}{(2\pi)^4} \text{Tr}_{\text{Dirac}} \left[\not{p} \Gamma_{\bar{\psi}(p) A_{\nu(q-p)}^A \psi(q)} S^M(q) \gamma_\mu \right] P^{\mu\nu}(q-p) G^M(q-p) \quad (3.39)$$

$$B^M(p^2) = m - \frac{1}{4} e \int \frac{d^4 q}{(2\pi)^4} \text{Tr}_{\text{Dirac}} \left[\Gamma_{\bar{\psi}(p) A_{\nu(q-p)}^A \psi(q)} S^M(q) \gamma_\mu \right] P^{\mu\nu}(q-p) G^M(q-p) \quad (3.40)$$

The truncations or vertex models we will investigate employ only tensor structures which may contain a scalar function multiplied by the perturbative vertex $ie\gamma_\nu V^M(q, p)$. As such, the traces can be explicitly carried out to yield:

$$A^M(p^2) = 1 + \frac{ie^2}{p^2} \int \frac{d^4q}{(2\pi)^4} \sigma_V^M(q^2) G^M(q-p) V^M(q, p) \times \left(\frac{2q^2p^2 + 4(p \cdot q)^2 - 3(p^2 + q^2)p \cdot q}{q^2 + p^2 - 2q \cdot p} \right) \quad (3.41)$$

$$B^M(p^2) = m - 3ie^2 \int \frac{d^4q}{(2\pi)^4} \sigma_S^M(q^2) G^M(q-p) V^M(q, p) \quad (3.42)$$

In order to obtain these equations of motion in Euclidean space, we must perform a Wick rotation. Any further appearance of an unlabeled four-momentum in the electron equation is to be understood as Euclidean, and we observe that the consequences of Wick rotation are:

$$A^M(p_M^2) \rightarrow A^E(p^2) = A^M(-p_M^2) \equiv A(p^2), \quad (3.43)$$

$$B^M(p_M^2) \rightarrow B^E(p^2) = B^M(-p_M^2) \equiv B(p^2), \quad (3.44)$$

$$\sigma_{V,S}^M(p_M^2) \rightarrow \sigma_{V,S}^E(p^2) = -\sigma_{V,S}^M(-p_M^2) \equiv \sigma_{V,S}(p^2), \quad (3.45)$$

$$G^M(p_M^2) \rightarrow G^E(p^2) = -G^M(-p_M^2) \equiv G(p^2), \quad (3.46)$$

$$V^M(q_M, p_M) \rightarrow V^E(q^2, p^2, q \cdot p) = V^M(-q_M^2, -p_M^2, -q_M \cdot p_M) \equiv V(q, p), \quad (3.47)$$

and so the Euclidean space equations of motion for the electron propagator are given by:

$$A(p^2) = 1 - e^2 \int \frac{d^4q}{(2\pi)^4} \sigma_V(q^2) G((q-p)^2) V(q, p) \times q^2 \left(\frac{2 + 4x^2 - 3\left(\frac{p}{q} + \frac{q}{p}\right)x}{q^2 + p^2 - 2qpx} \right) \quad (3.48)$$

$$B(p^2) = m + 3e^2 \int \frac{d^4q}{(2\pi)^4} \sigma_S(q^2) G((q-p)^2) V(q, p) \quad (3.49)$$

$$(\text{wavy line})^{-1} = (\text{wavy line with square loop})^{-1} + \text{wavy line with square loop and fermion loop}$$

Figure 17: Photon Gap Equation

3.3.2 Photons

Our treatment of the photon propagator will be done exclusively in covariant gauges, with a specific intent on working in Landau gauge. The Schwinger-Dyson equation for the photon propagator is shown diagrammatically in Figure 17. Considering first the perturbative propagator's contribution to this equation, we find that this quantity is given by:

$$\text{Covariant gauge : } \Delta^{(0)}_{\mu\nu}(p) = \frac{(-i) \left(g_{\mu\nu} + \frac{1-\lambda}{\lambda} \frac{p_\mu p_\nu}{p^2} \right)}{p^2 - \mu^2 + i\epsilon}, \quad (3.50)$$

$$\text{Feynman gauge : } \Delta^{(0)}_{\mu\nu}(p) = \frac{(-i) g_{\mu\nu}}{p^2 - \mu^2 + i\epsilon}, \quad (3.51)$$

$$\begin{aligned} \text{Landau gauge : } \Delta^{(0)}_{\mu\nu}(p) &= \frac{(-i) \left(g_{\mu\nu} - \frac{p_\mu p_\nu}{p^2} \right)}{p^2 - \mu^2 + i\epsilon} \\ &\equiv (-i) \frac{P_{\mu\nu}(p)}{p^2 - \mu^2 + i\epsilon}, \end{aligned} \quad (3.52)$$

where we have defined the transverse projection tensor $P_{\mu\nu}(p)$. The dressed propagators will be defined using the dressing functions:

$$\text{Covariant gauge : } \Delta_{\mu\nu}(p) = (-i) \left[P_{\mu\nu}(p) G_C^M(p^2) + \frac{1}{\lambda} \frac{p_\mu p_\nu}{p^4} \right], \quad (3.53)$$

$$\text{Feynman gauge : } \Delta_{\mu\nu}(p) = (-i) \left[P_{\mu\nu}(p) G_F^M(p^2) + \frac{p_\mu p_\nu}{p^4} \right], \quad (3.54)$$

$$\text{Landau gauge : } \Delta_{\mu\nu}(p) = (-i) P_{\mu\nu}(p) G^M(p^2) \equiv (-i) P_{\mu\nu}(p) \frac{Z^M(p^2)}{p^2}. \quad (3.55)$$

Starting from the general forms in covariant gauge, we observe that the inverse propagator appearing in the equation of motion (Figure 17 or (3.58)) can be expressed in the form:

$$\frac{i}{G_C^M(p^2)} \left(g_{\mu\nu} + (\lambda p^2 G_C^M(p^2) - 1) \frac{p_\mu p_\nu}{p^2} \right). \quad (3.56)$$

As such, we eliminate the dependence on Lorentz indices by contracting both sides with the projection tensor $P^{\mu\nu}(p)$. This yields:

$$P^{\mu\nu}(p) (\Delta_{\mu\nu}(p))^{-1} = \frac{3i}{G_C^M(p^2)}. \quad (3.57)$$

We thus find that the scalar dressing function $G_C^M(p^2)$ for any covariant gauge can be extracted in this manner. Now restricting ourselves to Landau gauge, we find the symbolic form for the photon propagator's equation of motion to be:

$$\frac{1}{G^M(p^2)} = \frac{1}{G^{M(0)}(p^2)} - \frac{e}{3} P^{\mu\nu}(p) \int \frac{d^4 q}{(2\pi)^4} \text{Tr}_{\text{Dirac}} \left[\gamma_\mu S^M(q-p) \Gamma_{\bar{\psi}(q-p)A_\nu(p)\psi(q)} S^M(q) \right] \quad (3.58)$$

As described in §3.3.1, the equations of motion will be truncated at the vertex level with either perturbative quantities or a model vertex which is proportional to the perturbative vertex and written as $ie\gamma_\nu V^M(q-p, q)$. This allows us to perform the trace over Dirac indices explicitly, to obtain:

$$\begin{aligned} \frac{1}{G^M(p^2)} = \frac{1}{G^{M(0)}(p^2)} - \frac{4ie^2}{3} \int \frac{d^4q}{(2\pi)^4} V^M(q-p, q) \left\{ 3\sigma_S^M((q-p)^2) \sigma_S^M(q^2) \right. \\ \left. - \left(4q^2 - 3q \cdot p + 2 \frac{(q \cdot p)^2}{p^2} \right) \sigma_V^M((q-p)^2) \sigma_V^M(q^2) \right\} \quad (3.59) \end{aligned}$$

We now perform the Wick rotation to obtain the Euclidean-space form for this equation of motion. All unlabeled four-momenta for the remaining discussion of QED are to be understood in Euclidean space. The effect on our dressing functions is found to be:

$$G^M(p_M^2) \rightarrow G^E(p^2) = -G^M(-p_M^2) \equiv G(p^2), \quad (3.60)$$

$$\sigma_{V,S}^M(p_M^2) \rightarrow \sigma_{V,S}^E(p^2) = -\sigma_{V,S}^M(-p_M^2) \equiv \sigma_{V,S}(p^2), \quad (3.61)$$

$$V^M(q_M - p_M, q_M) \rightarrow V^E(q^2, p^2, q \cdot p) = V^M(-q_M^2, -p_M^2, -q_M \cdot p_M) \equiv V(q-p, q), \quad (3.62)$$

which yields:

$$\begin{aligned} \frac{1}{G(p^2)} = \frac{1}{G^{(0)}(p^2)} + \frac{4e^2}{3} \int \frac{d^4q}{(2\pi)^4} V(q-p, q) \left\{ 3\sigma_S((q-p)^2) \sigma_S(q^2) \right. \\ \left. + \left(4q^2 - 3q \cdot p + 2 \frac{(q \cdot p)^2}{p^2} \right) \sigma_V((q-p)^2) \sigma_V(q^2) \right\} \quad (3.63) \end{aligned}$$

3.3.3 QED Interactions

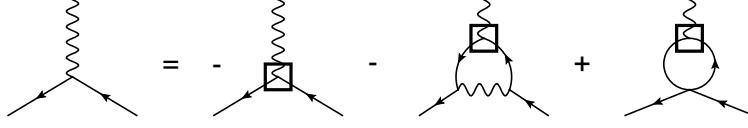


Figure 18: Electron-Photon Vertex Equation.

The equations of motion for electrons (3.48) and (3.49) and photons (3.63) which we consider here are to be truncated by introducing models for the electron-photon vertex. The perturbative truncation yields:

$$\Gamma_{\bar{\psi}A_{\mu}\psi}^{(0)} = ie\gamma_{\mu}, \quad (3.64)$$

which can be implemented in the equations of motion for the electron and photon propagators by choosing $V(q, p) = 1$.

The other truncation option we explore is to implement a vertex model for the electron-photon interaction based on the Ward-Takahashi Identities (WTIs)^[40,68] of QED. The appropriate WTI for this interaction is given by:

$$p^{\mu}\Gamma_{\mu}(q, k, p) = -e \left[S^{-1}(q) - S^{-1}(k) \right], \quad (3.65)$$

where $p = q - k$. The vertex model^[7] based on this identity is known as the Ball-Chiu vertex. The simplest solution which satisfies this identity based on the longitudinal constraints was found to be:

$$\Gamma_{\text{BC}\mu}(q, k, p) = ie \left[\frac{A(q^2) + A(k^2)}{2} \gamma_{\mu} + \frac{\left(\frac{\not{q} + \not{k}}{2} \right) \left(A(q^2) - A(k^2) \right) + \left(B(q^2) - B(k^2) \right)}{q^2 - k^2} (q + k)_{\mu} \right]. \quad (3.66)$$

For the purposes of this work, we will only be retaining the leading term of this vertex model which is proportional to γ_μ , and will refer to this as the “Central Ball-Chiu” (CBC) vertex:

$$\Gamma_{\text{CBC}\mu}(q, k, p) = ie \frac{A(q^2) + A(k^2)}{2} \gamma_\mu. \quad (3.67)$$

This model can be introduced into the equations of motion for electron and photon propagators by choosing $V(q, p) = \frac{A(q^2) + A(p^2)}{2}$.

3.3.4 QED Renormalization

In order to renormalize the equations of motion for QED, Z-factors are introduced into the Lagrangian (3.30) by the substitutions:

$$\psi_0 \ (\bar{\psi}_0) \rightarrow Z_F^{\frac{1}{2}} \psi_r \ \left(Z_F^{\frac{1}{2}} \bar{\psi}_r \right), \quad (3.68)$$

$$Z_F m_0 \rightarrow Z_m m_r, \quad (3.69)$$

$$A_0 \rightarrow Z_A^{\frac{1}{2}} A_r, \quad (3.70)$$

where, as in ϕ^4 theory, we understand all prior unlabeled variables in our equations of motion for QED as having been bare quantities and all that follow as the renormalized ones.

In order to perform our renormalization of the photon equation (which exhibits quadratic divergences in our regularization scheme), it is necessary to introduce some means of absorbing this divergence into our renormalization factors. It has been explicitly demonstrated in QED^[41] that the introduction of a photon mass term into the Lagrangian, which we shall express as $\mathcal{L}_{\mu^2} = \frac{\mu_0^2}{2} A \cdot A$, and renormalize it with a mass Z-factor as described in §subsection:RenormalizationPractice. The introduction of a momentum cutoff regulator in the loop integrals of (3.63) introduces mass-like terms into the dressed photon propagator,

and so the photon mass term serves only to cancel those contributions and restore the gauge-symmetry of the propagator. The renormalization of this mass term then follows according to:

$$Z_A \mu_0^2 \rightarrow Z_\mu \mu_r^2. \quad (3.71)$$

Finally, the field renormalization constants and unrenormalized charge e_0 represent another undetermined parameter of the theory. The vertex renormalization factor is thus defined as:

$$Z_A^{\frac{1}{2}} Z_f e_0 \rightarrow Z_e e. \quad (3.72)$$

The approach to determining these renormalization factors follows the general description of §3.1.3. The Z-factors defined in (3.68)-(3.71) are determined by fixing the values of A , B , or G at appropriate external momentum scales.

Since we are not considering the Schwinger-Dyson equation for the electron-photon vertex, we will not be explicitly determining the vertex Z-factor (3.72). For the computations described here, we choose to absorb the factor Z_e into the definition of the coupling e .

As shown in our discussion of the renormalization strategy in §3.1.3, we will determine these Z-factors such that they naturally introduce momentum subtraction terms into the loop integrals of (3.48), (3.49), and (3.63). If we schematically represent the equations of motion as:

$$A(p^2) = Z_F - I_A(p^2), \quad (3.73)$$

$$B(p^2) = Z_m m + I_B(p^2), \quad (3.74)$$

$$\frac{1}{G(p^2)} = Z_A p^2 + Z_\mu \mu^2 + I_G(p^2), \quad (3.75)$$

then we obtain for the renormalized forms:

$$A(p^2) = A(\mu_F^2) - (I_A(p^2) - I_A(\mu_F^2)) , \quad (3.76)$$

$$B(p^2) = B(\mu_F^2) + (I_B(p^2) - I_B(\mu_F^2)) , \quad (3.77)$$

$$\begin{aligned} \frac{1}{G(p^2)} &= \left(\frac{p^2 - \mu_2^2}{\mu_1^2 - \mu_2^2} \right) \frac{1}{G(\mu_1^2)} + \left(\frac{\mu_1^2 - p^2}{\mu_1^2 - \mu_2^2} \right) \frac{1}{G(\mu_2^2)} \\ &+ \left[I_G(p^2) - \left(\frac{p^2 - \mu_2^2}{\mu_1^2 - \mu_2^2} \right) I_G(\mu_1^2) - \left(\frac{\mu_1^2 - p^2}{\mu_1^2 - \mu_2^2} \right) I_G(\mu_2^2) \right] . \end{aligned} \quad (3.78)$$

3.3.5 Results

A sample of nonperturbative results for QED are shown in Figure 19, which were obtained with $e^2 = 1$ and renormalization conditions of $A(9 \text{ GeV}^2) = 1.1$, $B(9 \text{ GeV}^2) = .11$, $G(.01 \text{ GeV}^2) = 100$, and $G(9 \text{ GeV}^2) = \frac{4}{30}$. Since QED features a coupling which approaches the perturbative value in the IR (unlike QCD, which features asymptotic freedom in the UV regime), we arrange for these renormalization conditions to approach perturbation theory at low momentum. In particular, we emphasize that the photon propagator $G(p^2) \propto \frac{1}{p^2}$ at our IR external scale. Surprisingly, the photon propagator we obtain features the general shape of the decoupling (IR-finite) solutions for gluons in QCD. While it may be argued that this is due to the introduction of an (unphysical) bare photon mass term into the theory, we acknowledge that previous treatments^[41] demonstrate that such modifications can still respect the U(1) gauge symmetry in the dressed theory. In order to demonstrate that the renormalization was successful, the plots of Figure 19 are shown with two different sets of momentum grid points, $N_q = 40$ and $N_q = 80$. We observe that the photon solution and the electron dressing function $B(p^2)$ are stable under the variation in grid size, while the electron dressing function $A(p^2)$ seems to demonstrate dependence on the grid spacing in

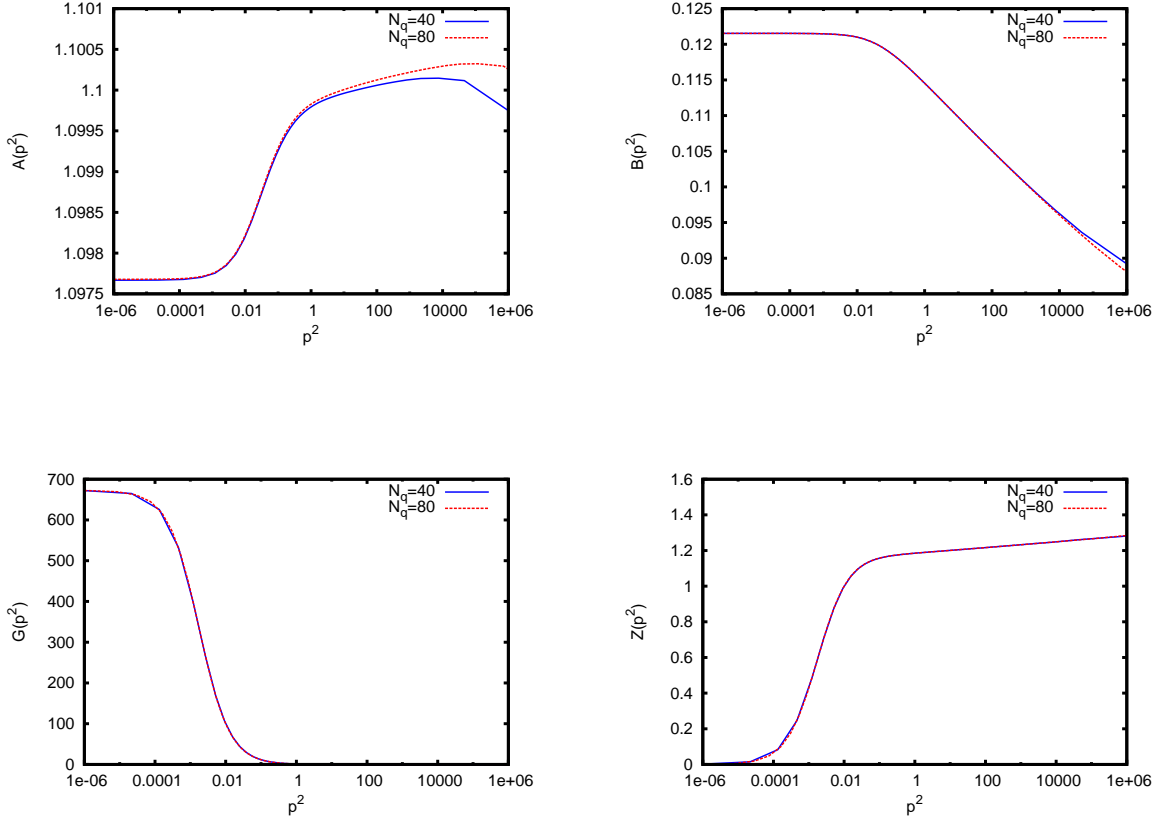


Figure 19: Plot of the electron propagator dressing functions A and B and the photon propagator dressing functions G and Z under a variation in momentum grid resolution. Solutions were obtained with $g^2 = 1$ and the set of toy model renormalization parameters shown in Table 2.

the UV. Recalling that QED is a low-momentum approximation to the Electroweak theory, we instead focus on the agreement of our various solutions in the IR and intermediate momentum regions. The observed consistency suggests that this is the proper behavior of the nonperturbative dressing functions in QED, and thus we aim to expand these techniques to investigations of QCD.

$A(9)$	1.1
$B(9)$.11
$G(.01)$	$\frac{1}{.01}$
$G(9)$	$\frac{1.2}{9}$

Table 2: Toy model renormalization parameters for the QED propagator functions of Figure 19.

3.4 QCD

Quantum Chromodynamics (QCD) consists of a fermion theory describing quarks and an $SU(3)$ Yang-Mills theory describing gauge particles called gluons. QCD behaves according to the Lagrangian introduced as (1.1):

$$\mathcal{L}_{\text{QCD}} = -\frac{1}{2}\text{Tr}_{SU(3)} [F_{\mu\nu}F^{\mu\nu}] + \bar{\psi}(i\not{D} - m)\psi + \mathcal{L}_{\text{gauge}} + \mathcal{L}_{\text{gh}}, \quad (1.1)$$

where:

$$A_\mu = T^A A_\mu^A \quad (3.79)$$

$$F_{\mu\nu} = D_\mu A_\nu - D_\nu A_\mu, \quad (3.80)$$

$$D_\mu = \partial_\mu + ig_s T^A A_\mu^A. \quad (3.81)$$

The fundamental degrees of freedom are the quark and gluon fields, $\psi(\bar{\psi})$ and A . The defining gauge symmetry of QCD is $SU_{\text{Color}}(3)$, which results in 3 color charge values for the quark sector and 8 color charge values for the Yang-Mills sector. These color charges are defined using the traceless 3×3 Gell-Mann matrices $T^A \equiv \frac{\lambda^A}{2}$ in the fundamental representation. The properties of these matrices which will be used here are^[44]:

$$[T^A, T^B] = if^{ABC}T^C \quad (3.82)$$

$$\text{Tr} [T^A T^B] = \frac{\delta^{AB}}{2} \quad (3.83)$$

$$f^{CDA} f^{CDB} = C_A \delta^{AB} \quad (3.84)$$

$$f^{DEA} f^{DFB} f^{EFC} = \frac{C_A}{2} f^{ABC} \quad (3.85)$$

$$f^{ACD} f^{BEF} f^{CEG} f^{DFG} = \frac{C_A^2}{2} \delta^{AB} \quad (3.86)$$

$$C_F = \frac{N_C^2 - 1}{2N_C} = \frac{4}{3} \quad (3.87)$$

$$C_A = N_C = 3 \quad (3.88)$$

The theory will be considered here in covariant gauge, specifically the Landau gauge. This gauge fixing is accomplished by introducing a gauge term (1.5) into the Lagrangian:

$$\text{covariant : } \mathcal{L}_{\text{gauge}} = -\lambda \text{Tr}_{\text{SU}(3)} [(\partial \cdot A)^2], \quad (1.5)$$

which produces the desired form for a general covariant gauge. Landau gauge is obtained by taking the limit $\lambda \rightarrow \infty$ once the equations of motion are defined. The equations of motion are obtained through functional derivatives of the Schwinger-Dyson master equations, which are shown in Figures 20–22.

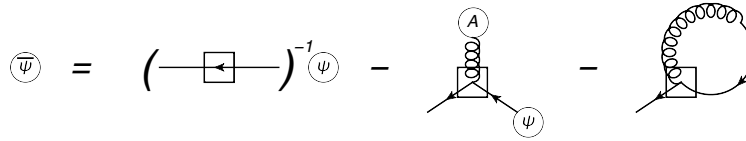


Figure 20: Quark Schwinger-Dyson Master Equation

Figure 21: Ghost Schwinger-Dyson Master Equation

Figure 22: Gluon Schwinger-Dyson Master Equation

3.4.1 Quark Sector

Treating the quark fields first, we obtain the gap equation (also shown diagrammatically in Figure 23):

$$S^{M^{-1}}(p) = -i(\not{p} - m) - g_s T^A \int \frac{d^4 q}{(2\pi)^4} \Gamma_{\bar{\psi}(p) A \psi(q-p)}^A \psi(q) S^M(q) \gamma_\mu P^{\mu\nu}(q-p) G^M(q-p). \quad (3.89)$$

This is cast into scalar integrals using the ansatz $S^{M^{-1}}(p) = -i\delta_{ab}(A^M(p^2)\not{p} - B^M(p^2))$. For convenience in expressing the involvement of quark propagators inside of loop integrals, we introduce the functions:

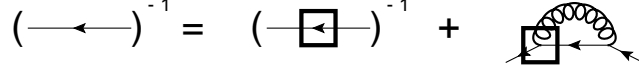
$$(\overrightarrow{\hspace{1.5cm}})^{-1} = (\overrightarrow{\hspace{1.5cm}} \boxed{\hspace{1.5cm}})^{-1} + \boxed{\hspace{1.5cm}} \overrightarrow{\hspace{1.5cm}}$$


Figure 23: Quark Gap Equation

$$\begin{aligned}\sigma_V^M(p^2) &\equiv \frac{A^M(p^2)}{A^{M^2}(p^2)p^2 - B^{M^2}(p^2)}, \\ \sigma_S^M(p^2) &\equiv \frac{B^M(p^2)}{A^{M^2}(p^2)p^2 - B^{M^2}(p^2)}.\end{aligned}\tag{3.90}$$

In order to extract our scalar functions from the quark gap equation, we observe that $A^M(p^2) = \frac{i}{12p^2} \text{Tr}_{\text{Dirac, SU}(3)} [\not{p} S^{M^{-1}}(p)]$ and $B^M(p^2) = \frac{-i}{12} \text{Tr}_{\text{Dirac, SU}(3)} [S^{M^{-1}}(p)]$. Applying these projectors, we obtain:

$$\begin{aligned}A^M(p^2) = \\ 1 - \frac{i}{12p^2} g_s \text{Tr}_{\text{SU}(3)} \left[T^A \int \frac{d^4 q}{(2\pi)^4} \text{Tr}_{\text{Dirac}} \left[\not{p} \Gamma_{\bar{\psi}_{(p)} A_{(q-p)}^{\nu} \psi_{(q)}}^{(3)} S^M(q) \gamma^\mu \right] P_{\mu\nu}(q-p) G^M(q-p) \right],\end{aligned}\tag{3.91}$$

$$\begin{aligned}B^M(p^2) = \\ m + \frac{i}{12} g_s \text{Tr}_{\text{SU}(3)} \left[T^A \int \frac{d^4 q}{(2\pi)^4} \text{Tr}_{\text{Dirac}} \left[\Gamma_{\bar{\psi}_{(p)} A_{(q-p)}^{\nu} \psi_{(q)}}^{(3)} S^M(q) \gamma^\mu \right] P_{\mu\nu}(q-p) G^M(q-p) \right].\end{aligned}\tag{3.92}$$

As we will see in §3.4.3, the truncations and vertex models we will consider for the quark-gluon interaction are all proportional to the perturbative vertex. We can thus perform the traces to find:

$$A^M(p^2) = 1 + \frac{i}{3p^2} g_s^2 \text{Tr}_{\text{SU}(3)} [T^A T^A] \int \frac{d^4 q}{(2\pi)^4} \sigma_V^M(q^2) G^M((q-p)^2) V_q^M(q, p) \times \left(\frac{2q^2 p^2 + 4(p \cdot q)^2 - 3(p^2 + q^2) p \cdot q}{q^2 + p^2 - 2q \cdot p} \right), \quad (3.93)$$

$$B^M(p^2) = m - i g_s^2 \text{Tr}_{\text{SU}(3)} [T^A T^A] \int \frac{d^4 q}{(2\pi)^4} \sigma_S^M(q^2) G^M((q-p)^2) V_q^M(q, p), \quad (3.94)$$

where $V_q^M(q, p)$ will be determined by the choice of truncation or model.

In order to obtain expressions in Euclidean space, we perform the conventional Wick rotation. For the remaining discussions of the quark sector, any unmarked momenta are to be understood as Euclidean 4-vectors. We observe:

$$A^M(p_M^2) \rightarrow A^E(p^2) = A^M(-p_M^2) \equiv A(p^2), \quad (3.95)$$

$$B^M(p_M^2) \rightarrow B^E(p^2) = B^M(-p_M^2) \equiv B(p^2), \quad (3.96)$$

$$\sigma_{V,S}^M(p_M^2) \rightarrow \sigma_{V,S}^E(p^2) = -\sigma_{V,S}^M(-p_M^2) \equiv \sigma_{V,S}(p^2), \quad (3.97)$$

$$G^M(p_M^2) \rightarrow G^E(p^2) = -G^M(-p_M^2) \equiv G(p^2), \quad (3.98)$$

$$V_q^M(q_M, p_M) \rightarrow V_q^E(q^2, p^2, q \cdot p) = V_q^M(-q_M^2, -p_M^2, -q_M \cdot p_M) \equiv V_q(q, p). \quad (3.99)$$

Our quark gap equations can thus be expressed in terms of purely Euclidean variables, where we define $x \equiv \frac{p \cdot q}{|p| |q|}$ as discussed in §3.1.1. Thus:

$$A(p^2) = 1 - \frac{4}{3} g_s^2 \int \frac{d^4 q}{(2\pi)^4} \sigma_V(q^2) G((q-p)^2) V_q(q, p) \left(\frac{2 + 4x^2 - 3x \left(\frac{p}{q} + \frac{q}{p} \right)}{q^2 + p^2 - 2qpx} \right), \quad (3.100)$$

$$B(p^2) = m + 4g_s^2 \int \frac{d^4 q}{(2\pi)^4} \sigma_S(q^2) G((q-p)^2) V_q(q, p). \quad (3.101)$$

$$(\text{dotted line with arrow})^{-1} = (\text{dotted line with arrow and a square box})^{-1} + \text{diagram with a square box and a wavy line loop}$$

Figure 24: Ghost Gap Equation

3.4.2 Yang-Mills Sector

3.4.2.1 Ghosts The SU(3) gauge invariance (as shown by the method of Faddeev and Popov^[26]) demands that the ghost fields be included. In any covariant gauge, one must add to the Lagrangian a term (1.6) given by:

$$\mathcal{L}_{\text{gh}} = -\bar{c}_A \left(\delta_{AB} \square + f_{ACB} A_C \cdot \partial \right) c_B \quad (1.6)$$

The gap equation for the ghost field is (also shown diagrammatically in Figure 24):

$$\begin{aligned} H^{M-1AB}(p^2) &= -ip^2 \delta^{AB} \\ &+ g_s f_{ECB} \int \frac{d^4 q}{(2\pi)^4} \Gamma_{\bar{c}_{(p)}^A A_{\mu_{(q-p)}^C} c_{(q)}^D} \delta^{DE} H^M(q) P^{\mu\nu}(q-p) G^M((q-p)^2) q^\nu, \end{aligned} \quad (3.102)$$

The perturbative propagator can be obtained from the first term of this equation, which yields:

$$H^{MAB}_{(0)}(p^2) = \frac{i\delta^{AB}}{p^2}, \quad (3.103)$$

while the dressed propagator has the form:

$$H^{MAB}(p^2) = i\delta^{AB} H^M(p^2) = i\delta^{AB} \frac{h^M(p^2)}{p^2} \quad (3.104)$$

As we had for the quarks, we will note in §3.4.3 that all of the truncations and models we employ for the ghost-gluon vertex are proportional to their perturbative interaction. We are thus free to perform all tensor contractions to find:

$$H^{M-1AB}(p^2) = -ip^2\delta^{AB} + g_s^2 N_c \delta^{AB} \int \frac{d^4 q}{(2\pi)^4} H^M(q^2) G^M((q-p)^2) V_c^M(q, p) \left(\frac{p^2 q^2 - (p \cdot q)^2}{q^2 + p^2 - 2q \cdot p} \right). \quad (3.105)$$

We now perform the Wick rotation to obtain this gap equation in Euclidean space. For the remainder of our discussions of ghost gap equations, any reference to unmarked momenta should be understood as Euclidean 4-vectors. We make the observation:

$$H^M(p_M^2) \rightarrow H^E(p^2) = -H^M(-p_M^2) \equiv H(p^2), \quad (3.106)$$

$$h^M(p_M^2) \rightarrow h^E(p^2) = h^M(-p_M^2) \equiv h(p^2). \quad (3.107)$$

$$V_c^M(q_M, p_M) \rightarrow V_c^E(q^2, p^2, q \cdot p) = V_c^M(-q_M^2, -p_M^2, -q_M \cdot p_M) \equiv V_c(q, p) \quad (3.108)$$

The Euclidean space ghost gap equation is thus given by:

$$H^{-1}(p^2) = p^2 - g_s^2 N_c \int \frac{d^4 q}{(2\pi)^4} H(q^2) G((q-p)^2) V_c(q, p) \left(\frac{p^2 q^2 (1-x^2)}{q^2 + p^2 - 2qpx} \right). \quad (3.109)$$

We prefer to write the gap equation in terms of the dressing function $h(p^2)$, thus:

$$h^{-1}(p^2) = 1 - g_s^2 N_c \int \frac{d^4 q}{(2\pi)^4} h(q^2) G((q-p)^2) V_c(q, p) \left(\frac{1-x^2}{q^2 + p^2 - 2qpx} \right). \quad (3.110)$$

$$\begin{aligned}
(\text{wavy line with box})^{-1} &= (\text{wavy line with box})^{-1} + \text{gluon loop with box} - \text{ghost loop with box} + \text{gluon loop with ghost line} \\
&+ \text{ghost loop with gluon line} + \text{gluon loop} - \text{ghost loop}
\end{aligned}$$

Figure 25: Gluon Gap Equation

3.4.2.2 Gluons We will consider the gluon field in the covariant gauges. First, we obtain the free field propagators from the terms in the Lagrangian

$$\text{Covariant gauge : } \Delta_{\mu\nu}^{(0)AB}(p) = \frac{(-i)\delta^{AB} \left(g_{\mu\nu} + \frac{1-\lambda}{\lambda} \frac{p_\mu p_\nu}{p^2} \right)}{p^2 - \mu^2 + i\epsilon} \quad (3.111)$$

$$\text{Feynman gauge : } \Delta_{\mu\nu}^{(0)AB}(p) = \frac{(-i)\delta^{AB} g_{\mu\nu}}{p^2 - \mu^2 + i\epsilon} \quad (3.112)$$

$$\begin{aligned}
\text{Landau gauge : } \Delta_{\mu\nu}^{(0)AB}(p) &= \frac{(-i)\delta^{AB} \left(g_{\mu\nu} - \frac{p_\mu p_\nu}{p^2} \right)}{p^2 - \mu^2 + i\epsilon} \\
&\equiv (-i)\delta^{AB} \frac{P_{\mu\nu}(p)}{p^2 - \mu^2 + i\epsilon}
\end{aligned} \quad (3.113)$$

While the dressed propagators become:

$$\text{Covariant gauge : } \Delta_{\mu\nu}^{AB}(p) = (-i)\delta^{AB} \left[P_{\mu\nu}(p)G_C^M(p^2) + \frac{1}{\lambda} \frac{p_\mu p_\nu}{p^4} \right] \quad (3.114)$$

$$\text{Feynman gauge : } \Delta_{\mu\nu}^{AB}(p) = (-i)\delta^{AB} \left[P_{\mu\nu}(p)G_F^M(p^2) + \frac{p_\mu p_\nu}{p^4} \right] \quad (3.115)$$

$$\text{Landau gauge : } \Delta_{\mu\nu}^{AB}(p) = (-i)\delta^{AB} P_{\mu\nu}(p)G^M(p^2) \equiv (-i)\delta^{AB} P_{\mu\nu}(p) \frac{Z^M(p^2)}{p^2} \quad (3.116)$$

This equation features more terms than either the quarks or ghosts, so we will represent the diagrams of Figure 25 in schematic form, with the labels corresponding to the loop diagrams in the order shown:

$$\begin{aligned} (\Delta_{\mu\nu}^{AB}(p))^{-1} = & \left(\Delta_{\mu\nu}^{(0)AB}(p) \right)^{-1} - \left((G_1^M)_{\mu\nu}^{AB} + (G_2^M)_{\mu\nu}^{AB} - (G_3^M)_{\mu\nu}^{AB} - (G_4^M)_{\mu\nu}^{AB} \right. \\ & \left. + (G_{\text{Sunset}}^M)_{\mu\nu}^{AB} + (G_{\text{Squint}}^M)_{\mu\nu}^{AB} \right) \end{aligned} \quad (3.117)$$

Since we intend to work primarily in Landau gauge, we will extract the scalar dressing function for the gluon propagator. First, in general covariant gauge we have

$$(\Delta_{\mu\nu}^{AB}(p))^{-1} = \frac{i\delta^{AB}}{G_C^M(p^2)} \left(g_{\mu\nu} + (\lambda p^2 G_C^M(p^2) - 1) \frac{p_\mu p_\nu}{p^2} \right). \quad (3.118)$$

We eliminate the Lorentz indices by contracting both sides with $P^{\mu\nu}(p)$. Tracing over color indices, we then obtain:

$$\text{Tr}_{\text{SU}(3)} \left[P^{\mu\nu}(p) (\Delta_{\mu\nu}^{AB}(p))^{-1} \right] = \frac{24i}{G_C^M(p^2)}, \quad (3.119)$$

which tells us that the scalar dressing function $G_C(p^2)$ for any covariant gauge can be extracted by this method. We thus conclude that the Landau gauge gap equation would be given by

$$\frac{i}{G^M(p^2)} = \frac{i}{G^{M(0)}(p^2)} - \frac{1}{24} \text{Tr}_{\text{SU}(3)} \left[P^{\mu\nu}(p) (G_1^M + G_2^M - G_3^M - G_4^M + G_{\text{Sunset}}^M + G_{\text{Squint}}^M)_{\mu\nu}^{AB} \right], \quad (3.120)$$

where all of the G_i which contribute to vacuum polarization are considered explicitly in Landau gauge.

We will present each diagram in two symbolic forms, one comprised of the tensors which appear from application of the nonperturbative diagrammatic rules, and one containing the symbolic results of carrying out the contractions of all indices. Both forms are to be understood in Euclidean space, as all factors pertaining to Wick rotation have already been taken into account. Simplifying our notation, we introduce the following definitions in Euclidean space and are to now understand all unmarked momenta as Euclidean 4-vectors. We observe:

$$G^M(p_M^2) \rightarrow G^E(p^2) = -G^M(-p_M^2) \equiv G(p^2), \quad (3.121)$$

$$G_i^M(p_M^2) \rightarrow G_i^E(p^2) = \frac{-i}{24} G_i^M(-p_M^2) \equiv G_i(p^2). \quad (3.122)$$

This results in our general form for the Euclidean equation of motion for the gluon propagator:

$$\frac{1}{G(p^2)} = \frac{1}{G^{(0)}(p^2)} + \text{Tr}_{\text{SU}(3)} \left[P^{\mu\nu}(p) (G_1 + G_2 - G_3 - G_4 + G_{\text{Sunset}} + G_{\text{Squint}})_{\mu\nu}^{AB} \right], \quad (3.123)$$

where for convenience we have absorbed the factor $\frac{1}{24}$ from (3.119) into the definition of the Euclidean G_i . As with the other fields, our gap equation can be expressed in terms

of purely Euclidean momentum variables. Since the general gluon equation features the nonperturbative two-loop diagrams G_{Sunset} and G_{Squint} , it is necessary to introduce a second loop variable k_μ . We thus define the orientation with respect to p_μ via $y \equiv \frac{p \cdot k}{|p| |k|}$, and the projection on q_μ according to $w \equiv \frac{q \cdot k}{|q| |k|}$, both as described in §3.1.1.

For brevity, we will also employ the shorthand $G_i \equiv \text{Tr}_{\text{SU}(3)} \left[P^{\mu\nu}(p) (G_i)_{\mu\nu}^{AB} \right]$. The contributions to vacuum polarization from each of the diagrams is thus:

$$G_1 = \left(\frac{1}{2} \right) \left(\frac{1}{24} \right) g_s^2 \text{Tr}_{\text{SU}(3)} [F_{ABCC}] \int \frac{d^4 q}{(2\pi)^4} P^{\mu\nu}(p) P^{\alpha\beta}(q) V^{\mu\nu\alpha\beta} G(q^2) \quad (3.124)$$

$$= \frac{g_s^2 N_C}{3} \int \frac{d^4 q}{(2\pi)^4} (7 - x^2) G(q^2), \quad (3.125)$$

$$G_2 = \left(\frac{1}{2} \right) \left(\frac{1}{24} \right) g_s^2 \text{Tr}_{\text{SU}(3)} [f_{ACD} f_{BCD}] \int \frac{d^4 q}{(2\pi)^4} G(q^2) G((q-p)^2) P^{\mu\nu}(p) P^{\alpha\beta}(q) P^{\gamma\delta}(q-p) \\ V_{\mu\alpha\gamma}(p, -q, q-p) V_{\nu\beta\delta}(-p, -q+p, q) \quad (3.126)$$

$$= -\frac{2g_s^2 N_C}{3} \int \frac{d^4 q}{(2\pi)^4} G(q^2) G((q-p)^2) \\ \times \left(\frac{3p^4 + 3q^4 - 6p^3 q x - 6p q^3 x + p^2 q^2 (8 + x^2)}{p^2 + q^2 - 2p q x} \right) (1 - x^2), \quad (3.127)$$

$$G_3 = \left(\frac{1}{24} \right) g_s^2 \text{Tr}_{\text{SU}(3)} [T^A T^B] \int \frac{d^4 q}{(2\pi)^4} P^{\mu\nu}(p) \text{Tr}_{\text{Dirac}} [\gamma_\mu S(q-p) \gamma_\nu S(q)] \quad (3.128)$$

$$= \frac{g_s^2 N_C C_F}{6} \int \frac{d^4 q}{(2\pi)^4} \left[3\sigma_S((q-p)^2) \sigma_S(q^2) \right. \\ \left. + \left(q^2 (1 + 2x^2) - 3q p x \right) \sigma_V((q-p)^2) \sigma_V(q^2) \right], \quad (3.129)$$

$$G_4 = - \left(\frac{1}{24} \right) g_s^2 \text{Tr}_{\text{SU}(3)} [f_{ACD} f_{BCD}] \int \frac{d^4 q}{(2\pi)^4} \frac{h(q^2)}{q^2} \frac{h((q-p)^2)}{(q-p)^2} (q-p)_\mu P^{\mu\nu}(p) q_\nu \quad (3.130)$$

$$= - \frac{g_s^2 N_C}{3} \int \frac{d^4 q}{(2\pi)^4} h(q^2) h((q-p)^2) \frac{1-x^2}{q^2 + p^2 - 2qpx}, \quad (3.131)$$

$$G_{\text{Sunset}} = - \left(\frac{1}{6} \right) \left(\frac{1}{24} \right) g_s^4 \text{Tr}_{\text{SU}(3)} [F_{ACDE} F_{BCDE}] \int \frac{d^4 q}{(2\pi)^8} G(q^2) G(k^2) G((p-q-k)^2) \\ P^{\mu\nu}(p) P^{\alpha\alpha'}(k) P^{\beta\beta'}(p-q-k) P^{\gamma\gamma'}(q) \\ V_{\mu\alpha\beta\gamma} V_{\nu\alpha'\beta'\gamma'} \quad (3.132)$$

$$= - \left(\frac{1}{12} \right) g_s^4 N_C^2 \int \frac{d^4 q}{(2\pi)^8} G(q^2) G(k^2) G((p-q-k)^2) \quad (3.133)$$

$$\times 2 \left[q^2 (11 + x^2 + w^2(1 + x^2) + 4wxy) \right. \\ + k^2 (11 + y^2 + w^2(1 + y^2) + 4wxy) \\ + qk (w(23 + 2x^2 + 2y^2 + w^2) + xy(3 + 5w^2)) \\ - pq (23x + x^3 + 3wy + 5wx^2y + 2w^2x + 2xy^2) \\ - pk (23y + y^3 + 3wx + 5wxy^2 + 2w^2y + 2x^2y) \\ \left. + p^2 (11 + x^2 + y^2 + x^2y^2 + 4wxy) \right] \\ \times \left[\frac{1}{p^2 + k^2 + q^2 - 2kpy - 2qpx + 2qkw} \right]. \quad (3.134)$$

$$\begin{aligned}
G_{\text{Squint}} &= - \left(\frac{1}{2} \right) \left(\frac{1}{24} \right) g_s^4 \text{Tr}_{\text{SU}(3)} [F_{ACED} f_{DEF} f_{BCF}] \\
&\quad \times \int \frac{d^4 q}{(2\pi)^8} \frac{d^4 k}{(2\pi)^8} G(q^2) G(k^2) G((q+k)^2) G((p-q-k)^2) \\
&\quad P^{\mu\nu}(p) P^{\alpha\alpha'}(k) P^{\beta\beta'}(q) P^{\gamma\gamma'}(q+k) P^{\delta\delta'}(p-q-k) \\
&\quad V_{\mu\delta\alpha\beta} V_{\beta'\alpha'\gamma}(-q, -k, k+q) V_{\nu\delta'\gamma'}(p, k+q-p, -k-q) \quad (3.135) \\
&= - \frac{g_s^4 N_C^2}{4} \int \frac{d^4 q}{(2\pi)^8} \frac{d^4 k}{(2\pi)^8} G(q^2) G(k^2) G((q+k)^2) G((p-q-k)^2) \\
&\quad \times 4 \left[q^6 (3 - 3x^2 - w^2(3 - x^2) + 2wxy) + k^6 (3 - 3y^2 - w^2(3 - y^2) + 2wxy) \right. \\
&\quad + q^5 k (13w(1 - w^2) - 3wx^2(3 - w^2) - 2xy(3 - 5w^2) + 2wy^2) \\
&\quad + qk^5 (13w(1 - w^2) - 3wy^2(3 - w^2) - 2xy(3 - 5w^2) + 2wx^2) \\
&\quad + q^4 k^2 (9 - 2x^2(3 - w^4) + w^2(7 - 16w^2) - 2wxy(8 - 7w^2) - 3y^2(1 - 3w^2)) \\
&\quad + q^2 k^4 (9 - 2y^2(3 - w^4) + w^2(7 - 16w^2) - 2wxy(8 - 7w^2) - 3x^2(1 - 3w^2)) \\
&\quad + q^3 k^3 (2w(13 - 11w^2 - 2w^4) - 4xy(3 - w^4) - w(x^2 + y^2)(7 - 11w^2)) \\
&\quad - pq^5 (x(5 - 7w^2) - x^3(5 - w^2) + 2wy + 4wx^2y) \\
&\quad - pk^5 (y(5 - 7w^2) - y^3(5 - w^2) + 2wx + 4wxy^2) \\
&\quad - pq^4 k (2wx(5 - 8w^2) - wx^3(6 - w^2) + y(5 + w^2) - x^2y(15 - 13w^2) + 7wxy^2) \\
&\quad - pqk^4 (2wy(5 - 8w^2) - wy^3(6 - w^2) + x(5 + w^2) - xy^2(15 - 13w^2) + 7wx^2y) \\
&\quad + pq^3 k^2 (-2x(5 - 5w^2 - 2w^4) + x^3(5 - 7w^2) + 15xy^2 \\
&\quad - 4wy(3 - 2w^2) + wx^2y(16 - 7w^2) - 3wy^3 - 19w^2xy^2) \\
&\quad + pq^2 k^3 (-2y(5 - 5w^2 - 2w^4) + y^3(5 - 7w^2) + 15x^2y \\
&\quad - 4wx(3 - 2w^2) + wxy^2(16 - 7w^2) - 3wx^3 - 19w^2x^2y) \\
&\quad + p^2 q^4 (5 - x^2(5 - w^2) - 5w^2 + 4wxy) \\
&\quad + p^2 k^4 (5 - y^2(5 - w^2) - 5w^2 + 4wxy) \\
&\quad + p^2 q^3 k (12w(1 - w^2) - wx^2(6 - w^2) - 2xy(5 - 6w^2) + 3wy^2) \\
&\quad + p^2 qk^3 (12w(1 - w^2) - wy^2(6 - w^2) - 2xy(5 - 6w^2) + 3wx^2) \\
&\quad \left. + p^2 q^2 k^2 (10 - 2w^2(3 + 2w^2) - 2wxy(5 - 3w^2) - (x^2 + y^2)(5 - 7w^2)) \right] \\
&\quad \times \left[\frac{1}{(k^2 + q^2 + 2qkw)(p^2 + k^2 + q^2 - 2pky - 2pqx + 2qkw)} \right], \quad (3.136)
\end{aligned}$$

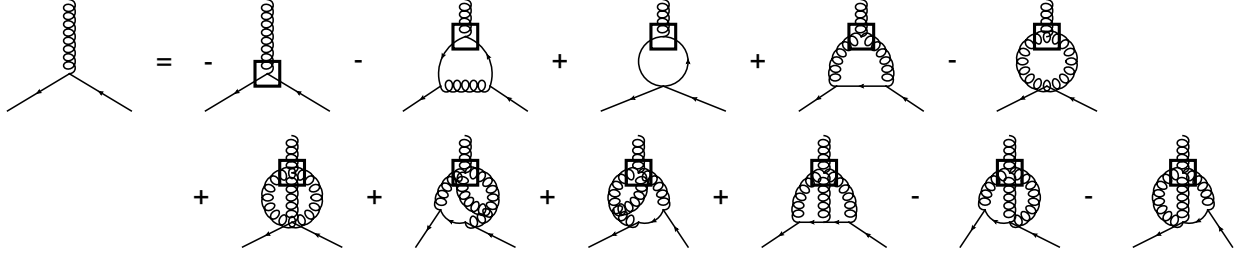


Figure 26: Quark-Gluon Vertex Equation

3.4.3 QCD Interactions

The Schwinger-Dyson equations for higher N -point 1PI correlation functions describe the interaction vertices present within QCD. As discussed in Section 2.3.3, we observe that these equations of motion couple to progressively higher interaction vertices of the nonperturbative quantum field theory. Figures 26–29 show the Schwinger-Dyson equations for the nonperturbative interactions of QCD which correspond to a dressing of one of the perturbative vertices (i.e. these are the only vertex equations which contain an inhomogeneous term given by one of the perturbative interactions). The solution of these vertex equations lies beyond the scope of this work, but recent efforts^[22,36] have begun including these equations into the coupled set of equations being solved.

The first interaction to consider is that of the quark-gluon vertex, whose Schwinger-Dyson equation is shown in Figure 26. The perturbative form of this equation is given by:

$$\Gamma_{\bar{\psi} A_{\mu}^A \psi}^{(0)} = ig_s T^A \gamma_{\mu}. \quad (3.137)$$

The vertex model we will consider is similar to the Ball-Chiu^[7] vertex of QED, and in fact, the original QED vertex model was explored in a paper published back-to-back with a second which explored the extension to QCD^[8]. As the QED Ball-Chiu vertex was designed to satisfy the (longitudinal) constraints of the Ward-Takahashi Identities (WTIs), we seek a generalization which satisfies the corresponding constraints of the Slavnov-Taylor Identities

(STIs) of QCD. Due to the influence of the Ball-Chiu model on nonperturbative studies of gauge symmetries in both QED and QCD, the generalizations considered in QCD will still be referred to as the “Ball-Chiu Vertex”. We will in fact be considering a set of closely related models [2,28,30] which differ by the extent to which the ghost dependence of the Slavnov-Taylor identity (3.138) has been considered in generalizing the original Ball-Chiu vertex model.

The appropriate Slavnov-Taylor identity to govern the quark-gluon vertex is given by:

$$p^\mu \Gamma_\mu^A(q, k, p) = -g_s T^A h(p) [S^{-1}(q) K_{\text{qc}}(q, k, p) - \overline{K}_{\text{qc}}(k, q, p) S^{-1}(k)], \quad (3.138)$$

where $p \equiv q - k$ is the gluon momentum and $K_{\text{qc}}(\overline{K}_{\text{qc}})$ refers to the quark-ghost scattering kernel (and adjoint). Treatment of the vertex appearing in this identity is made far more complicated than the case in QED due mainly to the influence of K_{qc} . The form for this vertex which will be used in the present study involves retaining only the “Central” term of the resulting Ball-Chiu (BC) vertex, which will be henceforth referred to as the “Central Ball-Chiu” (CBC) vertex:

$$\Gamma_{\text{CBC}\mu}^n(q, k, p) = ig_s T^A \gamma_\mu h^n(p^2) \frac{A(q) + A(k)}{2}, \quad (3.139)$$

where we allow the exponent of $h(p^2)$ to vary as a means of parametrizing the influence of ghost fields on the quark-gluon vertex. Choosing a value of $n = 1$ corresponds to neglecting the quark-ghost scattering kernel in 3.138 and having only the explicit dependence on $h(p^2)$ appear in the vertex model. We will find that a faithful replication of the lattice data is aided by considering a more significant influence of the ghost propagator, specifically the $n = 2$ form [2] for the vertex model as suggested by Aguilar & Papavassiliou. When introducing this vertex model into (3.100) and (3.101), we can now make the identification:

$$V_q(q, p) = h^n((q - p)^2) \frac{A(q^2) + A(p^2)}{2}, \quad (3.140)$$

and we note also that setting $V_q = 1$ would instead implement a truncation using only the perturbative vertex (3.137).

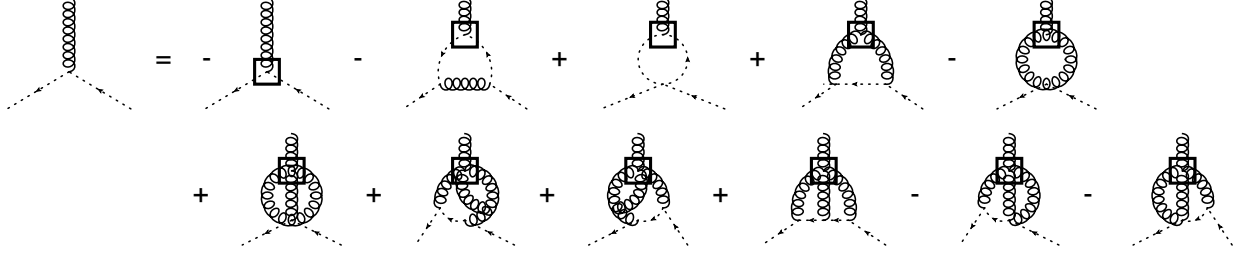


Figure 27: Ghost-Gluon Vertex Equation

The next interaction we consider is that of the ghost-gluon vertex, whose Schwinger-Dyson equation is shown in Figure 27. In its perturbative form, the interaction is given by:

$$\Gamma_{\bar{c}^A A_\mu^B c^C}^{(0)} = g_s f^{ABC} k_\mu, \quad (3.141)$$

where k corresponds to the incoming ghost momentum.

Modeling of the nonperturbative ghost-gluon interaction has also been considered by von Smekal, Hauck, and Alkofer^[67] who employed a direct treatment of the BRST invariance due to the lack of previous publication of the corresponding STI. They neglect the possibility of ghost-ghost scattering, and obtain:

$$\Gamma_\mu^{ABC}(q, k) = g_s f^{ABC} k_\mu \left(\frac{h(p^2)}{h(k^2)} + \frac{h(p^2)}{h(q^2)} - 1 \right), \quad (3.142)$$

where k is again the incoming ghost momentum, q is the outgoing ghost momentum, and $p = q - k$ is the incoming gluon momentum. Introducing this vertex model into (3.110) is accomplished by the identification of:

$$V_c(q, p) = \left(\frac{h((q-p)^2)}{h(q^2)} + \frac{h((q-p)^2)}{h(p^2)} - 1 \right), \quad (3.143)$$

while a choice of $V_c = 1$ would instead truncate the ghost equation with the perturbative vertex of (3.141).

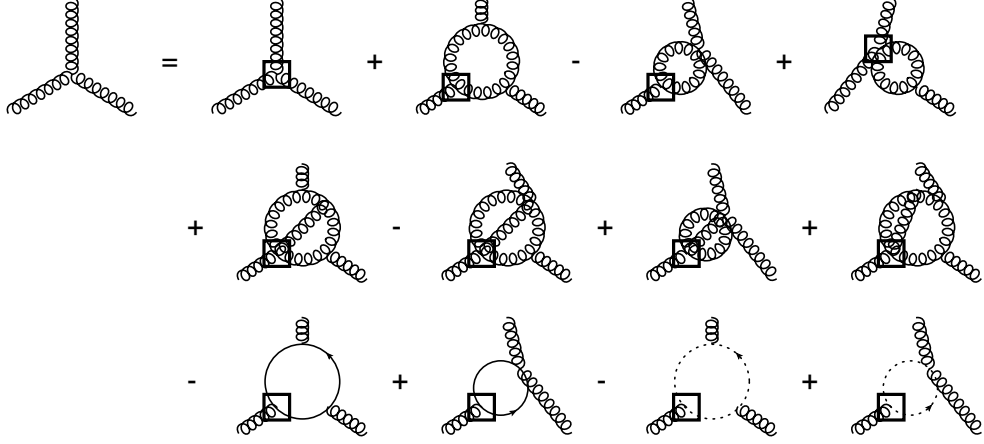


Figure 28: 3-Gluon Vertex Equation

Next we consider the 3-gluon vertex, whose Schwinger-Dyson equation is shown in Figure 28. The perturbative form of this interaction is given by:

$$\Gamma_{A_\alpha^A A_\beta^B A_\gamma^C}^{(0)}(p_1, p_2, p_3) = g_s f^{ABC} V_{\alpha\beta\gamma}(p_1, p_2, p_3) \quad (3.144)$$

$$= g_s f^{ABC} [g_{\alpha\beta}(p_2 - p_1)_\gamma + g_{\gamma\alpha}(p_1 - p_3)_\beta + g_{\beta\gamma}(p_3 - p_2)_\alpha], \quad (3.145)$$

where the momenta p_1 , p_2 , and p_3 are defined in the same cyclical order as the color and Lorentz indices.

The Slavnov-Taylor identities have also been used to build model vertices^[57,67] for the 3-gluon interaction. The appropriate STI for these models is given by:

$$p_3^\rho \Gamma_{\mu\nu\rho}(p_1, p_2, p_3) = -ih(p_3^2) \left[K_{cA}^\sigma(-p_3, p_2) P_{\sigma\nu}(p_2) \frac{p_2^2}{Z(p_2^2)} - K_{cA}^\sigma(-p_3, p_1) P_{\sigma\mu}(p_1) \frac{p_1^2}{Z(p_1^2)} \right], \quad (3.146)$$

where p_1 , p_2 , and p_3 are the four-momenta for each gluon leg, and $K_{cA}(\overline{K}_{cA})$ refers to the ghost-gluon scattering kernel.

The model developed by Pennington and Wilson^[57] is built by neglecting the contribution of the ghost-gluon scattering kernel in (3.146), and can be written in the form:

$$\Gamma^{\text{PW}}_{\mu\nu\rho}{}^{ABC}(p_1, p_2, p_3) = f^{ABC} \left[\tilde{A}_+(p_1^2, p_2^2; p_3^2) g_{\mu\nu}(p_2 - p_1)_\rho \text{ et cycl.} \right], \quad (3.147)$$

(where et cycl. implies two additional terms obtained by cyclic permutation of the Lorentz indices) with:

$$\tilde{A}_+(p_1^2, p_2^2; p_3^2) = \frac{h(p_3^2)}{2} \left(\frac{1}{Z(p_1^2)} + \frac{1}{Z(p_2^2)} \right) \quad (3.148)$$

Another model was developed by von Smekal, Hauck, and Alkofer^[67] which incorporates the ghost-gluon scattering kernel into (3.146) as it was obtained for their model of the ghost-gluon vertex (3.142). This vertex model can be written in the form:

$$\begin{aligned} \Gamma^{\text{vSHA}}_{\mu\nu\rho}{}^{ABC}(p_1, p_2, p_3) = f^{ABC} \left\{ \left[A_+(p_1^2, p_2^2; p_3^2) g_{\mu\nu}(p_2 - p_1)_\rho + A_-(p_1^2, p_2^2; p_3^2) g_{\mu\nu}(p_1 + p_2)_\rho \right. \right. \\ \left. \left. - 2 \frac{A_-(p_1^2, p_2^2; p_3^2)}{p_1^2 - p_2^2} (g_{\mu\nu} p_1 \cdot p_2 - p_{1\nu} p_{2\mu}) (p_2 - p_1)_\rho \right] \text{ et cycl.} \right\}, \end{aligned} \quad (3.149)$$

where:

$$A_\pm(p_1^2, p_2^2; p_3^2) = \frac{h(p_3^2)}{2} \left(\frac{h(p_2^2)}{h(p_1^2)Z(p_1^2)} \pm \frac{h(p_1^2)}{h(p_2^2)Z(p_2^2)} \right) \quad (3.150)$$

In the interest of our equations of motion for the propagators, and working specifically in Landau gauge, we recognize that each gluon leg of this vertex (either through internal lines or a transverse projector with respect to external momentum) will be acted upon by

a transverse projection tensor $P^{\alpha\beta}(p_i)$ with the momentum of that same leg. In the second term of the vertex model (3.149), we note that conservation of four-momentum tells us that $(p_1 + p_2) = -p_3$, and so:

$$P^{\rho'\rho}(p_3) (p_1 + p_2)_\rho = P^{\rho'\rho}(p_3) (-p_3)_\rho = 0.$$

Also, in the third term of this model vertex we observe the structure $p_{1\nu} p_{2\mu}$. Conservation of four-momentum tells us that $p_1 = -(p_2 + p_3)$ and $p_2 = -(p_1 + p_3)$. Thus:

$$\begin{aligned} P^{\mu'\mu}(p_1) P^{\nu'\nu}(p_2) [p_{1\nu} p_{2\mu}] &= P^{\mu'\mu}(p_1) P^{\nu'\nu}(p_2) [(p_2 + p_3)_\nu (p_1 + p_3)_\mu] \\ &= P^{\mu'\mu}(p_1) P^{\nu'\nu}(p_2) [p_{3\mu} p_{3\nu}], \end{aligned} \quad (3.151)$$

and so in Landau gauge the model vertex can be equivalently written as:

$$\begin{aligned} \Gamma_{\mu\nu\rho}^{\text{vSHA } ABC}(p_1, p_2, p_3) &= f^{ABC} \left\{ \left[A_+ (p_1^2, p_2^2; p_3^2) g_{\mu\nu} (p_2 - p_1)_\rho \right. \right. \\ &\quad \left. \left. - 2 \frac{A_- (p_1^2, p_2^2; p_3^2)}{p_1^2 - p_2^2} (g_{\mu\nu} p_1 \cdot p_2 - p_{3\nu} p_{3\mu}) (p_2 - p_1)_\rho \right] \text{ et cycl.} \right\}. \end{aligned} \quad (3.152)$$

We also consider an approximate form to this vertex model, in which we note that $h(p^2)$ and $Z(p^2)$ are $O(1)$ for wide ranges of momenta. As such, the assumption that $A_+ \gg A_-$ results in an approximate form for the interaction:

$$\Gamma_{\mu\nu\rho}^{\text{vSHA}' ABC}(p_1, p_2, p_3) = f^{ABC} \left\{ [A_+ (p_1^2, p_2^2; p_3^2) g_{\mu\nu} (p_2 - p_1)_\rho] \text{ et cycl.} \right\}. \quad (3.153)$$

Finally, we introduce a third 3-gluon interaction model, based on the analytic forms for the models discussed thus far. We consider also a “hybrid” interaction, which is similar to the Pennington-Wilson model but simply neglects the influence of the ghost dressing function:

$$\Gamma_{\mu\nu\rho}^{\text{hybrid } ABC}(p_1, p_2, p_3) = f^{ABC} \{ [A'_+(p_1^2, p_2^2; p_3^2) g_{\mu\nu}(p_2 - p_1)_\rho] \text{ et cycl.} \}. \quad (3.154)$$

with:

$$A'_+(p_1^2, p_2^2; p_3^2) = \frac{1}{2} \left(\frac{1}{Z(p_1^2)} + \frac{1}{Z(p_2^2)} \right) \quad (3.155)$$

The vertex models (3.147) and (3.153) have been introduced primarily for consideration in §4.3: [Glueballs](#). Our treatment in §3.4.5 and §3.4.6 of the equations of motion for the various propagators of QCD will tend not to employ vertex models for the gluon-self interactions (unless already included in published forms^[46,67] of the gluon equations we study).

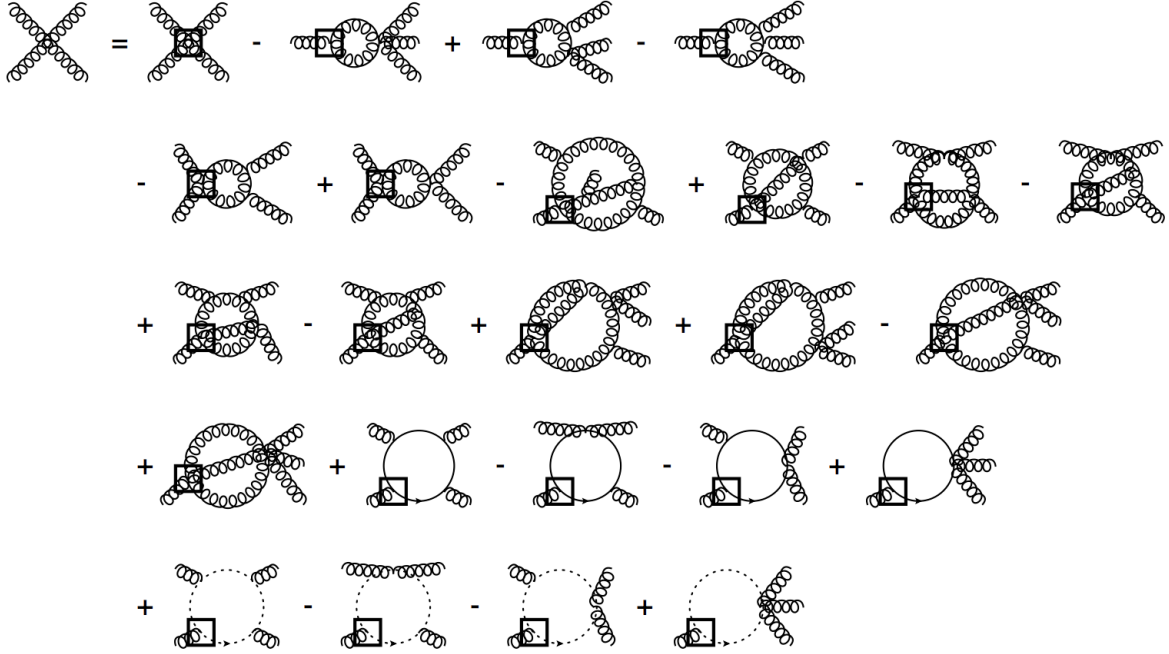


Figure 29: 4-Gluon Vertex Equation

The final interaction of QCD which corresponds to dressing a perturbative vertex is the 4-gluon interaction, whose equation of motion is shown in Figure 29. Any published efforts to model this vertex based on BRST invariance or well-established STIs are unknown to the author at this time. The inclusion of this vertex in Schwinger-Dyson equations as a non-perturbative entity has only recently been explored^[22]. For the purposes of our calculations here, we will make use of the perturbative form of the interaction, which is:

$$\Gamma_4^{(0)\alpha\beta\gamma\delta} = -ig_s^2 F_{ABCD} V^{\alpha\beta\gamma\delta} \quad (3.156)$$

$$\begin{aligned} &= -ig_s^2 \left[f_{iAB} f_{iCD} (g^{\alpha\gamma} g^{\beta\delta} - g^{\alpha\delta} g^{\beta\gamma}) \right. \\ &\quad + f_{iAC} f_{iDB} (g^{\alpha\delta} g^{\beta\gamma} - g^{\alpha\beta} g^{\gamma\delta}) \\ &\quad \left. + f_{iAD} f_{iBC} (g^{\alpha\beta} g^{\gamma\delta} - g^{\alpha\gamma} g^{\beta\delta}) \right]. \end{aligned} \quad (3.157)$$

3.4.4 QCD Renormalization

In order to renormalize the equations of motion for QCD, we introduce Z-factors into the Lagrangian (1.1). The factors introduced are defined as:

$$\psi_0 \ (\bar{\psi}_0) \rightarrow Z_F^{\frac{1}{2}} \psi_r \ \left(Z_F^{\frac{1}{2}} \bar{\psi}_r \right) \quad (3.158)$$

$$Z_F m_0 \rightarrow Z_m m_r \quad (3.159)$$

$$c_0 \ (\bar{c}_0) \rightarrow Z_c^{\frac{1}{2}} c_r \ \left(Z_c^{\frac{1}{2}} \bar{c}_r \right) \quad (3.160)$$

$$A_0 \rightarrow Z_A^{\frac{1}{2}} A_r \quad (3.161)$$

In addition to these renormalization factors, we introduce a bare gluon mass term $\frac{\mu_0^2}{2} A \cdot A$ into the Lagrangian as well, in an effort to formalize our ability to absorb and eliminate the

quadratic divergences we find in (3.123) (This is analogous to how we used the mass term in renormalizing the photon propagator in QED). This term is then renormalized according to:

$$Z_A \mu_0^2 \rightarrow Z_\mu \mu_r^2. \quad (3.162)$$

Finally, we acknowledge the introduction of Z-factors to each of the vertex terms of the Lagrangian. We define separate renormalization factors for each such coupling:.

$$Z_A^{\frac{1}{2}} Z_F g_0 \rightarrow Z_{g_F} g_F, \quad (3.163)$$

$$Z_A^{\frac{1}{2}} Z_c g_0 \rightarrow Z_{g_c} g_c, \quad (3.164)$$

$$Z_A^{\frac{3}{2}} g_0 \rightarrow Z_{g_{3A}} g_{3A}, \quad (3.165)$$

$$Z_A^2 g_0^2 \rightarrow Z_{g_{4A}} g_{4A}^2, \quad (3.166)$$

but note that they are constrained by the gauge symmetry of QCD^[66]. This symmetry requires that the definitions of (3.163)-(3.166) share only a single free parameter. The constraints can be expressed as:

$$\left(\frac{Z_{g_F} g_F}{Z_F} \right)^2 = \left(\frac{Z_{g_c} g_c}{Z_c} \right)^2 = \left(\frac{Z_{g_{3A}} g_{3A}}{Z_A} \right)^2 = \frac{Z_{g_{4A}} g_{4A}^2}{Z_A}. \quad (3.167)$$

The general approach to determining these factors again relies on the general approach as laid out in §3.1.3. Each Z-factor of (3.158)-(3.162) is determined by fixing the value of one of the scalar dressing functions A , B , h , or G at appropriate external momentum scales. For our treatment of QCD, we choose these values to agree with the scales used in lattice

studies^[15,16] of the same propagator functions, and so we can identify the units of these momentum scales and dressing functions as indicated in the plots of our results.

Determination of the vertex Z-factors (3.163)-(3.166) lies beyond the scope of the truncated set of Schwinger-Dyson equations which we are considering here. It is the author's opinion that renormalization of the vertices through their own equations of motion is the appropriate procedure for determining these factors in a way which is most consistent with (3.167). For the present treatment, we choose to absorb each vertex factor Z_{g_i} into the definition of its corresponding coupling g_i , and evaluate our equations of motion with independent inputs for each coupling with the exception of holding $g_{3A}^2 = g_{4A}^2$.

The result of our renormalization strategy is that the Z_i naturally introduce momentum subtractions, each of which serves to absorb a divergence which results from the loop integrals of Figures 23-25, and is as a result determined by one of the computation's input parameters.

If we represent the gap equations schematically as:

$$A(p^2) = Z_F - I_A(p^2), \quad (3.168)$$

$$B(p^2) = Z_m m + I_B(p^2), \quad (3.169)$$

$$\frac{1}{h(p^2)} = Z_c - I_h(p^2), \quad (3.170)$$

$$\frac{1}{G(p^2)} = Z_A p^2 + Z_\mu \mu^2 + \sum_i G_i(p^2), \quad (3.171)$$

then we obtain for the renormalized equations:

$$A(p^2) = A(\mu_F^2) - (I_A(p^2) - I_A(\mu_F^2)), \quad (3.172)$$

$$B(p^2) = B(\mu_F^2) + (I_B(p^2) - I_B(\mu_F^2)), \quad (3.173)$$

$$\frac{1}{h(p^2)} = \frac{1}{h(\mu_c^2)} - (I_h(p^2) - I_h(\mu_c^2)), \quad (3.174)$$

$$\begin{aligned} \frac{1}{G(p^2)} &= \left(\frac{p^2 - \mu_2^2}{\mu_1^2 - \mu_2^2} \right) \frac{1}{G(\mu_1^2)} + \left(\frac{\mu_1^2 - p^2}{\mu_1^2 - \mu_2^2} \right) \frac{1}{G(\mu_2^2)} \\ &+ \sum_i \left[G_i(p^2) - \left(\frac{p^2 - \mu_2^2}{\mu_1^2 - \mu_2^2} \right) G_i(\mu_1^2) - \left(\frac{\mu_1^2 - p^2}{\mu_1^2 - \mu_2^2} \right) G_i(\mu_2^2) \right]. \end{aligned} \quad (3.175)$$

The set of parameters chosen for the various couplings g_i serve as a means to evaluate how successfully the gauge invariance of our solutions has been maintained, by proxy of a comparison in the context of (3.167).

3.4.5 Truncation Examples

3.4.5.1 Swimming with Quarks Pennington's *Swimming with Quarks*^[58] considers a presentation of QCD in which only the quark equations (3.100) and (3.101) are considered dynamically. The truncations imposed on these equations is to employ the perturbative gluon propagator and quark-gluon vertex, which can be included as:

$$G_{\text{SwQ}}(p^2) = G^{(0)}(p^2) = \frac{1}{p^2} \quad (3.176)$$

$$V_q(q, p) = 1 \quad (3.177)$$

The gap equations for this truncation allow all external momenta to be expressed through either the integration kernel or the perturbative gluon propagator. As such, all angular variables appear in well-defined analytical expressions, and thus the angular integrals can be carried out explicitly. Performing these integrals yields gap equations involving only a single integration:

$$A(p^2) = Z_F, \quad (3.178)$$

$$B(p^2) = Z_F m + \frac{g_F^2}{4\pi^2} \int ds' \sigma_S(s') \left[\Theta(s' - p^2) + \frac{s'}{p^2} \Theta(p^2 - s') \right], \quad (3.179)$$

where in Landau gauge we find that upon angular integration the self-energy contribution to (3.178) vanishes. As a result, we simply use the perturbative value of $A(p^2) = Z_F = 1$. The step functions can be used to assign integration bounds, which display the dependence on the external momentum p^2 in an easily accessible way.

$$B(p^2) = Z_F m + \frac{g_F^2}{4\pi^2} \left[\int_0^{p^2} ds' \frac{s'}{p^2} \sigma_S(s') + \int_{p^2}^{\infty} ds' \sigma_S(s') \right] \quad (3.180)$$

This form of the integrals can be used to obtain a differential form for the quark gap equation. By applying $\frac{d}{ds} \equiv \frac{d}{d(p^2)}$, we obtain the differential form:

$$\frac{d}{ds} \left(s^2 \frac{dB}{ds} \right) = -\frac{g_F^2}{4\pi^2} s \sigma_S(s) \quad (3.181)$$

We note especially that the quark's mass renormalization does not appear in this expression. This implies that both the bare and renormalized solutions to the gap equations obey the same differential equation, and are thus solutions within the same “family of curves” which exhibit this behavior. Substitution of (3.181) into (3.180) yields a set of boundary conditions for the solutions of the differential equation. These boundary conditions are:

$$\left[s^2 \frac{dB}{ds} \right]_{s=0} = 0 \quad (3.182)$$

$$\left[B(s) + s \frac{dB}{ds} - Z_F m \right]_{s \rightarrow \infty} = 0 \quad (3.183)$$

Our method of solving these differential forms is to perform a stepping operation in momentum space, generating the solution from a fixed value and slope at $p^2 = 0$. Due to the nature of the differential equation, we will find that the boundary condition at $s \rightarrow \infty$ is satisfied automatically. In order to prime our solution with the proper slope, we must examine the asymptotic solutions in the IR region. Making the assumptions that $s^2 \frac{d^2 B}{ds^2} \ll 2s \frac{dB}{ds}$, we obtain the asymptotic form of the differential equation:

$$\frac{dB}{ds} = -\frac{g_F^2}{8\pi^2} \frac{1}{B} \quad (3.184)$$

We can solve this equation for $B(s)$, which yields:

$$B(s) \stackrel{s \rightarrow 0}{\Rightarrow} \sqrt{B^2(0) - \frac{g_F^2}{4\pi^2} s} \quad (3.185)$$

The solution to this quark model can thus be solved in two ways, either through the iterative method described in §3.1 [Numerical Methods](#), or through a numerical differential equation solver. A comparison of the results from these two methods is shown in Figure 30, in which the differential solution was primed with the same value of $B(0)$ which was implemented in the renormalization of the integral equation. The agreement between these two forms demonstrates that the renormalization in this model is equivalent to selecting a specific solution out of the “family of curves” by an arbitrary choice of boundary conditions.

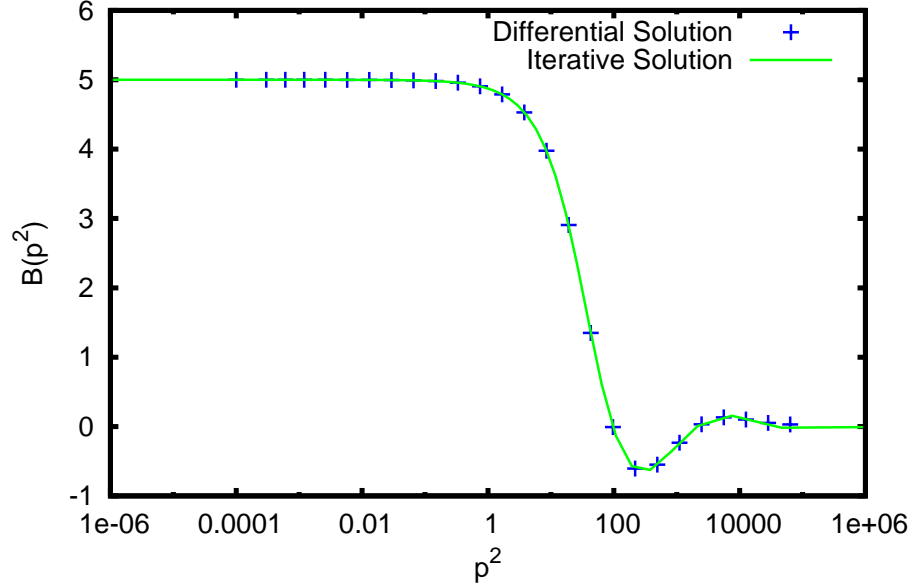


Figure 30: Comparison of solutions to the Swimming with Quarks^[58] model obtained through the integral form (3.180) and the differential form (3.184). Solutions were obtained with $g^2 = 50$ and toy model renormalization parameter (or boundary condition) $B(0) = 5$.

3.4.5.2 Fits to Lattice Gluons Another level of sophistication can be added to the quark-only dynamical model which started in [Swimming with Quarks](#). In that section we had considered the quarks under the influence of a specific gluon model: the perturbative propagator. Generalizing that method, we consider the quark gap equation where G can be replaced by an arbitrary analytical expression. This expression can relate to any of a number of gluon models, including the Maris-Tandy model^[48,49], a perturbative model based on a massive color-charged boson, or any other desired form. For the present example, in order to make contact with [Glueballs](#)^[50], we choose to employ analytical models based on fits to the lattice gluon results of Bogolubsky *et al.*^[15]. The lattice data is shown in Figure 32.

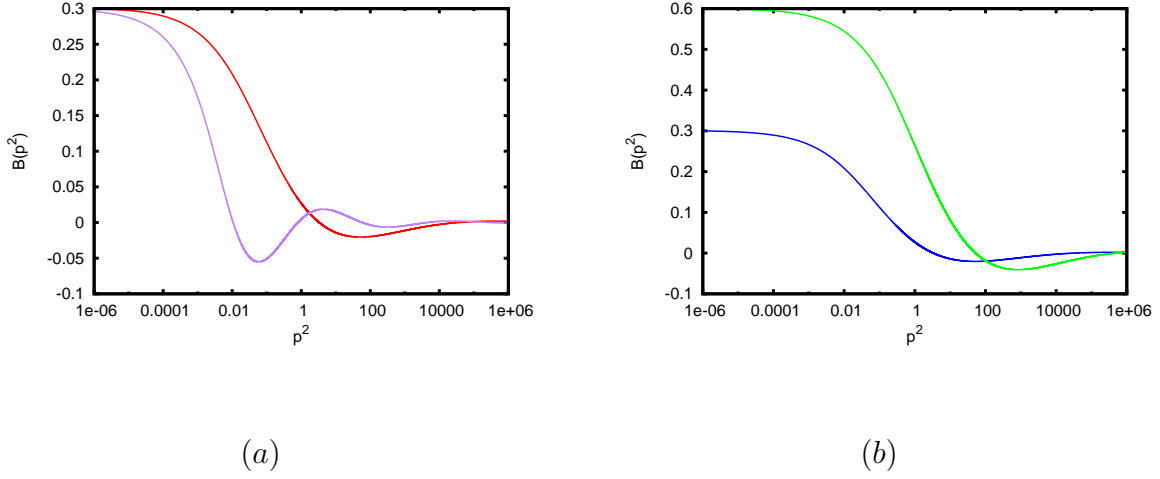


Figure 31: Comparison of solutions to the Swimming with Quarks^[58] model which have: (a) Identical (toy model) boundary conditions of $B(0) = .3$ but coupling values of $\alpha \equiv \frac{g^2}{4\pi} = 3$ (red) and $\alpha = 10$ (purple), and (b) Identical coupling $\alpha = 3$ but different (toy model) boundary conditions $B(0) = .3$ (blue) and $B(0) = .6$ (green).

Our fit to the Lattice gluon data was based on an “entire” model for the gluon function, in which the form is analytically defined as an entire function with a branch cut along the negative real axis. It has been suggested^[5] that this type of analytical behavior could function in such a way as to automatically incorporate confinement into QCD models due to the lack of any poles which could be associated with a propagating particle. The best fit in this form was obtained to be:

$$G_{\text{Entire}}(p^2) = 1.409 \left(\frac{1.0 - e^{-2.0(p^2 - 1.144)}}{p^2 - 1.144} \right). \quad (3.186)$$

In addition to the gluon models based on in-house fitting to the lattice data, we also considered published forms for the gluon propagator. One particular form was a fit^[2] to similar lattice data using more sophisticated expressions. The best fit under these conditions

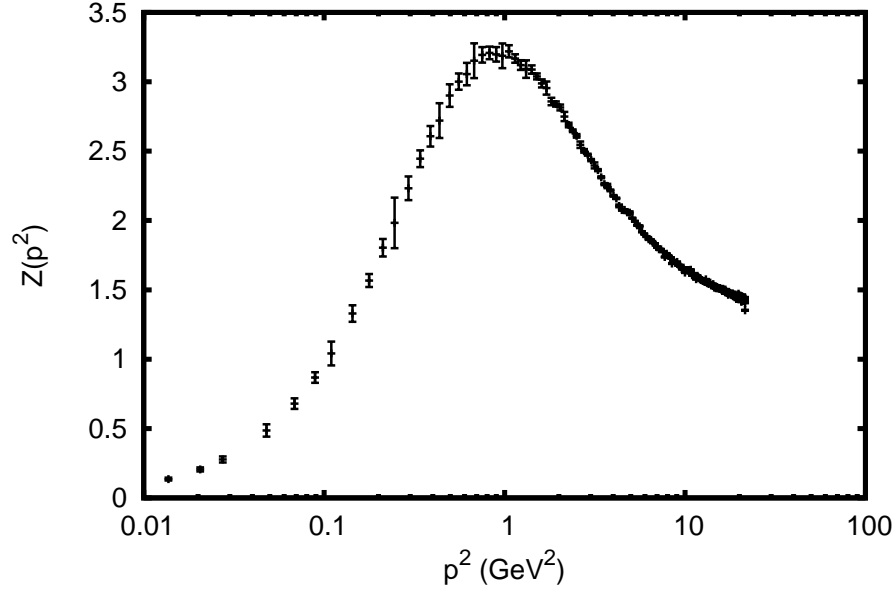


Figure 32: Plot of the Lattice Gluon Propagator as provided by Bogolubsky *et al.*^[15]

was shown to be:

$$G_{\text{AP}}(p^2) = \frac{1}{M^2(p^2) + p^2 \left(1 + \frac{13}{32} \frac{g^2}{\pi^2} \ln \left[p^2 + \frac{8.55 M^2(p^2)}{4.3^2} \right] \right)}, \quad (3.187)$$

where:

$$M^2(p^2) = \frac{.520^4}{p^2 + .520^2}. \quad (3.188)$$

The final gluon model we will consider here is the one presented by Maris and Tandy^[49].

The general form for this model is given by:

$$G_{\text{MT}}(p^2) = \frac{1}{p^2} \left[\frac{\pi}{\omega^6} D p^4 e^{-\frac{p^2}{\omega^2}} + \frac{2\pi\gamma_m \left(1 - e^{-\frac{q^2}{4m_t^2}}\right)}{\ln \left[\tau + \left(1 + \frac{q^2}{\Lambda_{\text{QCD}}^2}\right)^2 \right]} \right]. \quad (3.189)$$

We implement the parameter set used by Williams^[70] as listed in Table 3.

ω	.4
D	.933
γ_m	$\frac{12}{33-2*6}$
m_t	.5
τ	$e^2 - 1$
Λ_{QCD}	.234

Table 3: Set of parameters for the Maris-Tandy gluon propagator model.

The various analytic fits to the gluon propagator $G(p^2)$ were applied to the quark equations (3.100) and (3.101) as well as the ghost equation (3.110). The introduction of vertex models is left in the general sense, to explore the possible results that could be obtained with the various truncations and models discussed in §3.4.3.

In Figure 33 we show various solutions of the quark propagator's equations of motion with the Aguilar-Papavassiliou and Maris-Tandy gluon models as defined in (3.187) and (3.189). These solutions were obtained with the perturbative quark-gluon vertex truncation. In the investigation of dynamical Chiral Symmetry Breaking (XSB), we note that the mass renormalization parameter Z_m of (3.169) does not exist in the theory. As such, only the field renormalization Z_A can be carried out, and thus the equation for $B(p^2)$ can only be rendered finite if the resulting solution either vanishes or tends to zero in the UV more strongly than $A(p^2)$. This allows us to explore the phenomena of XSB in great detail, as a given gluon propagator model can produce the necessary XSB when the coupling is increased beyond a

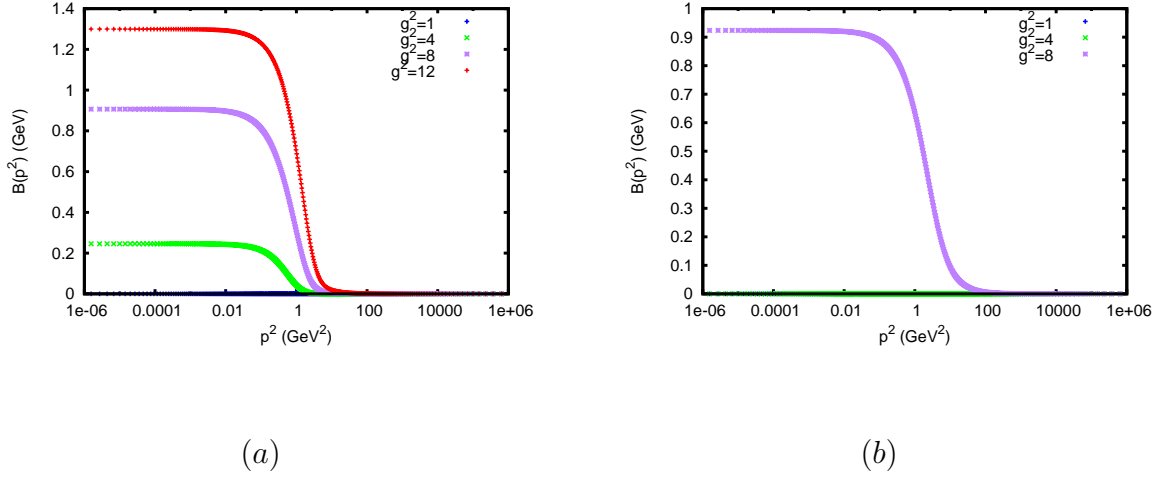


Figure 33: Demonstration of dynamical chiral symmetry breaking using the (a) Maris Tandy and (b) Aguilar-Papavassiliou gluon propagator models. Note that XSB solutions do not allow for renormalization of the equation for $B(p^2)$, but the renormalization parameter $A(9 \text{ GeV}^2) = 1$ was used, where the units of GeV arise from the scales introduced by the lattice $G(p^2)$.

certain critical value $g^2 > g_{\text{crit}}^2$. The critical value of coupling depends strongly on the gluon model employed in the equations, and we observe that the Maris-Tandy model produces XSB at a smaller coupling than what we show for the Aguilar-Papavassiliou model. The ability of these equations to incorporate arbitrary functions $G(p^2)$ with or without the inclusion of vertex models provide a robust framework for evaluating the behavior of quarks under varying behavior in the gluon propagator or the quark-gluon interaction.

Figure 34 shows that the computation can produce a wide array of results in the quark sector. Various cases involve unbroken chiral symmetry, XSB, and the dressing of massive quarks. These solutions were obtained using the entire gluon model (3.186), with a variety of couplings g^2 . We observe that the XSB cases require a critical coupling to dynamically generate a quark mass, but that the cases involving perturbatively massive quarks produce a nontrivial dressing for any value of coupling.

Finally, we consider the ability of these gluon models to reproduce available lattice data

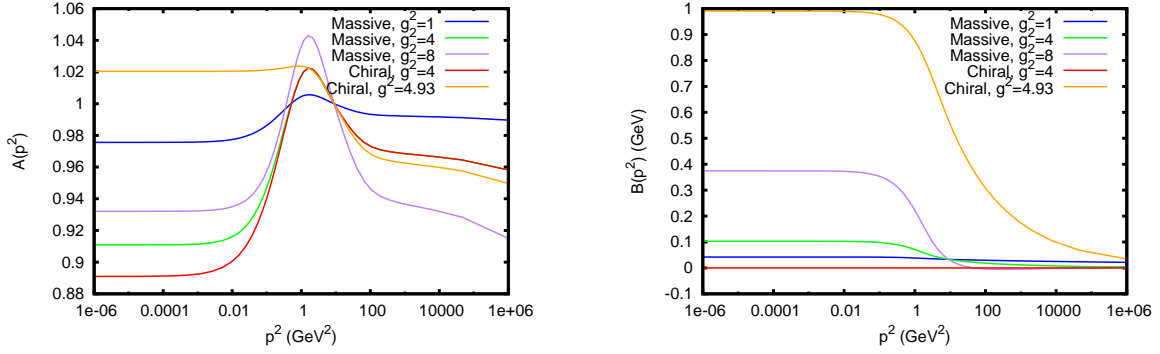


Figure 34: Plots of the quark propagator dressing functions A and B using the $n = 2$ CBC vertex and a variety of couplings and perturbative masses, obtained using the entire gluon model. The renormalization parameters $A(9 \text{ GeV}^2) = 1$ and (for massive quark cases) $B(9 \text{ GeV}^2) = .65 \text{ GeV}$ were used, and again the entire model fit to the lattice $G(p^2)$ implies units of GeV.

for the quarks and ghosts. Figure 35 shows comparisons of our solutions with the quark lattice data of Bowman *et al.* [16] and the ghost lattice data of Bogolubsky *et al.* [15]. The entire gluon model (3.186) was used for these computations. The quark equation was considered using perturbative vertices and the $n = 0$ CBC vertex, while the ghost equation was considered with a perturbative vertex but allowing for extra enhancement by a factor of $h(p_{\text{gluon}}^2)$ in the dressed vertex. We find that the potential agreement of quarks with the lattice data are improved slightly by the vertex model, but there is significant difficulty in obtaining a convincing match. We will revisit this difficulty in §3.4.6, and comment further on the role of vertex models. We find that the perturbative vertex solution for the ghost propagator can be tuned into good agreement with the lattice data, but the ad-hoc enhancement of the ghost-gluon interaction does not yield satisfactory results. Consideration of the ghost-gluon vertex model discussed in §3.4.3 will be considered in the fully-coupled propagator system, but we will find there also that the ghost results support the idea [3,19] that the ideal ghost-gluon vertex model will be very similar to the perturbative interaction.

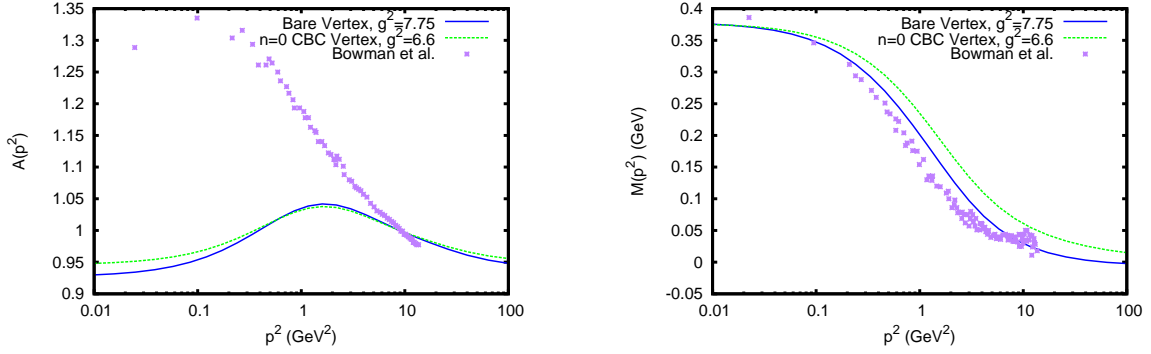


Figure 35: Plots using the entire gluon model of the quark propagator dressing functions A and $M = \frac{B}{A}$ with perturbative and $n = 0$ CBC vertices in comparison to the quenched massive quark lattice data of Bowman *et al* [16]. Renormalization parameters $A(9 \text{ GeV}^2) = 1$ and $B(9 \text{ GeV}^2) = .033 \text{ GeV}$ were used.

3.4.5.3 Mandelstam's Equation In Mandelstam's QCD approximation scheme [46], the gluon gap equation is considered first as truncated by considering only the gluon loop diagram in the vacuum polarization. It is argued that the Ward Identities serve to truncate the dressed 3-gluon vertex which remains, and that in doing so both the dressed vertex and one of the gluon propagators in the loop are replaced by their perturbative forms. Due to the more involved dependence on external momentum as compared to the quark equations of [Swimming with Quarks](#), this equation will only be considered in its integral form. Mandelstam had intended that the renormalization conditions would enforce a $1/p$ behavior in $Z(p)$, which at the time was believed to be the necessary condition for confinement. We choose here instead to introduce the field renormalization factor Z_A and (alternatively) either the gluon mass Z_μ or coupling Z_g renormalization factors according to our general scheme. The unrenormalized form of his equation is:

$$\frac{1}{Z(p^2)} = Z_A + Z_\mu \frac{\mu^2}{p^2} + \frac{Z_g g^2}{16\pi^2} \left[\int_0^{p^2} \frac{d(q^2)}{p^2} \left(\frac{7}{8} \frac{q^4}{p^4} - \frac{25}{4} \frac{q^2}{p^2} - \frac{9}{2} \right) Z(q^2) \right. \\ \left. + \int_{p^2}^{\Lambda^2} \frac{d(q^2)}{p^2} \left(\frac{7}{8} \frac{p^4}{q^4} - \frac{25}{4} \frac{p^2}{q^2} - \frac{9}{2} \right) Z(q^2) \right] \quad (3.190)$$

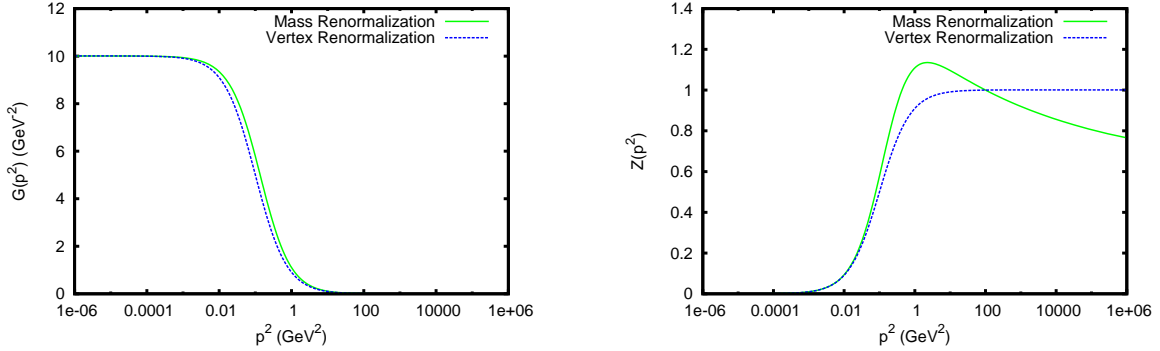


Figure 36: Results for the gluon propagator functions G and Z from Mandelstam's equation under two different approaches to renormalization. The solutions were obtained with $g^2 = 1$ and renormalization parameters were $G(0 \text{ GeV}^2) = 10 \text{ GeV}^{-2}$ and $G(0.01 \text{ GeV}^2) = \frac{1}{0.01} \text{ GeV}^2$.

The numerical approach to solving (3.190) was conducted in a number of ways to explore the robustness of our renormalization and numerical techniques. Since the renormalization intentions of Mandelstam are no longer in line with the modern understanding of confined gluon behavior (in particular the infrared behavior of decoupling or scaling solutions for the propagator), we take the liberty of introducing renormalization factors as described in §3.4.4 and implementing multiple interpretations of the Z-factors mentioned. Comparison of results from the various methods employed are shown in Figure 36, where the solutions were obtained in both schemes with identical values for the dressing functions at the same external scales μ_1^2 and μ_2^2 and the same coupling $g^2 = 1$. The first approach would be to follow our conventional description exactly, and introduce both field and mass renormalization

factors while absorbing Z_g into the coupling g^2 . What results is a renormalized equation taking a form as described in (3.175). Our alternative scheme was to abandon the mass renormalization approach, and instead try to use the as-yet undetermined vertex renormalization factor Z_g to serve as the means to absorb quadratic divergences. This method yields the renormalized equation:

$$\frac{1}{Z(p^2)} = \left(\frac{Z_2(\mu_2^2) - Z_2(p^2)}{Z_2(\mu_2^2) - Z_2(\mu_1^2)} \right) \frac{1}{Z(\mu_1^2)} + \left(\frac{Z_2(p^2) - Z_2(\mu_1^2)}{Z_2(\mu_2^2) - Z_2(\mu_1^2)} \right) \frac{1}{Z(\mu_2^2)}. \quad (3.191)$$

where we have introduced the notation $Z_i(p^2) = \frac{G_i(p^2)}{p^2}$. Solutions based on this method display unusual characteristics, notably that the field renormalization factor Z_A becomes vestigial and serves only to fix the value of $Z(p^2)$ at some external scale without actually absorbing any divergence. Comparison of solutions obtained with Z_A determined as described, or simply set as $Z_A = 1$, are practically equivalent (modulo a small scaling factor) provided that μ_1 lies in the region where asymptotic freedom takes effect. The reason for this is shown by consideration of what Z_g does when its renormalization is performed in the gap equations, which is to filter out the finite coefficient of the leading divergence while eliminating the contribution of any lower divergence. As such, only the quadratically divergent pieces of G_2 can actually contribute to the vacuum polarization in this equation of motion, and only finite coefficients of those divergent portions can appear. The solution obtained through the mass renormalization scheme displays the general shape characteristics of the lattice studies^[15] and looks distinctly different from the results of the vertex renormalization scheme. We interpret this difference to amount to an inconsistency in the meaning of the coupling g^2 in these two cases, and that the same physics should still result if the couplings were instead tuned to produce similar shapes for the solutions.

3.4.5.4 vSHA Equations In the same work^[67] which discussed the ghost-gluon model and one of the 3-gluon models of §3.4.3, von Smekal, Hauck, and Alkofer applied their vertex models to the propagators of the Yang-Mills sector. The resulting equations possessed a form

in which the angular integrals could be done analytically, and so again we consider integral equations involving only a single integration. The equations of motion for both gluon and ghost propagators in this approach were found to be (with augmentation of our gluon mass term, to be discussed below):

$$\begin{aligned} \frac{1}{Z(p^2)} = & Z_A + Z_\mu \frac{\mu^2}{p^2} + Z_g \frac{g^2}{16\pi^2} \frac{N_c}{3} \left[\int_0^{p^2} \frac{d(q^2)}{p^2} \left(\frac{7}{2} \frac{q^4}{p^4} - \frac{17}{2} \frac{q^2}{p^2} - \frac{9}{8} \right) h(q^2) Z(q^2) \right. \\ & \left. + \int_{p^2}^{\Lambda^2} \frac{d(q^2)}{p^2} \left(\frac{7}{8} \frac{p^2}{q^2} - 7 \right) h(q^2) Z(q^2) \right] \\ & + \frac{g^2}{16\pi^2} \frac{N_c}{3} \left[\frac{3}{2} \int_0^{p^2} \frac{d(q^2)}{p^2} \frac{q^2}{p^2} h(p^2) h(q^2) + \frac{1}{2} \int_{p^2}^{\Lambda^2} \frac{d(q^2)}{q^2} h^2(q^2) - \frac{1}{3} h^2(p^2) \right], \end{aligned} \quad (3.192)$$

$$\frac{1}{h(p^2)} = Z_c - \frac{g^2}{16\pi^2} \frac{3N_c}{4} \left[\frac{1}{2} h(p^2) Z(p^2) + \int_{p^2}^{\Lambda^2} \frac{d(q^2)}{q^2} h(q^2) Z(q^2) \right]. \quad (3.193)$$

This system of propagator equations of motion will be considered, as was done for Mandelstam's equation, under two approaches to renormalization. The first of these methods is that which was described generally in §3.4.4 using a gluon mass term to absorb quadratic divergences, while the second approach is analogous to the vertex renormalization described in §3.4.5.3 and uses the gluon propagator's equation to determine the vertex renormalization factor Z_g . This second method produces a slightly different form in this case, because we observe in (3.192) and (3.193) that the vertex renormalization factor only appears on the gluon loop term G_2 in the gluon propagator's equation. It may be difficult to recognize that this is the same diagram which we called G_2 in our general discussion, but the appearance of the combination $h(q^2)Z(q^2)$ instead of a pair of gluon propagators is a result of the vertex model employed. The vertex-based renormalization approach, if we start from a gluon equation in the schematic form:

$$\frac{1}{Z(p^2)} = Z_A + Z_g Z_2 + Z_4, \quad (3.194)$$

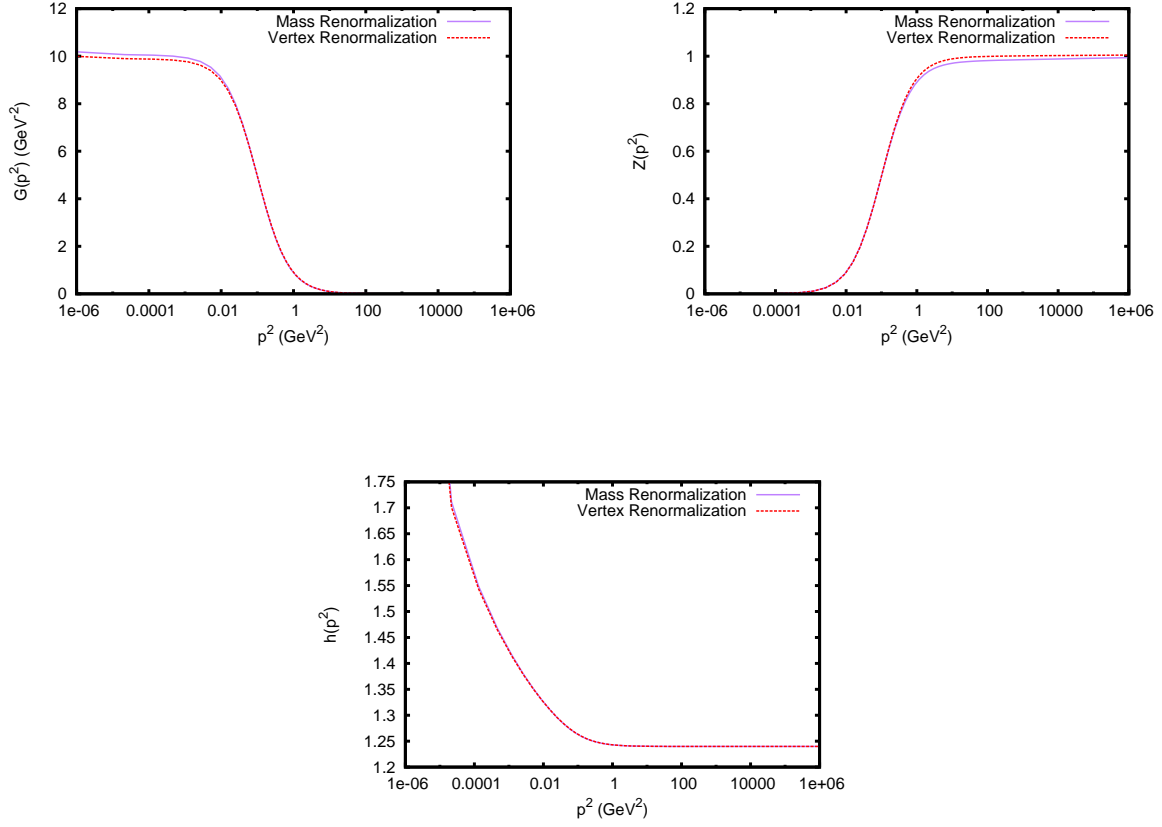


Figure 37: Results of the von Smekal, Hauck, and Alkofer propagator equations for the Yang-Mills system under two different approaches to renormalization of the gluon equation. Solutions were obtained with $g^2 = .11$ and renormalization parameters $G(0 \text{ GeV}^2) = 10 \text{ GeV}^{-2}$, $G(.01 \text{ GeV}^2) = \frac{1}{.01} \text{ GeV}^2$, and $h(16 \text{ GeV}^2) = 1.24$.

then this approach results in the renormalized equation:

$$\begin{aligned}
\frac{1}{Z(p^2)} &= \left(\frac{Z_2(\mu_2^2) - Z_2(p^2)}{Z_2(\mu_2^2) - Z_2(\mu_1^2)} \right) \frac{1}{Z(\mu_1^2)} + \left(\frac{Z_2(p^2) - Z_2(\mu_1^2)}{Z_2(\mu_2^2) - Z_2(\mu_1^2)} \right) \frac{1}{Z(\mu_2^2)} \\
&+ \left[Z_4(p^2) - \left(\frac{Z_2(\mu_2^2) - Z_2(p^2)}{Z_2(\mu_2^2) - Z_2(\mu_1^2)} \right) Z_4(\mu_1^2) - \left(\frac{Z_2(p^2) - Z_2(\mu_1^2)}{Z_2(\mu_2^2) - Z_2(\mu_1^2)} \right) Z_4(\mu_2^2) \right].
\end{aligned}
\tag{3.195}$$

We show in Figure 37 a comparison of our solutions to these equations (3.192) and (3.193) as obtained through the two renormalization methods. Unlike the plot we presented for Mandelstam's equation, we find that the two sets of solutions are very similar to each other and at the level of visual inspection are practically indistinguishable. We thus conclude that the interpretation of the coupling g^2 in this particular model is relatively insensitive to the details of renormalization procedure and so our solutions from the two methods are physically equivalent. While obtaining these solutions, it was noted that although agreement between the two renormalization methods was very good, both methods also suffered from severe numerical stability problems. The plots of Figure 37 were obtained as before with identical sets of renormalization parameters and coupling, but are shown for the case where $g^2 = .11$. Any attempts to increase the coupling much beyond this value caused unstable and non-converging numerical behavior in both schemes. It may be pointed out that the step functions which represent the integration bounds of these equations result in integrands which are, in various cases, either non-continuous or continuous and not smooth. Since our numerical integration algorithms are based on Gauss-Legendre grids over the full four-momentum space as discussed in §3.1.1, they are not well suited to resolving the transition regions of these integrands, and numerical errors are likely to be introduced as a result.

3.4.6 Fully Coupled System

The final truncation we will discuss here^[51] involves consideration of the fully coupled system of equations (3.100), (3.101), (3.110), and (3.123). The dressing functions for the quark,

ghost, and gluon propagators are all considered dynamically in the Landau gauge. The computations include the contributions of every diagram truncated and/or modeled at the vertex level, notably including the nonperturbative two-loop diagrams of the gluon equation (3.123) (Figure 25).

The full set of diagrams was built up slowly to explore the stability and contribution of the various parts. The initial stage was to include the self energy diagrams in the ghost and quark equations and only the ghost loop G_4 in the gluon vacuum polarization. This implies a coupled set of gluon and ghost equations, while the quarks depend only on the output of the gluon equation with no feedback. The next inclusion was the gluon loop G_2 , which presented certain numerical difficulties. Since the asymptotic behavior of the gluon propagator features more prominently in the renormalized convergence of this loop than the $O(1)$ ghost dressing function $h(p^2)$ did in G_4 , it was necessary to include a more robust means of extrapolating the UV behavior beyond our furthest grid point. An attempt was made to fit the perturbative behavior to the highest grid point and extrapolate in this manner, but the integral did not stabilize. We examined the behavior of our (naive) interpolation routine for $G(p^2)$, and noted that the function was continuous but not smooth when passing over a momentum grid point. We thus introduced a cubic spline interpolation routine to reduce the effects of discontinuous slope, but found that it did not match smoothly onto the extrapolation routine. Finally, we discovered that using applying the cubic spline interpolation to the propagators on a log-log scale (e.g. $\ln[G(e^{\ln(p^2)})]$) resulted in a sufficiently smooth interpolation routine which could also produce high-fidelity extrapolation in the far UV. This algorithm was then implemented for the other interpolations in $\sigma_{V,S}(p^2)$ and $h(p^2)$. Inclusion of further gluon diagrams was much simpler beyond this point, and so the quark loop G_3 and the two-loop diagrams G_{Sunset} and G_{Squint} were subsequently incorporated into the system with little difficulty.

The coupling values chosen for these computations can be divided into two general sets. The original intent (which we refer to as “universal coupling”) was to employ a single, universal coupling g^2 which applied to all of the vertices of (3.163)-(3.166). The second approach (which we refer to as “differentiated coupling”) was to independently specify the

couplings for each vertex in an effort to most closely reproduce the lattice data^[15,16] of dressing functions for all of the propagators.

The universal coupling value was chosen to provide the best possible fit to data^[15] of the lattice gluon propagator. Plots of the various dressing functions obtained in this scheme are shown in Figure 38. While this approach seemed to provide the most direct compatibility to the gauge symmetry constraints of (3.167), there were a number of shortcomings in the results. The best possible fits to the lattice gluon propagator resulted in poor agreement with the lattice data for the other propagators' dressing functions. In addition, the values of universal coupling which produced good agreement with the gluon lattice data (or in fact, any range of coupling which resulted in a stable computation of the gluon equation) were unable to simultaneously produce dynamical chiral symmetry breaking in the quark sector.

The universal coupling scheme was also used to investigate the contribution of each loop diagram of the gluon equation. The comparison of the various integrals is shown in Figure 39, in terms of the vacuum polarization Π_i for each loop i . The expression for Π_i is taken to mean the quantity in brackets in (3.175), which is then divided by p^2 and then plotted. The expression for Π_{tot} is obtained by considering the sum over the individual Π_i as shown in the same expression (3.175). The plots are shown for two different sets of renormalization parameters, but there are some common observations to be made in the two cases. The dominant contribution to the vacuum polarization for both cases is seen to come from the gluon loop term G_2 . The next largest contributions arise from G_{Squint} and then G_4 , again in both cases. As expected^[14], of the two-loop diagrams we find that $\Pi_{\text{Squint}} \gg \Pi_{\text{Sunset}}$. While we casually state that the contributions of the quark loop G_3 , the ghost loop G_4 , and the sunset diagram G_{Sunset} do not contribute significantly, it has been noted^[67] that the nonlinear nature of gap equations implies that every contribution does in fact have a fundamental impact on the solution obtained. Despite this aspect of nonlinear equations, we can compare to simpler computations which did not include all of the diagrams and thus observe that they were still very close approximations to the results of the more complete set of equations and so evaluating the relative significance of the various terms is not necessarily

inappropriate.

The differentiated coupling approach was able to improve the over-all agreement to the various sets of lattice data, and has the advantage that the solutions were obtained in a self-consistent manner. We find that the shift from universal to differentiated coupling schemes has a relatively minor impact on the solutions obtained from the gluon propagator, while at the same time providing vastly improved fits for the quark and ghost propagators.

The comparison to quark lattice data^[16] in Figure 40 shows the dressing functions $A(p^2)$ and $M(p^2) \equiv \frac{B(p^2)}{A(p^2)}$. The various solution curves plotted corresponded to changes in the quark-gluon vertex model. Solutions were obtained using the perturbative vertex (3.137) and the CBC vertex (3.139) with various values of n . We observe that agreement with lattice (particularly for A) is improved by use of the CBC vertex, and that as we increase the value of $n = 0, 1, 2$ we obtain further improvement and our solution for A matches the lattice data over a widening range.

The comparison to Yang-Mills lattice data^[15] of Figure 41 shows the ghost and gluon dressing functions $h(p^2)$ and $G(p^2)$ under two different sets of renormalization parameters, with the most obvious difference being the momentum scale at which the non-IR renormalization point μ_1^2 of the gluon propagator's equation of motion was matched onto the lattice. We find that the differentiated couplings could only suffice to mimic the lattice results at the IR and intermediate-momentum enhancement regions. Conversely, the ghost propagator's dressing function was relatively easy to tune into good agreement with the lattice. We can also quantify the agreement of our ghost and gluon solutions with their respective sets of lattice data. The anomalous dimension for each of these fields has been studied in literature^[30,67,70] in the general covariant gauge, and shown to correspond to the behavior of the correlation functions in the UV. Agreement between lattice results and the literature values is quite strong. The established behavior for the ghost and gluon propagators are:

$$G(p^2) \propto \frac{\ln(p^2)^{\gamma_G}}{p^2}, \quad (3.196)$$

$$h(p^2) \propto \ln(p^2)^{\gamma_h}. \quad (3.197)$$

The analytic values for the anomalous dimensions γ_G and γ_h in general covariant gauge at one-loop order are given by:

$$\gamma_G = \frac{3\xi N_c - 13N_c + 4n_f}{22N_c - 4n_f}, \quad (3.198)$$

$$\gamma_h = \frac{3\xi N_c - 9N_c}{44N_c - 8n_f}, \quad (3.199)$$

where $\xi = \frac{1}{\lambda}$ is another popular definition for the gauge fixing parameter from $\mathcal{L}_{\text{gauge}}$, N_c is the number of colors in the SU(N) Yang-Mills theory (in our case, $N_c = 3$), and n_f is the number of fermion species to which the Yang-Mills theory has been coupled (in our case $n_f = 1$). The comparison of these values to our numerical results is shown in Table 4, and is consistent with our qualitative statements regarding the agreement between our solutions and the lattice data in the UV. The vertex models for the gluon's self interactions in §3.4.3: [QCD Interactions](#) have not been explicitly included in these computations due primarily to the complicated contractions which would result in much slower computation of the two-loop diagrams in the gluon's equation of motion.

3.4.7 Comparison to Other Work

The equations and results presented here in Chapter 3 reflect a mixture of original research and reproductions of earlier work published by others. We now seek to clarify the distinction between these efforts.

The Schwinger-Dyson equations for QCD are well-established, and so the forms presented for various gap equations (in the sense of general vertex models or perturbative truncations) are well within the means of any practitioner of this type of nonperturbative quantum field theory. The diagrammatic rules and expressions presented here were a deliberate effort to describe a self-contained means of defining this framework, and are in full agreement with the symbolic forms which result from the functional calculus.

The default renormalization scheme presented here is common practice in the nonperturbative treatment of massive fields, and so for example the renormalized equation presented for ϕ^4 theory are in line with standard subtractive renormalization of such equations. The same method as applied to the gauge particles of QED and QCD are not such common practices, and to the author’s knowledge only a consideration of massive photons^[41] has ever been seriously explored as a means of renormalizing the gap equations. The introduction of Proca-like mass terms in these two theories are explorations into an unconventional (and in QCD, completely new) means of rendering the gauge sector’s propagators finite. As discussed in §3.1.3, the apparent conflict between the mass term and gauge symmetry is not actually a concern, as the mass is only introduced to absorb divergent mass-like terms which arise in the formulation of the nonperturbative regularization of integrals over loop momenta and thus serves to restore the gauge symmetry which the regulators would otherwise break. There has been much discussion preceding and since the writing of Meyers and Swanson (2014) regarding the proper means of introducing and determining Z-factors for QCD (and Schwinger-Dyson equations in general). The common discussions in literature tend to employ means of subtracting “spurious” behavior at each iteration of the gap equations, and the meaning of this undesired behavior evolves with the contemporary notions of confinement and gluon behavior. It may be particularly noted however, that a recent review^[37] sought to

categorize and describe many of the renormalization strategies in current practice in order to urge practitioners to converge on a standard method, but noted that the variation in results from these strategies are still no more significant than the numerical and systematic errors present in modern computations.

In the time of Mandelstam’s model^[46] discussed in §3.4.5.3, it was believed that confinement required the gluon propagator to diverge in the IR even more strongly than the perturbative $\frac{1}{p^2}$ behavior. In order to obtain this behavior, he parametrized the propagator into a $\frac{\text{const.}}{p^4}$ piece and a second dressing function. After solving for the constant coefficient, the integral equation was recast to solve for the new dressing function. In our treatment of the same equation examined by Mandelstam, we implemented the renormalization scheme discussed in §3.4.4 along with an alternative scheme which does not use the mass term. We obtained decoupling (IR-finite) solutions from both approaches, and have shown them here. We are currently unaware of any other treatment which has produced a decoupling-type solution to this particular equation.

The Yang-Mills model^[67] of von Smekal, Hauck, and Alkofer incorporated a more sophisticated set of vertex models. The renormalization approach used was focused predominantly on the running coupling and information from the renormalization group (RG). They performed the renormalization such that it would reproduce both the IR fixed point of QCD and an RG-invariant running coupling, and so obtained good agreement with the asymptotic behavior of lattice as discussed in §3.4.6. This treatment of renormalization required in-depth analysis of the vertex models’ behaviors in various momentum regimes, and was presented for their models as well as the Mandelstam truncation discussed above. The equations of motion which they obtained and solved were thus modified into a customized form for each truncation. In our own calculations, we were interested in the ability to swap out various vertex models in a modular fashion and so chose not to explicitly include RG considerations. As such, we instead introduced the interpretation of our results as described, in which agreement with lattice data and the asymptotic behavior were used to evaluate our solutions. Our solutions were obtained using two different renormalization approaches as we had done for

Mandelstam’s equation, and it was rather surprising to find that the two approaches were in very good agreement with each other. It is also clear that the shape of our solutions (especially in terms of $Z(p^2)$) are not in good agreement with the lattice results, but this shortcoming is due most likely to the rather limited range of couplings over which we could obtain stable solutions.

The fully-coupled system of gap equations for QCD as presented in §3.4.6 were obtained directly from the Lagrangian using the methods described in §2.3. To the author’s knowledge, this research was the first instance of all diagrams present in the QCD gap equations being included in a dynamical computation of the propagators. A previous investigation of the nonperturbative two-loop diagrams^[14] focused on evaluating the diagrams using an IR analysis and then approximating the two-loop integrals to a one-loop form which matched the IR behavior, and so the two-loop integrals were not actually performed across the full range of momenta. Other investigations^[22,36] which sought to expand the number of diagrams in the Schwinger-Dyson equations choose to maintain the gluon gap equation in terms of the one-loop diagrams and include interactions from truncated forms of the vertex equations shown in §3.4.3. While it would be a daunting task, a future computation combining the full suite of diagrams in the propagator equations with coupled vertex equations would have an easy claim to the state of the art in the Schwinger-Dyson equations of QCD.

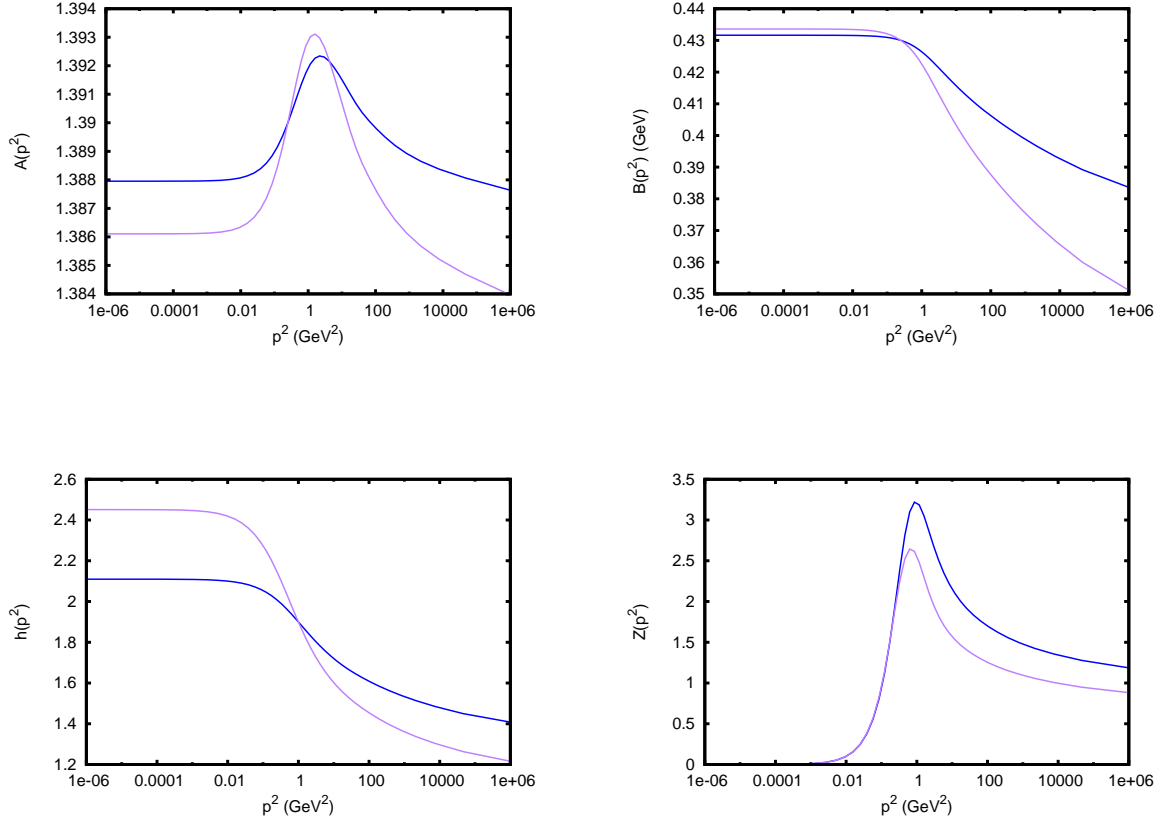
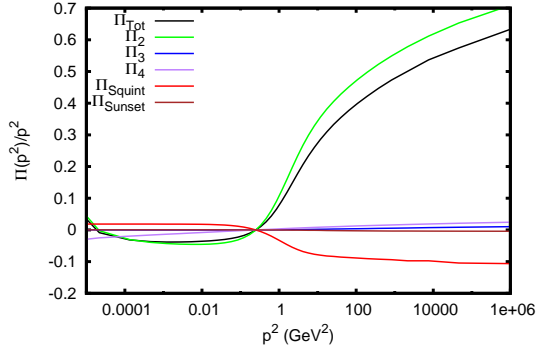
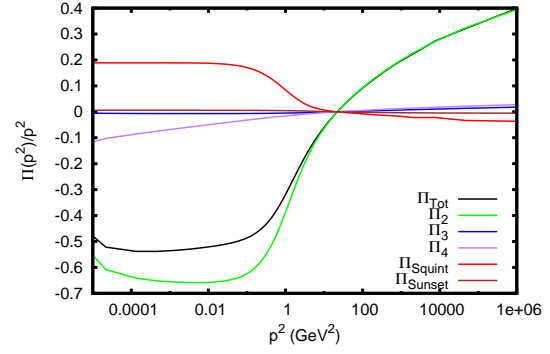


Figure 38: Plots of the solutions to the fully coupled system of QCD propagator dressing functions under two sets of renormalization parameters and a universal coupling value. The renormalization parameters for quarks, ghosts, and the IR point for gluons were $A(.25 \text{ GeV}^2) = 1.39$, $B(.25 \text{ GeV}^2) = .43$, $h(1 \text{ GeV}^2) = 1.9$, and $G(0 \text{ GeV}^2) = 10$ for all curves, while the second gluon renormalization point was $G(.25 \text{ GeV}^2) = 8 \text{ GeV}^{-2}$ with $g^2 = .36$ for the blue curves and $G(21.5 \text{ GeV}^2) = .0665$ with $g^2 = .83$ for the purple curves.



(a)



(b)

Figure 39: Plot of the relative contributions of the diagrams from (3.123) (Figure 25) to the gluon propagator's vacuum polarization, under two different sets of renormalization parameters. The renormalization parameters for quarks, ghosts, and the IR point for gluons were $A(.25 \text{ GeV}^2) = 1$, $B(.25 \text{ GeV}^2) = .033$, $h(1 \text{ GeV}^2) = 1.9$, and $G(0 \text{ GeV}^2) = 10$, while the second gluon renormalization point was $G(.25 \text{ GeV}^2) = 8 \text{ GeV}^{-2}$ with $g^2 = .36$; and (b) $G(21.5 \text{ GeV}^2) = .0665$ with $g^2 = .83$.

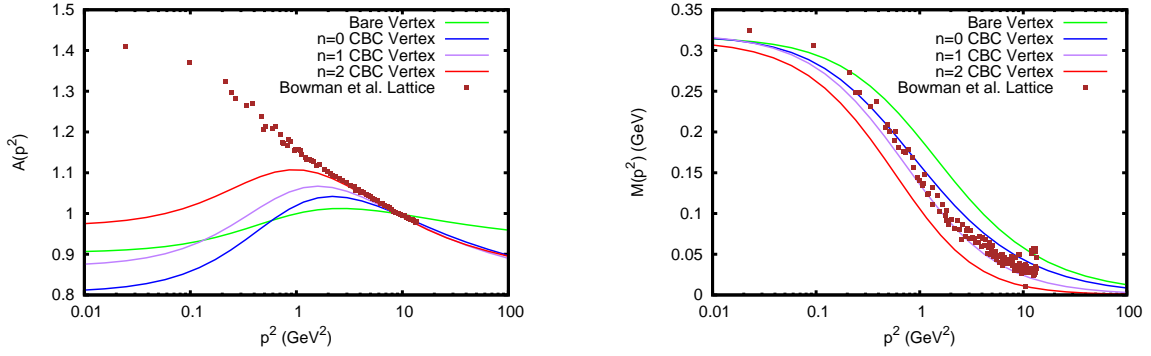


Figure 40: Comparison of the quark propagator dressing functions A and $M \equiv \frac{B}{A}$ to the lattice data of Bowman *et al.*^[16] Solutions were obtained with differentiated coupling values and variety of vertex models. Renormalization parameters were $A(.25 \text{ GeV}^2) = 1$, $B(.25 \text{ GeV}^2) = .033$, $h(16 \text{ GeV}^2) = 1.24$, $G(0 \text{ GeV}^2) = 10$, and $G(.25 \text{ GeV}^2) = 8 \text{ GeV}^{-2}$, while the couplings were $g_{AAA}^2 = .2$ and $g_{\bar{c}Ac}^2 = 1.57$, with $g_{\psi A\psi}^2 = 5.29$ for the bare vertex, $g_{\psi A\psi}^2 = 12.08$ for the $n = 0$ CBC vertex, $g_{\psi A\psi}^2 = 7.2$ for the $n = 1$ CBC vertex, and $g_{\psi A\psi}^2 = 3.85$ for the $n = 2$ CBC vertex.

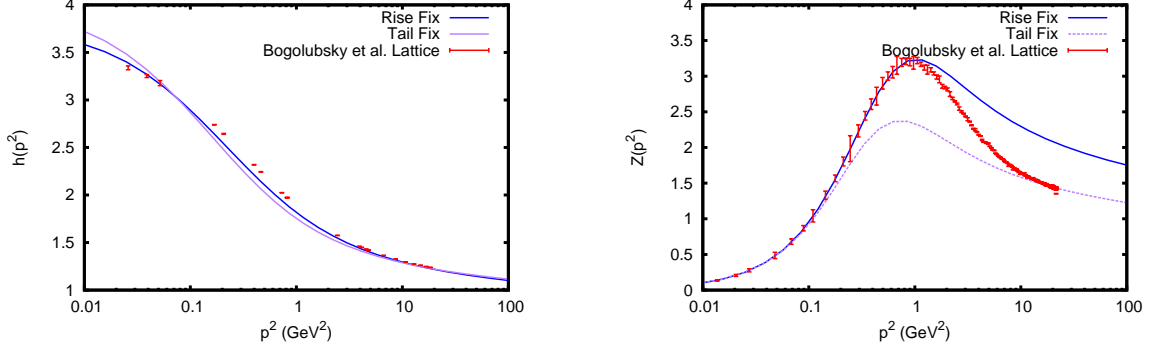


Figure 41: Comparison of the ghost and gluon propagator dressing functions h and Z to the lattice data of Bogolubsky *et al.* ^[15] The solutions were obtained using differentiated coupling values and two sets of renormalization parameters in the gluon equation. Renormalization parameters were $A(.25 \text{ GeV}^2) = 1$, $B(.25 \text{ GeV}^2) = .033 \text{ GeV}$, $h(16 \text{ GeV}^2) = 1.24$, and $G(0 \text{ GeV}^2) = 10 \text{ GeV}^{-2}$, with $G(.25 \text{ GeV}^2) = 8 \text{ GeV}^{-2}$ with couplings $g_{AAA}^2 = .2$, $g_{cAc}^2 = 1.6$, and $g_{\psi A\psi}^2 = 6.5$ for the blue curves, and $G(21.5 \text{ GeV}^2) = .0665 \text{ GeV}^{-2}$ with couplings $g_{AAA}^2 = .54$, $g_{cAc}^2 = 1.97$, and $g_{\psi A\psi}^2 = 8.4$ for the purple curves

	Literature (Lattice) γ_i	Numerical γ_i
$G(p^2)$	-.565	-.29
$h(p^2)$	-.218	-.21

Table 4: Comparison of anomalous dimension parameters γ_i exhibited by Lattice QCD results and the numerical results of our fully coupled system.

4.0 BOUND STATES

The bound states of a quantum field theory are typically studied using the quantities discussed in §2.4: [The Bethe-Salpeter Equation](#). In particular, we are interested in the resonance condition contained within (2.49) so that we may investigate the mass spectrum of the gluon bound states (Glueballs) of QCD. We recall that the bound state whose mass pole we approached to derive (2.48) corresponds to the Bethe-Salpeter Amplitude Φ (or χ) which solves the equation. The analytic behavior used to conduct that derivation assumes that there were not other bound states within an arbitrary but vanishing distance from that particular pole, but in the case of possible degeneracy we apply the equation with the intention that orthogonal Bethe-Salpeter amplitudes can be produced out of linear combinations of the solutions we find. The general approach will be to scan across regions of time-like Minkowski momenta and search for values which satisfy the resonance condition and thus represent the mass of a bound state.

4.1 ANALYTIC CONTINUATION

4.1.1 Necessity

The Bethe-Salpeter equation which we use to investigate bound states is based on the behavior of the scattering function G^{BS} in the vicinity of a mass pole. To correspond to a physical state, the four-momentum must have a time-like value related to the bound state's

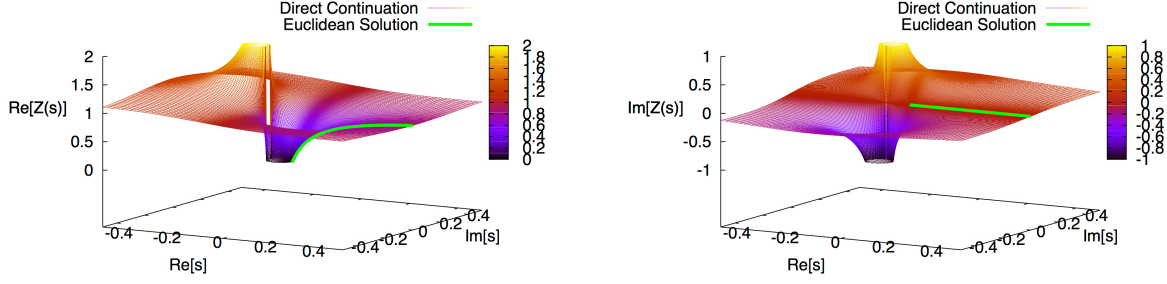


Figure 42: Plot of the real and imaginary parts of $Z(s)$ as obtained through direct continuation.

mass $p_M^2 = m_{\text{BS}}^2 > 0$. The results we have discussed for various propagators in Chapter 3: [Gap Equations](#) were primarily solved at space-like Euclidean values of momentum, $p_E^2 = -p_M^2 > 0$. As a result, we must investigate the effect of introducing an imaginary value of bound state momentum $P_B = \{ip; p \in \mathbb{R}\}$ into the arguments of those propagators. The propagators contained within the loop integrals we shall consider in the Bethe-Salpeter formalism have the arguments q_\pm^2 which we define as:

$$q_+^2 = (q + \eta ip)^2 = q^2 - \eta^2 p^2 + 2i\eta qpx, \quad (4.1)$$

$$q_-^2 = (q - (1 - \eta) ip)^2 = q^2 - (1 - \eta)^2 p^2 - 2i(1 - \eta)qpx, \quad (4.2)$$

and so we recognize that they must be analytically continued into a form which is valid within some region of a complex momentum plane $q_\pm^2 \rightarrow s \in \mathbb{C}$. We set the positive real s axis to correspond to space-like Euclidean values and maintain $q \in \mathbb{R}$. Choosing a value of $\eta = \frac{1}{2}$ results in the boundaries for q_\pm^2 being placed symmetrically in the upper and

lower half-planes^[25], with the extreme values occurring when the angular variable is at the integration bounds, $x = \pm 1$. The domain of q_{\pm}^2 we thus require is defined by a parabolic boundary encompassing the positive real axis, whose apex lies on the negative real axis. Once the propagators (and any dressed vertices involving similar arguments of complex four-momenta) are known within such a region, then the Bethe-Salpeter equation can be properly considered for a bound state of a physical mass up to the chosen value m^2 .

4.1.2 Methods – Direct Continuation

The simplest possible form of analytic continuation applies only in cases where the integral equation for a propagator can be cast in a linear form. This method can apply to situations such as §3.4.5.1 §3.4.5.2, or §3.4.5.3 where a gluon propagator is expressed symbolically. In these cases, the self-energy integral contains a factor of the unknown propagator along with an analytical expression for a gluon propagator. By choosing a fully asymmetric momentum routing, the external momentum P (and thus the dependence on complex values) can be placed entirely within the known gluon propagator. The assumption is then that the perturbative $\frac{1}{p^2}$ form or functions which were fit to the lattice gluon data^[15] can be relied upon for complex values as well. The procedure is then to solve for the unknown propagator along the Euclidean axis, and then evaluation of the gap equation at arbitrary complex momenta requires only that Euclidean solution and insertion of the complex value into the integration kernel and known form for the gluon propagator. We thus evaluate the gap equation as such and using the output to yield the continued propagator.

The Mandelstam gluon model of §3.4.5.3 is an example of a propagator which can be continued as such. Treatment of the angular integral for complex momenta reveals that the integrand of (3.190) generalizes to complex momenta if one simply replaces the argument inside of the step function (or the integration bounds) to refer to the magnitude $|p^2|$ instead of the Euclidean p^2 . The gluon propagator can then be obtained as described above. Plots of the real and imaginary parts of $G(p^2)$ are shown in Figure 42, along with a comparison to the initial solution obtained along the Euclidean axis. It is a rather surprising result, as the

decoupling solution requires $Z(0) = 0$, but the continued form reveals that the propagator is well described by a simple pole (as one would have in a massive boson's perturbation theory) along the Minkowski axis. The pole structure is visible in Figure 42, and attempts to fit this function as a simple pole on the complex s -plane are in agreement to the level of numerical precision.

4.1.3 Methods – Cauchy-Riemann Continuation

The dynamical functions needed on the complex plane can be obtained in a number of ways, all amounting to some form of analytic continuation within the propagator's equation of motion. One possible approach is to directly consider an analytic continuation of the purely Euclidean solution. The propagators are expected to be represented by analytic functions in some region enclosing the positive real axis, where our Euclidean momenta sit. The analytic nature of these functions means that they must obey the Cauchy-Riemann equations within this region. We choose to express these relations using a complex value of $z = re^{i\phi}$ in polar form. Analyticity of a function F then implies that the value of $\frac{dF}{dz}$ is independent of the direction from which the infinitesimal limit is taken. We use the polar form to compare the contributions along the radial and tangential directions:

$$\frac{dF}{dz} = e^{-i\phi} \frac{\partial F}{\partial r} = \frac{-ie^{-i\phi}}{r\phi} \frac{\partial F}{\partial \phi} \quad (4.3)$$

$$\Rightarrow \frac{\partial F}{\partial \phi} = ir\phi \frac{\partial F}{\partial r}. \quad (4.4)$$

We thus find that the function can be generated in the tangential direction by solving a first-order differential equation with the boundary conditions set by our Euclidean-axis solution. This method is cast as a stepping operation starting with a ray extending down the positive real axis, and using numerically calculated radial derivatives to generate the solution on an adjacent ray separated by a fixed polar angle $\Delta\phi$. While this is the simplest

and most easily implemented method of analytically continuing the propagator functions on the complex s plane, there are some technical barriers which cause this not to be the preferred approach. First, the rays generated in this fashion extend from the origin along a particular polar angle using our discretized momentum grid. Due to the required domain for the Bethe-Salpeter equation, one must perform the continuation the whole way to the negative real axis before the necessary region is obtained in full. In addition, the fact that we have primed our boundary condition using a discretized solution to the equation of motion and that the condition laid out as such is not known on a continuous boundary, numerical instability in the differential solution prevents this approach from yielding the complete continuation that we require.

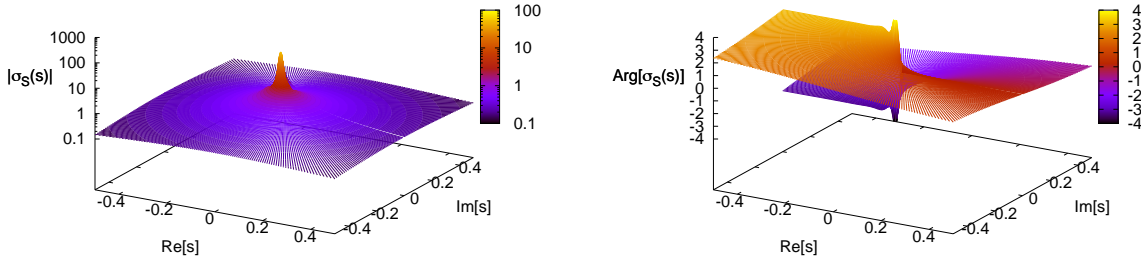


Figure 43: Plot of the magnitude and phase of the quark propagator function $\sigma_S(s)$ on the complex plane, as obtained using the entire gluon model and a Cauchy-Riemann algorithm.

In particularly well-behaved examples, it is possible for this approach to yield the continued propagator on the whole complex plane. Figure 43 shows an example of a successful Cauchy-Riemann continuation for the quark function $\sigma_S(s)$. The propagator was obtained on the Euclidean axis using the entire gluon model. In this example, we found that continuing the dressed propagator in the form of σ_S produced a more stable computation than attempting to treat A or B individually. We note also that the quark propagator appears to

have inherited a branch cut along the negative real axis which was also present in the entire model for the gluon propagator.

4.1.4 Methods – Double-Grid Continuation

Another approach can be formulated using the rays described in §4.1.3. Instead of solving the Euclidean equations first, we choose to discretize the complex solutions in the radial and angular directions, and employ a 2-dimensional interpolation routine to obtain the argument for arbitrary points on the complex plane. The radial interpolation is performed as in the purely real Euclidean examples of Chapter 3 as discussed in §3.1, but we now introduce a cubic spline fit in a purely linear fashion along the angular direction. We are thus able to iterate the full complex plane to obtain a solution at all points, but there are some considerations and limitations.

The domain of complex momentum points discussed in §4.1.1 apply also to the propagators appearing in the gap equations for complex momenta. Since the integration grids for an arbitrary point fall into a parabolic region about the positive real axis (and extending somewhat into the left half-plane where $\text{Re}[s] < 0$), the function on or near the Euclidean axis tends to converge most rapidly. It cannot be expected that the solution at an arbitrary point will converge to a stable solution until its domain has done so, and so we find that the solution's convergence spreads outward from the positive real axis where the initial stabilization occurs. The time required to obtain stable solutions is thus increased by both the expanded number of grid points and the means by which the solution converges.

A common discussion^[4,5,11,24,25,29,31] among studies which perform analytic continuations of propagator functions is the appearance of singularities, typically in the left half-plane and appearing at paired locations of complex conjugates. In the method to be discussed in §4.1.5, it is required for the continuation to be valid that the unknown solution is purely analytic within the parabolic region. If that method encounters an unexpected singularity, then the assumptions made in its definition are invalid. What occurs in the current method is that the appearance of a singularity at any point in the complex plane will prevent the

valid solution from being found at any point whose complex domain includes the singularity. The reason for this is that the function is known only in a discrete numerical sense, and neither the integration grids nor interpolation routine are well-suited to resolving the location or analytic structure of such singularities. The direct continuation method is thus most beneficial in exploring the unknown analytic behavior of solutions to the propagators' equations of motion, but at the same time requires vastly increased computation times which may include significant devotion to regions which cannot be expected to produce a stable or valid solution. We thus conclude that this method is sufficient for bound state studies, but in the interest of computational efficiency may not be the most advantageous option available.

4.1.5 Methods – Contour Continuation

An alternative approach^[11,25,31] to continuing the propagators onto the complex s plane is based on an application of the Cauchy Integral Theorem. Suppose that we evaluate the propagator's equation of motion for an arbitrary complex point $p^2 \in \mathbb{C}$. Expressing this in Cartesian form as $p = P + i\alpha$, and generalizing our angular parameter as $x \equiv \frac{q \cdot p}{|q|(P+i\alpha)}$, we find for q_{\pm}^2 :

$$q_+^2 = q^2 + \eta^2(P^2 - \alpha^2) + 2\eta qPx + 2i\eta\alpha(qx + \eta P) \quad (4.5)$$

$$q_-^2 = q^2 + (1 - \eta)^2(P^2 - \alpha^2) - 2(1 - \eta)qPx - 2i(1 - \eta)\alpha(qx - (1 - \eta)P) \quad (4.6)$$

Consider a momentum point on the boundary of q_+^2 when $x = \pm 1$ and $\eta = 1$. If we define $p' = P' + i\alpha'$, then we make the identifications:

$$P' = q \pm P, \quad (4.7)$$

$$\alpha' = \alpha, \quad (4.8)$$

with complementary expressions should we consider q_{\pm}^2 and $\eta = 0$. Thus, the extreme values required by q_{\pm}^2 under a fully asymmetric momentum routing scheme define a contour of complex momenta P which share a constant imaginary component α . We conclude that should we define a contour C in the complex s -plane lying on values where $s = \{(P \pm i\alpha)^2; P, \alpha \in \mathbb{R}; \alpha = \text{const.}\}$ (plus a closure line at the infinite limit of $\text{Re}[s]$), then any possible argument using this routing would lie upon or within the contour. We could thus use the contour to host our discretized solutions for various propagators, and use Cauchy's Integral Theorem to generate them at any point within the contour:

$$\Delta_{\phi\phi}(s) = \frac{1}{2\pi i} \oint_C dz \frac{\Delta_{\phi\phi}(z)}{z - s}. \quad (4.9)$$

In considering the closure line at the mouth of our parabolic contour, we note that the integrand of (4.9) must vanish more rapidly than $\frac{1}{z}$ as $\text{Re}[z] \rightarrow \infty$ for it to be properly neglected.

We define our discretized solution along this contour, with the input value α to characterize the largest bound state mass m_B we could consider. The solution is discretized along grid points defined by setting $q = 0$ in (4.5) or (4.6) with fully asymmetric momentum routing, and using the integration/discretization momentum grid of §3.1.1 as the set of values for P . Since we must define the discretized solution along both arcs of the contour (or modify our prior integrands to take advantage of the conjugation symmetry implied by the Schwarz Reflection Principle), we must (effectively) perform twice as many updates at each iteration. Also, the computation time for this method involves an additional integration over the contour in place of our interpolation routine. We find that this is still preferable to the brute force continuation method of §4.1.4 provided that the chosen contour with parameter α contains a purely analytic region for the propagators being considered.

It turns out that the fully asymmetric routing presents a “worst-case scenario” as far as the integration domain is concerned. If we revisit the forms of (4.5) and (4.6) with $\eta = \frac{1}{2}$, we would instead find that the complex values of q_{\pm}^2 are now bounded by the contour we would obtain with $\alpha' = \frac{\alpha}{2}$. We could have argued in the asymmetric case that our integration

grids never quite reach $x = \pm 1$ and so we only require points within the original contour (otherwise we would have to impose an additional factor of 2 in (4.9) for points lying on the contour), but the equal sharing case of momentum routing avoids this discussion entirely. We may note also, that despite the lack of requiring the continued propagators at points lying in the band between the α and $\frac{\alpha}{2}$ contours, the fundamental assumption made in the definition of (4.9) is that the propagator has no singularities in the full α -contour region. As such, we cannot forcibly extend this continuation beyond the same limiting singularities (if present) which were discussed in §4.1.4. While this presents a possibility that the input value of α may cause unexpected instability, we choose to take that risk in the interest of computational efficiency when a stable solution does exist.

4.2 NUMERICAL METHODS

In order to find solutions to the resonance condition implied by the Bethe-Salpeter equation (2.49), we employ the same discretized integration grids which were described in §3.1.1. Multiple methods have been explored in this work, with distinct methods of characterizing the angular dependence of the (amputated) Bethe-Salpeter amplitude $\chi_{B,r}(q_+, q_-; P)$. Since this function has only two independent four-momenta as arguments, we will discuss the numerical approach using the generic structure function $F(q, P)$. The Bethe-Salpeter equation will be expressed in terms of loop integrals having the general form:

$$F(k, P) = \int \frac{d^4 q}{(2\pi)^4} K(q, k, P) F(q, P). \quad (4.10)$$

We note that the momentum dependence of $F(q, P)$ can be expressed in terms of three parameters, which as discussed in §3.1.1 are given by $q \equiv |q|$, $x \equiv \frac{q \cdot P}{q^2 P^2}$, and $P \equiv \sqrt{P \cdot P}$ (the last of which has been modified from our earlier definition to incorporate the complex nature of P). The integration kernel $K(q, k, P)$ contains an analogous dependence on the radial and angular parameters of the two-loop integrals of Chapter 3: [Gap Equations](#). We thus employ

the angular definitions for k as described in §3.1.1 by introducing the parameters $y \equiv \frac{k \cdot P}{kP}$ and $w \equiv \frac{q \cdot k}{qk}$, where $w = w(x, y, z)$ with $z \equiv \cos(\theta_2^{(q)})$.

One trivial angular integral can be done analytically, while the one over z can be (numerically) performed since only K depends on this parameter. We thus have left only the variables required to express $F(k, P)$ and $F(q, P)$, which are P, q, k, x , and y . As mentioned at the beginning of the chapter, we will scan over values of bound state momentum to search for resonances, and so for the computation at any particular value P it is essentially a fixed parameter. We must thus devise a method of expressing the momentum and angular dependence of F in a way that takes the form of matrix multiplication, and have explored two different approaches. The first approach will be to simply map the discretized radial and angular momentum variables into a single “Super-Index”, and the second will be to expand the angular dependence in terms of Chebyshev polynomials and employ a mapping of radial and Chebyshev indices in F to express it as another column vector.

4.2.1 Eigensystem Representation

In order to examine our resonance condition (2.49) for arbitrary values of P , we can express it in a generalized form for arbitrary bound state momentum:

$$\lambda \chi = K \cdot \chi. \quad (4.11)$$

We thus note that a solution χ to this generalized equation is represented by an eigenvector, and that examination of the structure of K (which has been conveniently represented above as a matrix) will suffice to find the possible eigenvalues $\{\lambda\}$. The search for bound state masses which can satisfy the resonance condition is thus reduced to a search for values of P at which one (or more) eigenvalue satisfies $\lambda = 1$. Should one desire to then examine dynamical bound state properties, then the corresponding eigenvector is a discretized representation of the Bethe-Salpeter amplitude χ .

It is important to implement a numerical eigensystem routine which is capable of diagonalizing complex-valued matrices due to the nature of P . A number of such routines are

available^[32,59] with this capability, and have been used to a various extent in this work.

4.2.2 Chebyshev vs. Super-Index

As mentioned above, we explore two methods of discretizing the unknown Bethe-Salpeter amplitude χ such that the resonance condition can be expressed as matrix multiplication. The two methods differ primarily on their treatment of the angular parameters x and y , as the same momentum grid from §3.1.1 is used for the radial parameters q and k . We shall now describe and compare these two methods.

4.2.2.1 Point Basis Diagonalization The Point Basis or Super-Index method is based on simply discretizing the radial and angular dependence on momentum. For example, the function $F(q_i, x_j; P)$ (recall P is effectively fixed) could be easily represented as a 2-dimensional array with index $[i, j]$. We choose to map this into a single parameter, which we shall represent as $[i + j \times N_q]$. We see that the matrix is thus expressed in block form, where each block (of which there are $N_x \times N_x$) is $N_q \times N_q$ and corresponds to a pair of x and y grid points. This matrix is filled with the arguments of the kernel along with necessary factors from integration measures and weights. We perform the integral over z numerically on the fly as we fill the matrix, and so it is put into a form sufficient for the discussions of §4.2.1. The advantage of this form is its conceptual simplicity, as well as the clear dependence on the discretized grid resolutions. For a particular choice of grid points N_q and N_x , the error arises purely from the numerical integration in z and the integrations in q and x which are represented by the matrix multiplication.

4.2.2.2 Chebyshev Basis Diagonalization To analytically express the expansion of the structure function in some complete set of functions, we first introduce a generic form for the bound state equation:

$$F(k, y; P) = \int \frac{d^4 q}{(2\pi)^4} K(q, k, x, y, z; P) F(q, x; P). \quad (4.12)$$

We seek the analogue of a partial wave expansion in 4D Minkowski space, as opposed to the quantum mechanical wave expansion in 3D Euclidean space. The measure of d^4q introduces a weight factor $\sqrt{1-x^2}$, which suggests that the ideal basis functions may be one of the kinds of Chebyshev polynomials. Should we choose to expand the combination $(1-y^2)F(k, y; P)$, the weight function in the integral would allow us to choose the Chebyshev polynomials of the first kind, $T_n(y)$. Instead, we shall choose to expand $F(k, y; P)$ alone, which demands that we use Chebyshev polynomials of the second kind, $U_n(y)$. We shall use:

$$F(k, y; P) = \sum_n f_n(k; P) U_n(y) \quad (4.13)$$

$$\text{and} \quad (4.14)$$

$$K(q, k, x, y, z; P) = \sum_{l,m,n} h_{lmn}(q, k; P) U_m(x) U_n(y) P_l(z). \quad (4.15)$$

The resonance condition, in this expansion, yields:

$$f_n(k; P) = \frac{1}{8\pi^2} \sum_m \int q^3 dq f_m(q; P) h_{0mn}(q, k; P), \quad (4.16)$$

where

$$h_{0mn}(k_E^2, P_E^2, q_E^2) = \frac{4}{\pi^2} \int \sqrt{1-x^2} dx \sqrt{1-y^2} dy U_m(x) U_n(y) \int d\phi_2 \mathcal{H}(P_E^2, k_E^2, q_E^2, y, x, \cos \phi_2). \quad (4.17)$$

We note in particular that the lack of any z dependence outside of K produces the orthogonality condition for $P_0(z)$, and so we set $l = 0$ in (4.15) with no loss of generality. This would allow us (given the particular form and manageability of K) to hypothetically produce an analytic expansion in the Chebyshev polynomials, but as we shall see in §4.3.2 and §4.3.3, the symbolic form for the kernels is incredibly complicated.

To obtain a finite-dimensional matrix, it is necessary to truncate the Chebyshev expansion at a particular order of polynomial n_{MAX} . We thus form (once again) a block diagonal

representation of the kernel K . The blocks are still of dimension $N_q \times N_q$ as for the Point basis, but now we have $n_{\text{MAX}} \times n_{\text{MAX}}$ blocks. The mapping described is also in a form to which the discussion of §4.2.1 applies.

The discussion of numerical errors in the Chebyshev basis is more complicated than for the point basis. In addition to the series truncation at n_{MAX} , the evaluation of the orthogonality integrals to obtain (4.17) were performed using the discretized angular grid, and so the series truncation error is further compounded by the numerical error from integration of both x and z (which we also had in the point basis). So while we may have avoided explicit dependence on the discretized integrals while filling the matrix representation of K , we acknowledge that the errors of §4.2.2.1 apply in addition to the exclusion of higher-order Chebyshev polynomials.

In addition to the need for a discretized angular grid (to perform the projection integrals), this approach also requires that we set a maximum order of Chebyshev polynomials, n_{MAX} , to obtain a finite-dimensioned eigensystem. This introduces an additional level of approximation to this method, and is among the reasons why we developed a preference for the Point Basis.

4.2.2.3 Results and Comparison Both the Point Basis and Chebyshev Basis methods were successful in calculating the eigenvalues which result from the resonance condition (4.37) over a range of pseudoscalar masses. The agreement is impressive for the low-lying resonances, particularly the ground state. These comparisons validate both methods, but expose a weakness in the Chebyshev Basis. In order to obtain a finite-dimensioned eigensystem, it was necessary to truncate the function expansion at a certain order of Chebyshev polynomial, n_{MAX} , where in this case $n_{\text{MAX}} = 5$. We see in this graph that the solutions produced by such a calculation are only reliable for the first n_{MAX} resonances, beyond which the truncation of the Chebyshev expansion introduces increasing levels of error. A comparison of the eigenvalue curves which demonstrates this departure is shown in Figure 44.

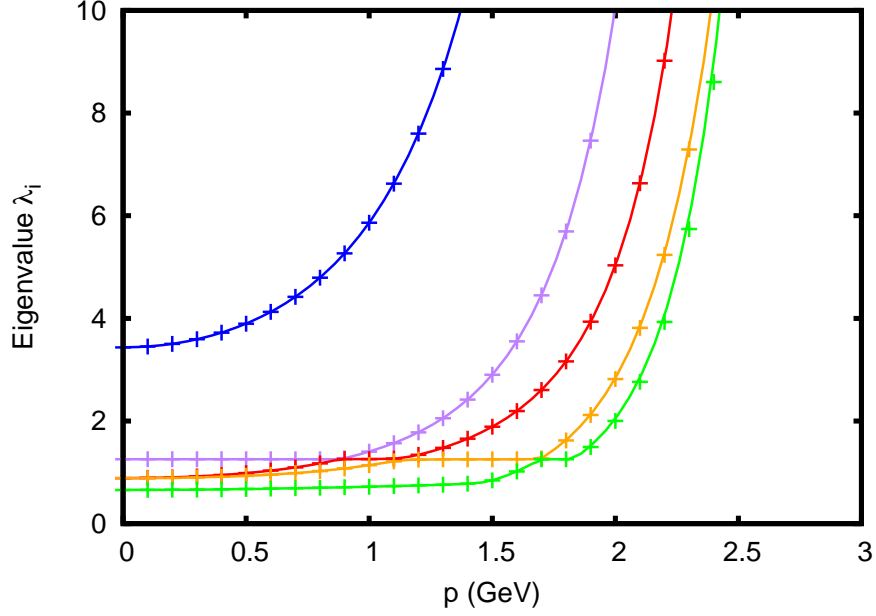


Figure 44: Comparison of the eigenvalue curves for the 0^{-+} glueball, calculated using both the Point Basis (lines) and Chebyshev Basis (points) methods, obtained with $g^2 = 1$ and the entire gluon model.

4.3 GLUEBALLS

As mentioned, the defining property of the $SU(3)$ symmetry underlying Quantum Chromodynamics is the existence of a color charge possessed by the constituents of all Baryons, the quarks, and featuring gluons as the mediator of the strong nuclear force. Unlike the (macroscopically) more familiar electromagnetism based on $U(1)$ charges, the gluons also carry a value of color charge, though in an adjoint representation to the three quark color charges. As charged particles, we have seen in §3.4.3 QCD Interactions that the gluons are capable of interacting not only with quarks, but with themselves as well. It has been long suspected^[18,39,64] that in addition to the familiar baryon states, there could also be

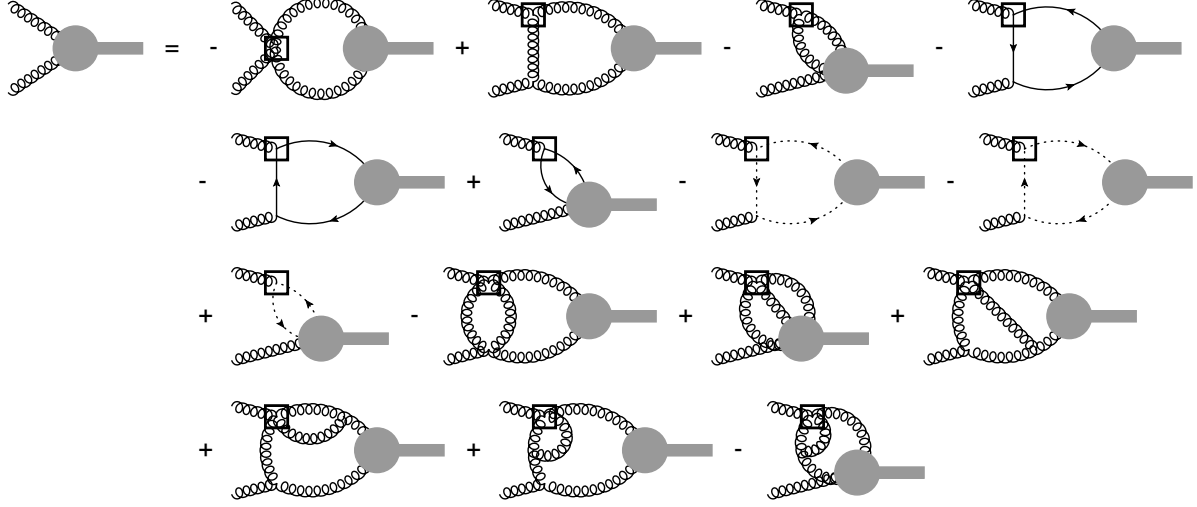


Figure 45: Functional expression for the 2-gluon glueball Bethe-Salpeter amplitude



Figure 46: Functional expression for the ghost-antighost mixing contribution to the glueball Bethe-Salpeter amplitude

bound states of QCD having only gluons as the constituents. These hypothetical bound states are known as Glueballs. We consider here the simplest valence contribution to glueballs, consisting of a bound pair of gluons. The development and continued improvement of the analysis presented here would seek to make contact with recent experimental results^[35] which suspect that higher excited states of these glueballs have already been detected. If one were to use the functional approach to deriving the Bethe-Salpeter amplitude as though the bound state were another field in our Lagrangian (though one which cannot propagate as an internal line), we would obtain the equation of motion shown in Figure 45 for the 2-gluon valence Bethe-Salpeter amplitude. The functional nature of this equation explicitly

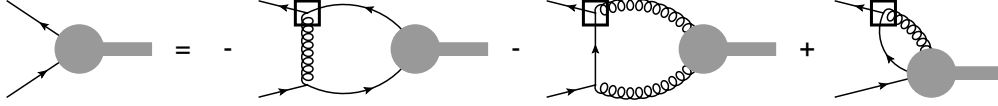


Figure 47: Functional expression for the quark-antiquark mixing contribution to the glueball Bethe-Salpeter amplitude

shows the coupling to other valence states, as one might expect given our experiences with the Schwinger-Dyson equations. We observe Bethe-Salpeter amplitudes which would couple the 2-gluon glueball to the 3-gluon and 4-gluon glueballs, a quark-antiquark (meson) bound state, a ghost-antighost bound state, as well as quark-antiquark-gluon and ghost-antighost-gluon hybrid states. The functional approach thus naturally incorporates the possibility of valence particles mixing through intermediate bound states. In order to fully characterize the system, we thus require the equivalent expressions for the ghosts and quarks, which are shown in Figures 46 and 47 respectively.

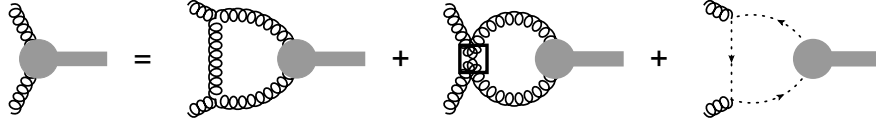


Figure 48: Equation for the gluon Bethe-Salpeter amplitude which was used in the present computation.

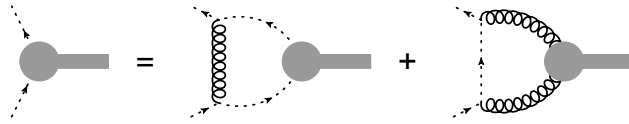


Figure 49: Equation for the ghost Bethe-Salpeter amplitude which was used in the present computation.

The truncated kernels which we considered for the computation discussed here are shown in Figure 48 and Figure 49 for the gluon and ghost amplitudes, respectively. A simple

ansatz for the vertex dressings was made^[50] before examination of the functional forms shown in Figures 45-47 were examined, and consistency with the gap equations for QCD would suggest that one of the vertices attached to a valence leg should have been left bare. This modification might be a first step toward improving upon the computation we have performed. In addition, early attempts were made to include a coupling to the truncated quark Bethe-Salpeter equation shown in Figure 50 (and the additional diagram in the gluon equation shown in Figure 51), but the choice of structure functions employed did not lead to a well-conditioned matrix for our eigensystem routine.

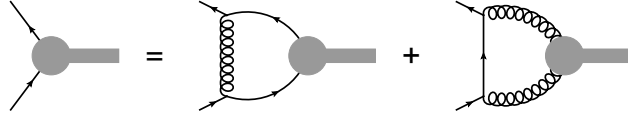


Figure 50: Equation for the quark Bethe-Salpeter amplitude which was initially attempted for the extension to glueball-meson mixing of §4.4.

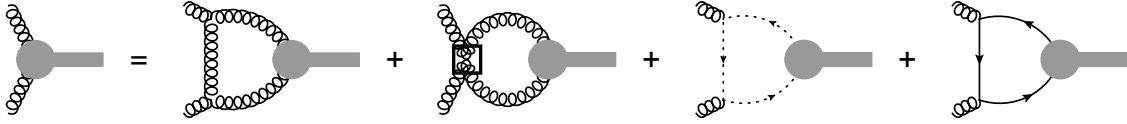


Figure 51: Extended equation for the gluon Bethe-Salpeter amplitude which was initially attempted for the extension to glueball-meson mixing of §4.4.

4.3.1 Symmetries of the 2-gluon Valence Contribution

In order to consider the glueball Bethe-Salpeter amplitude, we return to our definition 2.31 and apply it to the present case:

$$\Gamma^{\mu\nu}(x, y; P, \lambda) = \left\langle 0 \left| T(A^\mu(x) A^\nu(y)) \right| M(P, \lambda) \right\rangle \quad (4.18)$$

Our studies of the Bethe-Salpeter amplitudes will be based upon a general ansatz for a

2^{nd} rank Lorentz tensor. Given the available elements, and noting that we would prefer to define our ansatz for the Fourier transform of (4.18), we obtain:

$$\Gamma_{ab}^{\mu\nu}(q_+, q_-; \lambda) = \delta_{ab} \left(Q_\lambda g^{\mu\nu} + R_\lambda q_+^\mu q_+^\nu + S_\lambda q_-^\mu q_-^\nu + T_\lambda q_+^\mu q_-^\nu + U_\lambda q_-^\mu q_+^\nu + V_\lambda \epsilon^{\mu\nu\alpha\beta} q_{+\alpha} q_{-\beta} \right) \quad (4.19)$$

We will investigate which forms from a general ansatz can be made consistent with a gluonic bound state. We will accomplish this by imposing gluon field symmetries and the commutator for general times (to represent Bose symmetry):

$$\mathcal{T} A^\mu(x) \mathcal{T}^\dagger = \tilde{A}^\mu(-\tilde{x}) \quad (4.20)$$

$$\mathcal{P} A^\mu(x) \mathcal{P}^\dagger = \tilde{A}^\mu(\tilde{x}) \quad (4.21)$$

$$\mathcal{C} A^\mu(x) \mathcal{C}^\dagger = -A^{T\mu}(x) = -\frac{\lambda_a^T}{2} A_a^\mu(x) \quad (4.22)$$

$$[A^\mu(x), A^\nu(y)] = \Delta_{\mu\nu}(x - y) \quad (4.23)$$

where we employ the four-vector transformation $\tilde{a}^\mu \equiv (a^0, -\vec{a})^\mu$. Application of the time-reversal (4.20), parity (4.21), and charge-conjugation (4.22) transformations to the Bethe-Salpeter amplitude yields:

$$\Gamma^{\mu\nu}(x, y; P, \lambda) \xrightarrow{\mathcal{T}} \langle 0 | \overline{T}(\tilde{A}^\mu(-\tilde{x}) \tilde{A}^\nu(-\tilde{y})) | M(\tilde{P}, \lambda_T) \rangle, \quad (4.24)$$

$$\Gamma^{\mu\nu}(x, y; P, \lambda) \xrightarrow{\mathcal{P}} \eta_P^{(M)} \langle 0 | T(\tilde{A}^\mu(\tilde{x}) \tilde{A}^\nu(\tilde{y})) | M(\tilde{P}, \lambda_P) \rangle, \quad (4.25)$$

$$\Gamma^{\mu\nu}(x, y; P, \lambda) \xrightarrow{\mathcal{C}} \eta_C^{(M)} \langle 0 | T(A^\mu(x) A^\nu(y)) | M(P, \lambda_C) \rangle. \quad (4.26)$$

Aside from identifying that $\eta_C^{(M)} = +1$ for the 2-gluon glueball, the only transformation which we will consider by itself is the parity transformation (4.25). Instead, we will combine all three of these transformations to obtain:

$$\Gamma^{\mu\nu}(x, y; P, \lambda) \xrightarrow{\mathcal{CPT}} \eta_P^{(M)} \eta_C^{(M)} \langle 0 | \overline{T}(A^\mu(-x) A^\nu(-y)) | M(P, \lambda) \rangle \quad (4.27)$$

Next, we shall apply Bose symmetry. Due to the fact that $\Delta_{\mu\nu}(x-y)$ can be factored out of the scalar product, we are left with terms proportional to $\langle 0|M(P, \lambda)\rangle = 0$ from the RHS of (4.23). As such, our surviving terms yield:

$$\Gamma^{\mu\nu}(x, y; P, \lambda) \xrightarrow{Bose} \left\langle 0 \left| \overline{T}(A^\mu(x)A^\nu(y)) \right| M(P, \lambda) \right\rangle \quad (4.28)$$

Finally, we demand that $\Gamma^{\mu\nu}$ is invariant under $\mathcal{CP}\mathcal{T}$ and the Bose symmetry, so we can equate results of (4.27) and (4.28) to eliminate the anti-time ordering and find:

$$\overline{\Gamma}^{*\mu\nu}(x, y; P, \lambda) = \eta_P^{(M)} \eta_C^{(M)} \overline{\Gamma}^{*\mu\nu}(-x, -y; P, \lambda) \quad (4.29)$$

$$\Rightarrow \Gamma^{\mu\nu}(x, y; P, \lambda) = \eta_P^{(M)} \eta_C^{(M)} \Gamma^{\mu\nu}(-x, -y; P, \lambda) \quad (4.30)$$

where the last of these was obtained by assuming that $\eta_P^{(M)}$ and $\eta_C^{(M)}$ are real. Fourier transforming this yields:

$$\Gamma^{\mu\nu}(q_+, q_-; P, \lambda) = \eta_P^{(M)} \eta_C^{(M)} \Gamma^{\mu\nu}(-q_+, -q_-; P, \lambda). \quad (4.31)$$

Comparison to our general form shows that all of our 2nd rank terms in (4.19) are consistent with this result.

Next, we shall investigate the effects of the parity transformation. This transformation implies that we should flip the sign of all spatial 4-vector components, and it is clear from (4.25) that the time-time and space-space elements are unchanged while mixed time-space elements receive a sign change, as shown schematically in (4.32).

$$\left[\begin{array}{c|ccc} + & - & - & - \\ \hline - & + & + & + \\ - & + & + & + \\ - & + & + & + \end{array} \right] \quad (4.32)$$

Examination of (4.19) reveals that the metric term and all outer products of momenta transform in the same way. As such, we conclude that the even parity Bethe-Salpeter amplitude is given by

$$\Gamma_{ab}^{\mu\nu}(q_+, q_-; P, 0^{++}) = \delta_{ab} (Qg^{\mu\nu} + Rq_+^\mu q_+^\nu + Sq_-^\mu q_-^\nu + Tq_+^\mu q_-^\nu + Uq_-^\mu q_+^\nu). \quad (4.33)$$

The final term, which includes the antisymmetric tensor $\epsilon^{\mu\nu\alpha\beta}$, transforms with an additional sign change on all elements, as shown schematically in (4.34). This can be seen by recalling that the antisymmetric tensor is only nonzero if $\{\mu\nu\alpha\beta\}$ are some permutation of $\{0123\}$. The time-time element, as well as the diagonal space-space elements, are strictly zero. Of the remaining elements, the mixed time-space elements are only nonzero if $q_{+\alpha} q_{-\beta}$ are both spatial components, thus no sign flip. Similarly, the nonvanishing space-space elements are only nonzero if one of α and β is a time component and the other a spatial component, which results in a sign flip.

$$\left[\begin{array}{c|ccc} - & + & + & + \\ \hline + & - & - & - \\ + & - & - & - \\ + & - & - & - \end{array} \right] \quad (4.34)$$

As such, we conclude that the odd parity Bethe-Salpeter amplitude is given by

$$\Gamma_{ab}^{\mu\nu}(q_+, q_-; P, 0^{-+}) = \delta_{ab} V \epsilon^{\mu\nu\alpha\beta} q_{+\alpha} q_{-\beta}. \quad (4.35)$$

4.3.2 The 0^{-+} Glueball

From our earlier discussions of parity, we learn that the only available tensor for a 0^{-+} glueball amplitude is $\epsilon_{\mu\nu\alpha\beta} k_+^\alpha k_-^\beta$. We define the reduced Bethe-Salpeter amplitude with its structure function as:

$$\chi_{\mu\nu}^{0^{-+}}(k_+, k_-) \delta^{AB} = F(k, P) \delta^{AB} \epsilon_{\mu\nu\alpha\beta} k_+^\alpha k_-^\beta \quad (4.36)$$

4.3.2.1 Perturbative Vertices The resonance condition from gluon exchange (the second integral in the gluon equation (4.38)) is the only nonzero contribution to the (Yang-Mills) 0^{-+} glueball. In Landau gauge, this yields:

$$\begin{aligned}
F(k, P) = & \frac{ig_s^2 N_c}{k^2 P^2 - (k \cdot P)^2} \int \frac{d^4 q}{(2\pi)^4} F(q, P) G(q_+^2) G((q-k)^2) G(q_-^2) \\
& \times \left\{ 8P^2(q \cdot k)^2 + 8k^2(P \cdot q)^2 + 8q^2(P \cdot k)^2 - 8P^2 q^2 k^2 \right. \\
& - 16(P \cdot q)(P \cdot k)(q \cdot k) + P^4(q \cdot k) - P^2(P \cdot q)(P \cdot k) \\
& \left. - (P^2(q \cdot k) - (P \cdot q)(P \cdot k)) \left(\frac{4q^2 k^2 - 2(q \cdot k)^2 + (P \cdot (q-k))^2}{(q-k)^2} \right) \right\}
\end{aligned} \tag{4.37}$$

In general, other contributions are possible from the ghost fields. In particular, we consider the mixing kernel diagrams shown in Figure 52.

Careful examination of the term denoted $\gamma_{g \ gh}$ in Figure 52 shows that the integrand contains the combination $(q-k)_\mu k_{-\nu} \epsilon^{\mu\nu\alpha\beta} q_{+\alpha} q_{-\beta}$. This quantity vanishes due to the fact that there are four contractions involving combinations of only three vectors k_μ , q_μ , and P_μ . The term denoted $\gamma_{gh \ g}$ in Figure 52 contains the combination $q_{+\mu}(q-k)_\nu$. This does not by itself vanish, however the scalar combination we employed to obtain (4.37) yields $q_{+\mu}(q-k)_\nu \epsilon^{\mu\nu\alpha\beta} k_{+\alpha} k_{-\beta}$ in the integrand, which vanishes for the same reason. We conclude that there is no gluon-ghost mixing for the 0^{-+} glueball, and so (4.37) is our complete resonance condition in the Landau gauge.

4.3.2.2 Dressed Vertices The inclusion of the vertex dressing functions in our bound state equation leads to considerable complication of the integrand, and so the computation is defined at the level of (4.38)–(4.40) with the dressing functions $V^{\alpha\beta\gamma}(P_1, P_2, P_3)$ unspecified. This allows for investigation of various vertex dressing models with a single input parameter at runtime, where the appropriate scalar dressing functions $V(P_1, P_2, P_3)$ as called in the

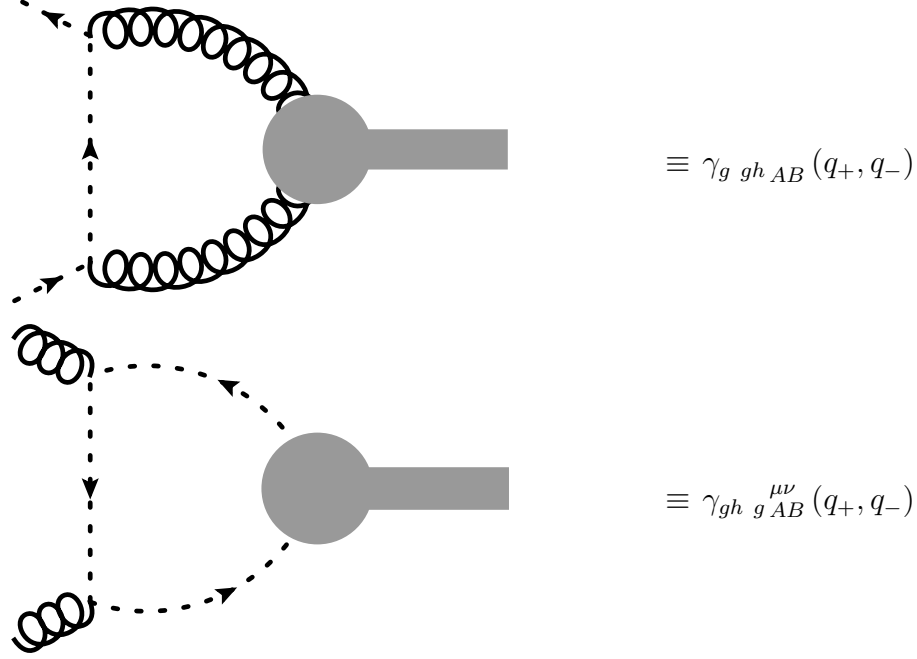


Figure 52: Bethe-Salpeter terms involving the gluon-ghost mixing kernel.

code are the only difference between models which share a common tensor structure. We are considering first the approximate form of the vSHA gluon vertex (3.153), the Pennington-Wilson model (3.147), and the hybrid dressing model (3.154). The dressing in these cases can be seen as introducing a scalar function with each metric term in the perturbative gluon vertex, where the three functions are related by cyclic permutations of the arguments. The dressed ghost vertex can similarly be expressed as a scalar function multiplying the perturbative vertex, and so there is an identical argument for neglecting the ghost equations as with the perturbative vertices. This also allows us to include the preceding perturbative case by providing an option for $V(P_1, P_2, P_3) = 1$, such that the form (4.37) is recovered numerically.

4.3.3 The 0^{++} Glueball

Since no Lorentz indices are needed to characterize a $J = 0$ state, the Bethe-Salpeter amplitude for a $J = 0$ glueball can be expressed as an outer product of a 2nd-rank Lorentz tensor with a 2nd-rank color tensor. As we will see, the color dimensions arise in forms which reduce to an identity matrix and so do not need to be considered extensively. This behavior is reasonable, as the color-singlet nature of any physically-observed particle should imply that there should be no preference for any particular gluon color state. In terms of the (reduced) Bethe-Salpeter amplitude, propagators, and generalized vertex functions, the coupled system of bound state equations, for the gluons, ghosts, and fermions respectively, are:

$$\begin{aligned}
\chi^{\mu\nu}(k_+, k_-)\delta^{AB} = & ig_0^2 f^{ACD} f^{BCD} \int \frac{d^4 q}{(2\pi)^4} [2g^{\mu\nu} g^{\alpha\beta} - g^{\mu\alpha} g^{\nu\beta} - g^{\mu\beta} g^{\nu\alpha}] \\
& \chi_{\alpha\beta}(q_+, q_-) G(q_+) G(q_-) \\
& + ig_0^2 f^{ACD} f^{BCD} \int \frac{d^4 q}{(2\pi)^4} \chi_{\alpha\beta}(q_+, q_-) G(q_+) G(q_-) G(Q) \\
& \quad \times P_{\gamma\gamma'}(Q) V^{\mu\gamma\alpha}(-k_+, -Q, q_+) V^{\nu\gamma'\beta}(-k_-, Q, q_-) \\
& - g_0^2 \frac{\delta^{AB}}{2} \int \frac{d^4 q}{(2\pi)^4} Tr [\gamma^\mu S(q_+) \chi_F(q_+, q_-) S(-q_-) \gamma^\nu S(Q)] \\
& \quad \times \frac{h^n(k_+) h^n(k_-)}{4} [A(q_+) + A(Q)] [A(q_-) + A(Q)] \\
& + ig_0^2 f^{ACD} f^{BCD} \int \frac{d^4 q}{(2\pi)^4} \chi_G(q_+, q_-) H(q_+) H(q_-) H(Q) \\
& \quad \times \left[q_+^\mu \frac{h(k_+)}{h(q_+)} + Q^\mu \left(\frac{h(k_+)}{h(Q)} - 1 \right) \right] \\
& \quad \times \left[Q^\nu \frac{h(k_-)}{h(Q)} - q_-^\nu \left(\frac{h(k_-)}{h(q_-)} - 1 \right) \right], \tag{4.38}
\end{aligned}$$

$$\begin{aligned}
\chi_G(k_+, k_-; P) \delta^{AB} = & -ig_0^2 f^{ACD} f^{BCD} \int \frac{d^4 q}{(2\pi)^4} k_{+\mu} k_{-\nu} \chi^{\mu\nu}(q_+, q_-) G(q_+) G(q_-) H(Q) \\
& \times \left[\frac{h(q_+)}{h(Q)} + \frac{h(q_+)}{h(k_+)} - 1 \right] \left[\frac{h(q_-)}{h(Q)} + \frac{h(q_-)}{h(k_-)} - 1 \right] \\
& + ig_0^2 f^{ACD} f^{BCD} \int \frac{d^4 q}{(2\pi)^4} k_{+\mu} k_{-\nu} P^{\mu\nu}(Q) \chi_G(q_+, q_-) H(q_+) H(q_-) G(Q) \\
& \times \left[\frac{h(Q)}{h(q_+)} + \frac{h(Q)}{h(k_+)} - 1 \right] \left[\frac{h(Q)}{h(q_-)} + \frac{h(Q)}{h(k_-)} - 1 \right], \tag{4.39}
\end{aligned}$$

$$\begin{aligned}
\chi_F(k_+, k_-; P) = & g_0^2 T^A \cdot T^A \int \frac{d^4 q}{(2\pi)^4} \gamma_\mu S(-Q) \gamma_\nu \chi^{\mu\nu}(q_+, q_-) G(q_+) G(q_-) \\
& \times \frac{h^n(q_+) h^n(q_-)}{4} [A(k_+) + A(Q)] [A(Q) + A(k_-)] \\
& + ig_0^2 T^A \cdot T^A \int \frac{d^4 q}{(2\pi)^4} \gamma_\mu S(q_+) \chi_F(q_+, q_-) S(-q_-) \gamma_\nu P^{\mu\nu}(Q) G(Q) \\
& \times \frac{h^{2n}(Q)}{4} [A(k_+) + A(q_+)] [A(q_-) + A(k_-)], \tag{4.40}
\end{aligned}$$

where we have suppressed the fermion's Dirac and color indices. For the present computation we do not directly consider (4.40) as it pertains to Glueballs, but the extension it provides will be discussed in §4.4. The equations include the possibility for the modeled gluon self interaction discussed in §3.4.3 and §4.3.2.2, where:

$$V^{\alpha\beta\gamma}(1, 2, 3) = V_1^{\beta\gamma}(P_2 - P_3)^\alpha + V_2^{\gamma\alpha}(P_3 - P_1)^\beta + V_3^{\alpha\beta}(P_1 - P_2)^\gamma. \tag{4.41}$$

For the vertex models (3.153), (3.147), and (3.154), the dressing functions are simply terms involving a metric tensor like $V_3^{\alpha\beta} = V_3 g^{\alpha\beta}$. As mentioned previously, the bare vertex case can be recovered by $V(P_1, P_2, P_3) = 1$.

As described in the §4.3.1, the most general form for the 0^{++} glueball Bethe-Salpeter amplitude is shown in (4.33).

If we were working in Feynman gauge, it would be obvious that the tensors are unaffected by amputation of the gluon lines and so the only difference between Γ and χ is the definition of the structure functions. The ansatz for χ would thus be:

$$\chi_{AB}^{\mu\nu}(q_+, q_-; P, 0^{++}) = \delta_{AB} (Ag^{\mu\nu} + Bq_+^\mu q_+^\nu + Cq_-^\mu q_-^\nu + D'q_+^\mu q_-^\nu + Eq_-^\mu q_+^\nu), \quad (4.42)$$

where multiplication of the structure functions $\{ABCD'E\}$ by the scalar portions of the gluon propagators yields the structure functions $\{QRSTU\}$.

In Landau gauge, the investigation of the reduced amplitude must be performed carefully due to the presence of projection operators $P^{\mu\nu}(q_\pm)$ in the gluon propagators. As such, there is no inverse operator which can directly transform Γ into χ , and so the definition of χ appears to be ambiguous. Instead, we note that the projection operators allow only the transverse components of χ to appear in the integral. If we contract the entire gluon Bethe-Salpeter equation with appropriate projection operators, we can similarly reduce the equation to only the equivalent transverse forms on the LHS. Since we obtain our scalar equations by contracting the equation with a 2nd rank tensor which shares these transversality properties, this has no effect on our resonance condition. We could alternatively state that the structure functions introduced with the transverse terms are the only independent functions in the resonance equation, where all other possible structure functions are functionally dependent on the transverse portions and can be determined by using more general projectors on the LHS.

Due to the restriction of functional independence to transverse components, we take advantage of the fact that the (physically relevant) Bethe-Salpeter amplitude is transverse to the momentum of each gluon leg contracted to that particular index:

$$q_{+\mu} \chi^{\mu\nu} = \chi^{\mu\nu} q_{-\nu} = 0, \quad (4.43)$$

which yields three scalar equations among the structure functions

$$0 = q_+ \cdot \chi \cdot q_+ = Aq_+^2 + Bq_+^4 + C(q_+ \cdot q_-)^2 + D'q_+^2(q_+ \cdot q_-) + Eq_+^2(q_+ \cdot q_-), \quad (4.44)$$

$$0 = q_- \cdot \chi \cdot q_- = Aq_-^2 + B(q_+ \cdot q_-)^2 + Cq_-^4 + D'q_-^2(q_+ \cdot q_-) + Eq_-^2(q_+ \cdot q_-), \quad (4.45)$$

$$0 = q_+ \cdot \chi \cdot q_- = A(q_+ \cdot q_-) + Bq_+^2(q_+ \cdot q_-) + Cq_-^2(q_+ \cdot q_-) + D'q_+^2q_-^2 + E(q_+ \cdot q_-)^2. \quad (4.46)$$

Solution of this system of equations yields the final ansatz for the 0^{++} glueball amplitude, which depends on only two structure functions, A and D' .

$$\chi_{AB}^{\mu\nu}(q_+, q_-; P, 0^{++}) = \delta_{AB} \left\{ A \left(g^{\mu\nu} - \frac{q_-^\mu q_+^\nu}{q_+ \cdot q_-} \right) \right. \quad (4.47)$$

$$\left. + D' \left[q_+^\mu q_-^\nu - \left(\frac{q_-^2}{q_+ \cdot q_-} \right) q_+^\mu q_+^\nu - \left(\frac{q_+^2}{q_+ \cdot q_-} \right) q_-^\mu q_-^\nu + \frac{q_+^2 q_-^2}{(q_+ \cdot q_-)^2} q_-^\mu q_+^\nu \right] \right\}$$

$$= \delta_{AB} \left\{ A \left(g^{\mu\nu} - \frac{q_-^\mu q_+^\nu}{q_+ \cdot q_-} \right) + D' \left(q_+^\mu - \left(\frac{q_-^2}{q_+ \cdot q_-} \right) q_-^\mu \right) \otimes \left(q_-^\nu - \left(\frac{q_+^2}{q_+ \cdot q_-} \right) q_+^\nu \right) \right\} \quad (4.48)$$

$$= \delta_{AB} \left\{ A \left(g^{\mu\nu} - \frac{q_-^\mu q_+^\nu}{q_+ \cdot q_-} \right) + D \frac{\left(q_+^\mu - \left(\frac{q_-^2}{q_+ \cdot q_-} \right) q_-^\mu \right) \otimes \left(q_-^\nu - \left(\frac{q_+^2}{q_+ \cdot q_-} \right) q_+^\nu \right)}{\left(q_+ - \left(\frac{q_-^2}{q_+ \cdot q_-} \right) q_- \right) \cdot \left(q_- - \left(\frac{q_+^2}{q_+ \cdot q_-} \right) q_+ \right)} \right\}, \quad (4.49)$$

where we have rescaled the structure function $D = D' \left(q_+ - \left(\frac{q_-^2}{q_+ \cdot q_-} \right) q_- \right) \cdot \left(q_- - \left(\frac{q_+^2}{q_+ \cdot q_-} \right) q_+ \right)$.

Truncating at the perturbative vertices, we see that the ghost fields can potentially mix with the gluon bound state. The Bethe-Salpeter equation for the ghost's contribution is shown in Figure 49, which must be considered in conjunction with the gluon's equation to preserve consistency with gauge invariance to the level of our truncations and modeling. Figure 51 also shows the Bethe-Salpeter equation for the quark fields, which is also able to mix with the gluons when we generalize beyond the pure Yang-Mills theory, but for now the consideration will only include the valence gluon/ghost content.

Consideration of the structure of the ghost Bethe-Salpeter amplitude is much simpler, as the same color-diagonal arguments apply and there are no further tensor indices to represent. The ghost amplitude contains a single structure function F , and the requirement for 0^{++} symmetry is consistent with a scalar function:

$$\chi_G^{AB}(k_+, k_-; P) = \delta^{AB} F(k_+, k_-; P). \quad (4.50)$$

Due to the complicated nature of the contractions expressed in (4.38)–(4.40), the symbolic form for these equations will not be given explicitly, as each required term can be most simply expressed using hundreds or thousands of lines when expressed in code (if not careful about obtaining the most fully simplified form from Mathematica, the expressions can easily reach tens of thousands of lines).

The various structure functions, 1 for the ghosts and 2 for the gluons, require an expansion of the eigensystem matrix described in §4.2.1. We thus express the kernel in matrix form such that each structure function contributes to an $N_q \times N_x$ “Super-Block” as describe above. For the 0^{++} glueball, we thus have a $3 \times N_q \times N_x$ -dimensioned square matrix subdivided by such Super-Blocks. For example, the diagonal Super-Blocks represent a structure function’s contribution to its own scalar equation, while the off-diagonal Super-Blocks express the mixing between distinct structure functions and/or valence particles. The significance of this form for valence-mixing situations will be further discussed in §4.4

4.3.4 Glueball Results

As discussed in §4.2, the Point basis (Super-Index) is our preferred method of expressing the resonance equation as an eigensystem. Furthermore, we choose to employ the symbolic expressions for the tensor contractions as obtained from Mathematica, since the in-code contractions result in computationally intensive summation loops which lack the speed and increased precision of evaluating the (rather complicated) symbolic expressions. These symbolic expressions depend on a generic form for the gluon propagator, provided that it is an analytic function on the complex plane and thus well-suited to inclusion in the integrands.

The various continuation methods discussed in §4.1 could be successfully applied to a relative few of the gluon propagator models discussed in QCD, and even then only under very restrictive sets of input parameters. As a result, the glueball resonances were investigated using only the entire model gluon propagator of (3.186) as fit to the lattice data of Bogolubsky *et al*^[15].

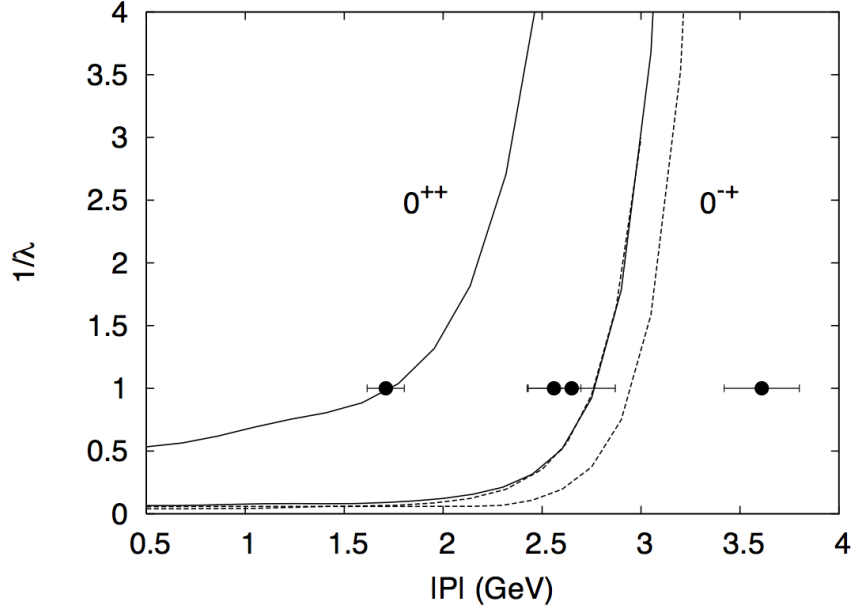


Figure 53: Comparison of resonance eigenvalues to the lattice results for glueball masses of Morningstar *et al.*^[52]. Solid lines represent 0^{++} eigenvalues, dashed lines are 0^{-+} . All solutions were obtained with the entire gluon model and $g^2 = .1681$

Our findings are consistent with a glueball ground state of mass $O(1\text{GeV})$ for both parity states^[52], and the existence of several excited states with slightly greater mass. A comparison to lattice QCD results for the ground and first excitation glueball states is shown in Figure 53.

Unfortunately for experimental verification, the observed resonances that can be clearly identified^[35] by modern detectors lie in the $2 - 3 \text{ GeV}$ mass range and represent $O(10)$ excited states that are beyond our current capability for computing bound state spectra. Nonetheless, the possibility of fitting pure-gluon bound states to experimental observation

represents an exciting extension to the theoretical understanding of QCD and the nature of of nuclear and particle physics.

4.4 GLUEBALL + MESON STUDIES

The expansion of the eigensystem representation to describe the 0^{++} glueball describes a clear path for consideration of the mixed-valence bound states. We did not call much attention to the ghost valence content of these glueball states, because despite the unobservable nature of the fundamental particles of QCD the ghosts are suppressed by a further layer of conceptual understanding. The ghosts are not meant to be fundamental dynamical degrees of freedom (i.e. fundamental particles) of the theory, but only to serve as a mathematical crutch to preserve the gauge symmetry for gluons through the gauge-fixing procedure. Despite this interpretation of unphysical ghosts, they serve (along with the multiple structure functions for the 0^{++} gluon contribution) to reveal the nonperturbative treatment of valence particle states.

As mentioned in §4.2.1, the identification of a resonance state implies that the corresponding eigenvector is a discretized representation of the Bethe-Salpeter amplitude(s) χ . Despite the expansion of “Super-Block” contributions from various structure functions and valence states, the eigenvector provides a telling and conclusive means to assess the true valence contribution of any resonance.

Conventional practice has declared the observable states of QCD to fall into categories such as mesons and baryons, but to date the possibility of gluon binding had been lacking from these definitions. The conditions imposed by confinement merely suggest that no color-charged entity can be observed as an asymptotic state. The benefit of extending valence content beyond the quark sector is that any solution (eigenvector) that satisfies the resonance condition is a recipe for the physically realistic and relevant particle content of that state. For example, if a meson state consisted purely of a quark and anti-quark with no gluon

contributions, then the eigenvector produced at that resonance would contain a discretized Bethe-Salpeter amplitude for the quark sector and a null set for any other valence sector. The only means by which such an assessment could be made is to include potential contributions from gluons, ghosts, and quarks in any imaginable (and computationally feasible) consideration of the generalized Bethe-Salpeter equation for all observed bound states.

In particular, the coupling of the scalar glueball to the meson sector has been investigated at the perturbative level^[17]. In that investigation, it was noted that the coupling to quark fields was proportional to the current quark mass and thus the pion decay channels would be suppressed by the light quark masses and kaons would instead dominate. Our preliminary studies of this mixing revealed that the quark contributions in a nonperturbative approach are proportional to factors of $B(p^2)$ and so are consistent with the earlier attempts.

5.0 CONCLUSIONS

The nonperturbative treatment of quantum field theory has been presented here in a pedagogical manner that should suffice to instruct a future practitioner in the methods and content required to reproduce and expand upon the investigations described. The formalism was developed out of the context of a textbook-level understanding of field theory to provide a sure basis for the study of these nonperturbative equations.

The nonperturbative methods have been applied to a number of quantum field theories with multiple choices of modeling or truncation. These theories were presented to illustrate the methods and capability of the Schwinger-Dyson equations, and to provide context for the computation of the fully coupled system of gap equations for QCD. In the context of the gluon gap equation, we were able to compare the relative contributions of the various diagrams and identify a clear and persistent hierarchy in the significance of each term. As mentioned, the fact that these solutions result from nonlinear equations might make arguments of significance seem dubious, but it can be confirmed through comparison to previous treatments of the equations, by myself and others, that approximations based on arguments such as these can provide useful insight into the dynamics and physical content of the theory. As another example, we were able to develop a set of equations for the quark propagator which depends in a very general way on the gluon propagator's dressing function. As a result, the comparison between the various models such as *Swimming with Quarks*, fits to the lattice gluon propagator, or even the inclusion of a dynamically calculated gluon propagator can be directly compared based on the change of only a single contribution to the integrand. This example also shows the versatility of the Schwinger-Dyson formalism,

as the cases involving modeled or perturbative gluon propagators can be easily revisited and reproduced using the same computational tools as the fully coupled model by making relatively simple modifications. These comparisons across many levels of approximation provide a high level of confidence that we are able to produce consistent results from these equations, and that our interpretations and conclusions are built on a solid analytical and computational foundation.

The Schwinger-Dyson equations thus provide a clear and reliable method for advancing the understanding of how our approximations affect the quality of the solutions we obtain. From any starting approximation, the option to expand the set of equations or introduce more sophisticated treatments is always available, and it is relatively easy to compare to previous efforts and assess the importance of the new elements in the calculation. As mentioned, the fact that these solutions result from nonlinear equations might make arguments of significance seem dubious, but it can be confirmed through comparison to previous treatments of the equations, by myself and others, that approximations based on arguments such as these can provide useful insight into the dynamics and physical content of the theory. We obtained solutions within QCD which demonstrated many different situations which could produce decoupling solutions for the gluon propagator or chiral symmetry breaking in the quark sector.

Our computation of the fully coupled system of QCD gap equations with the inclusion of nonperturbative two-loop diagrams for the gluon propagator represents the most complete treatment of these equations to date. The agreement of our results with lattice QCD was impressive but not perfect. Future research with a special focus on improving the dynamical models for interaction vertices is sure to provide a corresponding improvement in the quality of solutions obtained. This dynamical treatment and renormalization of the vertex equations could provide an unambiguous means of performing nonperturbative renormalization, which have the potential to absorb or prevent the quadratic divergences of the gluon equation without recourse to schemes involving the introduction of gluon mass terms or the fitting and subtraction of the unphysical behaviors that may arise. Much as the gauge symmetry

causes such divergences to cancel in perturbation theory, the issues discussed regarding their appearance in the nonperturbative treatment seem to imply that the vertex models do not sufficiently represent those symmetries. The consideration of these interactions in the Schwinger-Dyson formalism would be increasingly difficult, but the benefit they would provide has the potential to be equally great.

The Schwinger-Dyson equations are a powerful means for studying quantum field theory. Further investigation of their structure and continued progress beyond the current state of truncations and models promise to yield valuable insights into the physical content of Quantum Chromodynamics and other quantum field theories. While progress in this formalism is sometimes overlooked in favor of the complementary nonperturbative methods of lattice gauge theory, there are properties that can be more easily examined through one method or the other. We have demonstrated that the Schwinger-Dyson equations can produce reliable calculations of the propagators across many different field theories, and that the analytical formulation of these equations of motion can be easily compared across seemingly different theories. We have shown that the diagrammatic expressions for the equations of motion are based on very general properties of the particles and interactions, and that for example the c-number or Grassmann nature of a field variable or the number of particles in a perturbative vertex have a more significant affect on these expressions than the particular quantum numbers or tensor structures which define the fields. These other properties feature heavily in the translation between the diagrammatic and analytical expressions, but we have shown that the structure of perturbative interactions or propagators can provide a great deal of information for the choice of tensor expansions, dressing functions, and vertex models, and so the translation between these representations can be easily generalized and applied to a new theory. In addition to the particular field content, we have shown that a consistent set of nonperturbative renormalization strategies can be easily applied across a wide range of quantum field theories. This is a powerful application of the Schwinger-Dyson formalism, as information regarding the success or failure of a renormalization approach in one situation can be extremely useful in the consideration of other theories whose equations of motion

describe similar analytic behavior or perturbative expressions.

Along with the physical motivations for the continued pursuit of nonperturbative quantum field theory, there are technological reasons as well. The continued improvement of computer technology has made it possible for rapid advances in many topics of computational physics, including the ability to obtain good approximations to the continuum solutions of Schwinger-Dyson equations on a consumer-end machine and the progressively finer grid spacings now possible in lattice QCD. Since computational limitations are part of the difficulty in extending the Schwinger-Dyson formalism to include dressed interactions, it is likely that continued improvement of the technology will allow for further investigation of these quantities even without significant progress in the analytical development. As a comparison, the computation of propagators as discussed here would have been prohibitively intense even as of a few decades ago and so we cannot rule out the possibility of great progress from brute-force applications of future technology.

The discussions of gluon content in the bound states of QCD provide another interesting application of nonperturbative quantum field theory. Since the fundamental degrees of freedom in this theory are strictly unobservable due to confinement, its bound states are the experimentally observable entities and their spectra and properties are the measurable quantities we can obtain. The conventional explanation for the particle zoo is built around the simplest valence combinations of quarks that can have the properties used to define mesons and baryons, but experimental evidence is mounting for the existence of more exotic states such as diquarks and glueballs. The traditional definitions of the hadrons may thus merely be a representation of the leading contribution to these states, while comparison to the tower of Schwinger-Dyson equations would suggest that it is quite likely that more complex and exotic valence states have some level of influence on these states and perhaps even a direct contribution.

Investigations of the Bethe-Salpeter equation as presented here have the potential to shine some light on these exotic states and the possibility of mixing into more familiar ones. As the quality of nonperturbative solutions for propagators and interactions are improved, the

ability of bound state computations to faithfully include dynamical properties will likewise improve. Improvement of the dynamical ingredients and computational tools that have been developed here may allow for more direct comparison to observations and experiment. The main difficulty in expanding this approach is that the simplistic scattering kernel we described does not seem to provide a good description of glueball dynamics, and so it would be necessary to develop a far more robust and sophisticated kernel before the desired results would be possible. As an additional challenge, lattice results have suggested phenomena such as gluelumps and flux tubes which involve massive numbers of gluons and suggest that many-particle states make significant contributions to glueballs and related structures. Since large numbers of particles are a particular weakness of the current state of Schwinger-Dyson equations, it is possible and in fact extremely likely that this bound state formalism would require a significant amount of progress and development before these computations could prove themselves useful.

BIBLIOGRAPHY

- [1] Stephen L. Adler. Axial-Vector Vertex in Spinor Electrodynamics. *Phys. Rev.*, 177: 2426–2438, Jan 1969. doi: 10.1103/PhysRev.177.2426. URL <http://link.aps.org/doi/10.1103/PhysRev.177.2426>.
- [2] A. C. Aguilar and J. Papavassiliou. Chiral Symmetry Breaking With Lattice Propagators. *Phys. Rev. D*, 83:014013, Jan 2011. doi: 10.1103/PhysRevD.83.014013. URL <http://link.aps.org/doi/10.1103/PhysRevD.83.014013>.
- [3] A. C. Aguilar, D. Ibáñez, and J. Papavassiliou. Ghost Propagator and Ghost-Gluon Vertex from Schwinger-dyson Equations. *Phys. Rev. D*, 87:114020, Jun 2013. doi: 10.1103/PhysRevD.87.114020. URL <http://link.aps.org/doi/10.1103/PhysRevD.87.114020>.
- [4] R. Alkofer, W. Detmold, C. S. Fischer, and P. Maris. Analytic Properties of the Landau Gauge Gluon and Quark Propagators. *Phys. Rev. D*, 70:014014, Jul 2004. doi: 10.1103/PhysRevD.70.014014. URL <http://link.aps.org/doi/10.1103/PhysRevD.70.014014>.
- [5] Reinhard Alkofer and Lorenz von Smekal. The Infrared Behaviour of QCD Green’s Functions: Confinement, Dynamical Symmetry Breaking, and Hadrons as Relativistic Bound States. *Physics Reports*, 353(56):281 – 465, 2001. ISSN 0370-1573. doi: [http://dx.doi.org/10.1016/S0370-1573\(01\)00010-2](http://dx.doi.org/10.1016/S0370-1573(01)00010-2). URL <http://www.sciencedirect.com/science/article/pii/S0370157301000102>.
- [6] D. Bailin and A. Love. *Introduction to Gauge Field Theory: Revised Edition*. Graduate Student Series in Physics. Taylor & Francis, 1993. ISBN 9780750302814. URL <http://books.google.com/books?id=A9MU9pvcEGQC>.
- [7] James S. Ball and Ting-Wai Chiu. Analytic Properties of the Vertex Function in Gauge Theories. I. *Phys. Rev. D*, 22:2542–2549, Nov 1980. doi: 10.1103/PhysRevD.22.2542. URL <http://link.aps.org/doi/10.1103/PhysRevD.22.2542>.

- [8] James S. Ball and Ting-Wai Chiu. Analytic Properties of the Vertex Function in Gauge Theories. II. *Phys. Rev. D*, 22:2550–2557, Nov 1980. doi: 10.1103/PhysRevD.22.2550. URL <http://link.aps.org/doi/10.1103/PhysRevD.22.2550>.
- [9] C Becchi, A Rouet, and R Stora. Renormalization of Gauge Theories. *Annals of Physics*, 98(2):287 – 321, 1976. ISSN 0003-4916. doi: [http://dx.doi.org/10.1016/0003-4916\(76\)90156-1](http://dx.doi.org/10.1016/0003-4916(76)90156-1). URL <http://www.sciencedirect.com/science/article/pii/0003491676901561>.
- [10] J.S. Bell and R. Jackiw. A PCAC Puzzle: $\pi^0 \rightarrow \gamma\gamma$ in the σ -Model. *Il Nuovo Cimento A*, 60(1):47–61, 1969. ISSN 0369-3546. doi: 10.1007/BF02823296. URL <http://dx.doi.org/10.1007/BF02823296>.
- [11] Martina Blank. *Properties of Quarks and Mesons in the Dyson-Schwinger/Bethe-Salpeter Approach*. PhD thesis, University of Graz, 2011. URL <http://arxiv.org/abs/1106.4843>. arXiv:1106.4843 [hep-ph].
- [12] J. C. R. Bloch. Multiplicative Renormalizability of Gluon and Ghost Propagators in QCD. *Phys. Rev. D*, 64:116011, Nov 2001. doi: 10.1103/PhysRevD.64.116011. URL <http://link.aps.org/doi/10.1103/PhysRevD.64.116011>.
- [13] J. C. R. Bloch. Multiplicative Renormalizability and Quark Propagator. *Phys. Rev. D*, 66:034032, Aug 2002. doi: 10.1103/PhysRevD.66.034032. URL <http://link.aps.org/doi/10.1103/PhysRevD.66.034032>.
- [14] J. C. R. Bloch. Two-Loop Improved Truncation of the Ghost-Gluon Dyson-Schwinger Equations: Multiplicatively Renormalizable Propagators and Nonperturbative Running Coupling. *Few-Body Systems*, 33(2-3):111–152, 2003. ISSN 0177-7963. doi: 10.1007/s00601-003-0013-3. URL <http://dx.doi.org/10.1007/s00601-003-0013-3>.
- [15] I.L. Bogolubsky, E.-M. Ilgenfritz, M. Müller-Preussker, and A. Sternbeck. Lattice Gluodynamics Computation of Landau-Gauge Green’s Functions in the Deep Infrared. *Physics Letters B*, 676(13):69 – 73, 2009. ISSN 0370-2693. doi: <http://dx.doi.org/10.1016/j.physletb.2009.04.076>. URL <http://www.sciencedirect.com/science/article/pii/S0370269309005206>.
- [16] Patrick O. Bowman, Urs M. Heller, Derek B. Leinweber, Maria B. Parappilly, Anthony G. Williams, and Jianbo Zhang. Unquenched Quark Propagator in Landau Gauge. *Phys. Rev. D*, 71:054507, Mar 2005. doi: 10.1103/PhysRevD.71.054507. URL <http://link.aps.org/doi/10.1103/PhysRevD.71.054507>.
- [17] Michael Chanowitz. Chiral Suppression of Scalar-Glueball Decay. *Phys. Rev. Lett.*, 95:172001, Oct 2005. doi: 10.1103/PhysRevLett.95.172001. URL <http://link.aps.org/doi/10.1103/PhysRevLett.95.172001>.

- [18] Frank E. Close. Scalar Glueballs and Friends. *Nuclear Physics A*, 623(12):125 – 134, 1997. ISSN 0375-9474. doi: [http://dx.doi.org/10.1016/S0375-9474\(97\)00430-2](http://dx.doi.org/10.1016/S0375-9474(97)00430-2). URL <http://www.sciencedirect.com/science/article/pii/S0375947497004302>.
- [19] Attilio Cucchieri, Tereza Mendes, and Antonio Mihara. Numerical Study of the Ghost-Gluon Vertex in Landau Gauge. *Journal of High Energy Physics*, 2004(12):012, 2004. URL <http://stacks.iop.org/1126-6708/2004/i=12/a=012>.
- [20] D. C. Curtis and M. R. Pennington. Truncating the Schwinger-Dyson Equations: How Multiplicative Renormalizability and the Ward Identity Restrict the Three-Point vertex in QED. *Phys. Rev. D*, 42:4165–4169, Dec 1990. doi: 10.1103/PhysRevD.42.4165. URL <http://link.aps.org/doi/10.1103/PhysRevD.42.4165>.
- [21] R. E. Cutkosky and M. Leon. Normalization of Bethe-Salpeter Wave Functions and Bootstrap Equations. *Phys. Rev.*, 135:B1445–B1446, Sep 1964. doi: 10.1103/PhysRev.135.B1445. URL <http://link.aps.org/doi/10.1103/PhysRev.135.B1445>.
- [22] Anton K. Cyrol, Markus Q. Huber, and Lorenz von Smekal. A Dyson-Schwinger Study of the Four-Gluon Vertex. *arXiv*, arXiv:1408.5409 [hep-ph], 2014. URL <http://arxiv.org/abs/1408.5409>.
- [23] F. Dyson. The s Matrix in Quantum Electrodynamics. *Phys. Rev.*, 75:1736–1755, Jun 1949. doi: 10.1103/PhysRev.75.1736. URL <http://link.aps.org/doi/10.1103/PhysRev.75.1736>.
- [24] G. Eichmann, A. Krassnigg, M. Schwinzerl, and R. Alkofer. A Covariant View on the Nucleons Quark Core. *Annals of Physics*, 323(10):2505 – 2553, 2008. ISSN 0003-4916. doi: <http://dx.doi.org/10.1016/j.aop.2008.02.007>. URL <http://www.sciencedirect.com/science/article/pii/S0003491608000328>.
- [25] Gernot Eichmann. *Hadron Properties from QCD Bound-State Equations*. PhD thesis, University of Graz, 2009. URL <http://arxiv.org/abs/0909.0703>. arXiv:0909.0703 [hep-ph].
- [26] L.D. Faddeev and V.N. Popov. Feynman diagrams for the yang-mills field. *Physics Letters B*, 25(1):29 – 30, 1967. ISSN 0370-2693. doi: [http://dx.doi.org/10.1016/0370-2693\(67\)90067-6](http://dx.doi.org/10.1016/0370-2693(67)90067-6). URL <http://www.sciencedirect.com/science/article/pii/0370269367900676>.
- [27] R.P. Feynman and A.R. Hibbs. *Quantum Mechanics and Path Integrals*. International series in pure and applied physics. McGraw-Hill, 1965. URL <http://books.google.com/books?id=14ApAQAAMAAJ>.
- [28] C. S. Fischer and R. Alkofer. Nonperturbative Propagators, Running Coupling, and the Dynamical Quark Mass of Landau Gauge QCD. *Phys. Rev. D*, 67:094020, May

2003. doi: 10.1103/PhysRevD.67.094020. URL <http://link.aps.org/doi/10.1103/PhysRevD.67.094020>.
- [29] C. S. Fischer, P. Watson, and W. Cassing. Probing Unquenching Effects in the Gluon Polarization in Light Mesons. *Phys. Rev. D*, 72:094025, Nov 2005. doi: 10.1103/PhysRevD.72.094025. URL <http://link.aps.org/doi/10.1103/PhysRevD.72.094025>.
- [30] Christian S. Fischer. *Nonperturbative Propagators, Running Coupling and Dynamical Mass Generation in Ghost - Anti-Ghost Symmetric Gauges in QCD*. PhD thesis, University of Tübingen, 2003. URL <http://arxiv.org/abs/hep-ph/0304233>.
- [31] Christian S. Fischer, Dominik Nickel, and Richard Williams. On Gribovs Supercriticality Picture of Quark Confinement. *The European Physical Journal C*, 60(1):47–61, 2009. ISSN 1434-6044. doi: 10.1140/epjc/s10052-008-0821-1. URL <http://dx.doi.org/10.1140/epjc/s10052-008-0821-1>.
- [32] Galassi, M. et al. *GNU Scientific Library Reference Manual*, 3rd edition, 2013. URL <http://www.gnu.org/software/gsl/>.
- [33] Murray Gell-Mann and Francis Low. Bound States in Quantum Field Theory. *Phys. Rev.*, 84:350–354, Oct 1951. doi: 10.1103/PhysRev.84.350. URL <http://link.aps.org/doi/10.1103/PhysRev.84.350>.
- [34] Pavel Holoborodko. Gauss-Legendre Quadrature for C/C++. URL <http://www.holoborodko.com/pavel/numerical-methods/numerical-integration/>.
- [35] Y.K. Hsiao and C.Q. Geng. Identifying Glueball at 3.02 GeV in Baryonic B Decays. *Physics Letters B*, 727(13):168 – 171, 2013. ISSN 0370-2693. doi: <http://dx.doi.org/10.1016/j.physletb.2013.10.008>. URL <http://www.sciencedirect.com/science/article/pii/S0370269313008010>.
- [36] Markus Q. Huber and Lorenz Smekal. On the Influence of Three-Point Functions on the Propagators of Landau Gauge Yang-Mills Theory. *Journal of High Energy Physics*, 2013(4):1–33, 2013. doi: 10.1007/JHEP04(2013)149. URL <http://dx.doi.org/10.1007/JHEP04%282013%29149>.
- [37] Markus Q. Huber and Lorenz von Smekal. Spurious Divergences in Dyson-Schwinger Equations. *Journal of High Energy Physics*, 2014(6):15, 2014. doi: 10.1007/JHEP06(2014)015. URL <http://dx.doi.org/10.1007/JHEP06%282014%29015>.
- [38] M.Z. Iofa and I.V. Tyutin. Gauge Invariance of Spontaneously Broken Non-Abelian Theories in the Bogolyubov-Parasyuk-Hepp-Zimmermann Method. *Theoretical and Mathematical Physics*, 27(1):316–322, 1976. ISSN 0040-5779. doi: 10.1007/BF01036547. URL <http://dx.doi.org/10.1007/BF01036547>.

- [39] Kenzo Ishikawa. Glueballs. *Scientific American*, 247(5):142–156, November 1982. ISSN 0036-8733 (print), 1946-7087 (electronic). doi: <http://dx.doi.org/10.1038/scientificamerican1182-142>. URL <http://www.nature.com/scientificamerican/journal/v247/n5/pdf/scientificamerican1182-142.pdf>.
- [40] C. Itzykson and J.B. Zuber. *Quantum Field Theory*. Dover Books on Physics. Dover Publications, 2012. ISBN 9780486134697. URL <http://books.google.com/books?id=CxYCMNrUnTEC>.
- [41] Josef M. Jauch and F. Rohrlich. *The Theory of Photons and Electrons: The Relativistic Quantum Field Theory of Charged Particles with Spin One-Half*. Springer-Verlag New York, 2nd expanded edition, 1976. ISBN 0387072950.
- [42] Hideji Kita. Relativistic Two-Body Problem. *Progress of Theoretical Physics*, 7(2): 217–224, 1952. doi: 10.1143/ptp/7.2.217. URL <http://ptp.oxfordjournals.org/content/7/2/217.abstract>.
- [43] D. Lurié, A. J. Macfarlane, and Y. Takahashi. Normalization of Bethe-Salpeter Wave Functions. *Phys. Rev.*, 140:B1091–B1099, Nov 1965. doi: 10.1103/PhysRev.140.B1091. URL <http://link.aps.org/doi/10.1103/PhysRev.140.B1091>.
- [44] A.J. Macfarlane, A. Sudbery, and P.H. Weisz. On Gell-Mann’s λ -Matrices, d- and f-Tensors, Octets, and Parametrizations of SU(3). *Communications in Mathematical Physics*, 11(1):77–90, 1968. ISSN 0010-3616. doi: 10.1007/BF01654302. URL <http://dx.doi.org/10.1007/BF01654302>.
- [45] S. Mandelstam. Dynamical Variables in the Bethe-Salpeter Formalism. *Proceedings of the Royal Society of London. Series A. Mathematical and Physical Sciences*, 233(1193):248–266, 1955. doi: 10.1098/rspa.1955.0261. URL <http://rspa.royalsocietypublishing.org/content/233/1193/248.abstract>.
- [46] S. Mandelstam. Approximation Scheme for Quantum Chromodynamics. *Phys. Rev. D*, 20:3223–3238, Dec 1979. doi: 10.1103/PhysRevD.20.3223. URL <http://link.aps.org/doi/10.1103/PhysRevD.20.3223>.
- [47] F. Mandl and G. Shaw. *Quantum Field Theory*. A Wiley-Interscience publication. John Wiley & Sons, 2010. ISBN 9780471496830. URL <http://books.google.com/books?id=Ef4zDW1V2LkC>.
- [48] Pieter Maris and Craig D. Roberts. π - and k-meson Bethe-Salpeter Amplitudes. *Phys. Rev. C*, 56:3369–3383, Dec 1997. doi: 10.1103/PhysRevC.56.3369. URL <http://link.aps.org/doi/10.1103/PhysRevC.56.3369>.

- [49] Pieter Maris and Peter C. Tandy. Bethe-Salpeter Study of Vector Meson Masses and Decay Constants. *Phys. Rev. C*, 60:055214, Oct 1999. doi: 10.1103/PhysRevC.60.055214. URL <http://link.aps.org/doi/10.1103/PhysRevC.60.055214>.
- [50] Joseph Meyers and Eric S. Swanson. Spin Zero Glueballs in the Bethe-Salpeter Formalism. *Phys. Rev. D*, 87:036009, Feb 2013. doi: 10.1103/PhysRevD.87.036009. URL <http://link.aps.org/doi/10.1103/PhysRevD.87.036009>.
- [51] Joseph Meyers and Eric S. Swanson. The Gluon Propagator with Two-Loop Schwinger-Dyson Equations. *Phys. Rev. D*, 90:045037, Aug 2014. doi: 10.1103/PhysRevD.90.045037. URL <http://link.aps.org/doi/10.1103/PhysRevD.90.045037>.
- [52] Colin J. Morningstar and Mike Peardon. Glueball Spectrum from an Anisotropic Lattice Study. *Phys. Rev. D*, 60:034509, Jul 1999. doi: 10.1103/PhysRevD.60.034509. URL <http://link.aps.org/doi/10.1103/PhysRevD.60.034509>.
- [53] Noboru Nakanishi. Normalization Condition and Normal and Abnormal Solutions of the Bethe-Salpeter Equation. *Phys. Rev.*, 138:B1182–B1192, Jun 1965. doi: 10.1103/PhysRev.138.B1182. URL <http://link.aps.org/doi/10.1103/PhysRev.138.B1182>.
- [54] Noboru Nakanishi. A General Survey of the Theory of the Bethe-Salpeter Equation. *Progress of Theoretical Physics Supplement*, 43:1–81, 1969. doi: 10.1143/PTPS.43.1. URL <http://ptps.oxfordjournals.org/content/43/1.abstract>.
- [55] Yoichiro Nambu. Force Potentials in Quantum Field Theory. *Progress of Theoretical Physics*, 5(4):614–633, 1950. doi: 10.1143/ptp/5.4.614. URL <http://ptp.oxfordjournals.org/content/5/4/614.short>.
- [56] K.A. Olive et al. Review of particle physics. *Chin.Phys.*, C38:090001, 2014. doi: 10.1088/1674-1137/38/9/090001.
- [57] M. R. Pennington and D. J. Wilson. Are the Dressed Gluon and Ghost Propagators in the Landau Gauge Presently Determined in the Confinement Regime of QCD? *Phys. Rev. D*, 84:094028, Nov 2011. doi: 10.1103/PhysRevD.84.094028. URL <http://link.aps.org/doi/10.1103/PhysRevD.84.094028>.
- [58] M.R. Pennington. Swimming with Quarks. *J.Phys.Conf.Ser.*, 18:1–73, 2005. doi: 10.1088/1742-6596/18/1/001. URL <http://arxiv.org/abs/hep-ph/0504262>.
- [59] Roldan Pozo. Template Numerical Toolkit (TNT) and JAMA/C++. URL <http://math.nist.gov/tnt/index.html>.
- [60] E. E. Salpeter and H. A. Bethe. A Relativistic Equation for Bound-State Problems. *Phys. Rev.*, 84:1232–1242, Dec 1951. doi: 10.1103/PhysRev.84.1232. URL <http://link.aps.org/doi/10.1103/PhysRev.84.1232>.

- [61] D.V. Schroeder. *An Introduction to Quantum Field Theory*. Levant Books, 2005. ISBN 9788187169529. URL <http://books.google.com/books?id=yL3PnQk84HwC>.
- [62] Julian Schwinger. On the Greens Functions of Quantized Fields. i. *Proceedings of the National Academy of Sciences*, 37(7):452–455, 1951. doi: 10.1073/pnas.37.7.452. URL <http://www.pnas.org/content/37/7/452.short>.
- [63] Julian Schwinger. On the Greens Functions of Quantized Fields II. *Proceedings of the National Academy of Sciences*, 37(7):455–459, 1951. doi: 10.1073/pnas.37.7.455. URL <http://www.pnas.org/content/37/7/455.short>.
- [64] J. Sexton, A. Vaccarino, and D. Weingarten. Numerical Evidence for the Observation of a Scalar Glueball. *Phys. Rev. Lett.*, 75:4563–4566, Dec 1995. doi: 10.1103/PhysRevLett.75.4563. URL <http://link.aps.org/doi/10.1103/PhysRevLett.75.4563>.
- [65] A.A. Slavnov. Ward Identities in Gauge Theories. *Theoretical and Mathematical Physics*, 10(2):99–104, 1972. ISSN 0040-5779. doi: 10.1007/BF01090719. URL <http://dx.doi.org/10.1007/BF01090719>.
- [66] J.C. Taylor. Ward Identities and Charge Renormalization of the Yang-Mills Field. *Nuclear Physics B*, 33(2):436 – 444, 1971. ISSN 0550-3213. doi: [http://dx.doi.org/10.1016/0550-3213\(71\)90297-5](http://dx.doi.org/10.1016/0550-3213(71)90297-5). URL <http://www.sciencedirect.com/science/article/pii/0550321371902975>.
- [67] Lorenz von Smekal, Andreas Hauck, and Reinhard Alkofer. A Solution to Coupled Dyson-Schwinger Equations for Gluons and Ghosts in Landau Gauge. *Annals of Physics*, 267(1):1 – 60, 1998. ISSN 0003-4916. doi: <http://dx.doi.org/10.1006/aphy.1998.5806>. URL <http://www.sciencedirect.com/science/article/pii/S0003491698958067>.
- [68] S. Weinberg. *The Quantum Theory of Fields: Foundations*. Number V. 1 in The Quantum Theory of Fields. Cambridge University Press, 1995. ISBN 9780521550017. URL http://books.google.com/books?id=doeDB3_WLvwC.
- [69] S. Weinberg. *The Quantum Theory of Fields*. Number V. 2 in The Quantum Theory of Fields 3 Volume Hardback Set. Cambridge University Press, 1996. ISBN 9780521550024. URL <http://books.google.com/books?id=sn9QvU5dmBQC>.
- [70] Richard Williams. *Schwinger-Dyson Equations in QED and QCD and the Calculation of Fermion-Antifermion Condensates*. PhD thesis, Durham University, 2007. URL <http://etheses.dur.ac.uk/2558/>. Available at Durham E-Theses Online.
- [71] Kenneth Wilson. Confinement of Quarks. *Phys. Rev. D*, 10:2445–2459, Oct 1974. doi: 10.1103/PhysRevD.10.2445. URL <http://link.aps.org/doi/10.1103/PhysRevD.10.2445>.

[72] Wolfram Research, Inc. Mathematica, Version 10.0, Champaign, IL (2014).